Computer Simulations of Polymers and Tethered Membranes

by

Sandra Barsky

B.Sc.H., Queen's University, 1987

M.Sc., University of Western Ontario, 1989

A THESIS SUBMITTED IN PARTIAL FULFILLMENT
OF THE REQUIREMENTS FOR THE DEGREE OF
DOCTOR OF PHILOSOPHY
in the Department
of
Physics

SIMON FRASER UNIVERSITY
April 1996

APPROVAL

Name: Sandra Barksy

Degree: Doctor of Philosophy

Title of thesis: Computer Simulations of Polymers and Tethered Membranes

Examining Committee: Dr. Jeffrey Dahn
Chair

Dr. Michael Plischke, Senior Supervisor

Dr. David Boal

Dr. Michael Wortis

Dr. Barbara Frisken, Internal Examiner

Dr. Gary Grest, External Examiner
Corporate Research Science Laboratory,
Exxon Research and Engineering Company
Annandale New Jersey

Date Approved: April 19, 1996

PARTIAL COPYRIGHT LICENSE

I hereby grant to Simon Fraser University the right to lend my thesis, project or extended essay (the title of which is shown below) to users of the Simon Fraser University Library, and to make partial or single copies only for such users or in response to a request from the library of any other university, or other educational institution, on its own behalf or for one of its users. I further agree that permission for multiple copying of this work for scholarly purposes may be granted by me or the Dean of Graduate Studies. It is understood that copying or publication of this work for financial gain shall not be allowed without my written permission.

Title of Thesis/Project/Extended Essay

COMPUTER SIMULATIONS OF POLYMERS AND TETHERED MEMBRANES

Author: _____
(signature)

_____
(name)

April 19, 1996.
(date)

Abstract

Tethered membranes are a natural two-dimensional generalization of linear polymers. They can be thought of as a collection of monomers that are permanently connected to their neighbours in two-dimensions. When embedded in three dimensions a generalized Flory theory predicts that the membrane should be crumpled. However, computer simulations indicate that membranes remain flat except in models where the monomers occupy no volume. I report on simulations done on membranes embedded in four and five dimensions. It is found that membranes in four dimensions remain flat, even with a limited amount of excluded volume. In five dimensions the membranes are crumpled even with a very high degree of excluded volume.

The remaining chapters focus on the vulcanization transition of linear polymers. This transition is normally described by incorporating crosslinks into a melt of linear polymers. Both the classical theory of vulcanization and a more recent model proposed by Goldbart *et al.* are reviewed. In the latter model, when the density of crosslinks in a polymer melt is increased beyond a critical number n_c, then a fraction of monomers acquire fixed mean positions. The localized monomers fluctuate normally about these mean positions. Both the critical density of crosslinks and the distribution of localization lengths are predicted. Also, an order parameter that differentiates liquid from amorphous solid is derived.

I report on computer simulations of randomly crosslinked melts of linear polymers. The density of crosslinks is varied and both the order parameter and the distribution of localization lengths are monitored. The order parameter describes the crosslinked melt as predicted. The distribution of localization lengths collapses to a universal function when scaled by an appropriate variable. The collapse occurs for a wide range of crosslink densities and for different system sizes.

A final study examines how the shear modulus varies with crosslink density in the

crosslinked polymer melts. The system acquires a non-zero shear modulus at approximately the same density of crosslinks that the order parameter becomes non-zero.

Acknowledgements

In appreciating the many contributions from different sources, the biggest thanks must to go my supervisor Dr. Michael Plischke. His patience, generosity and caring made this degree possible. He never tired of answering my questions, no matter how basic nor how often I asked the same question; he never showed his frustration at my errors. He considerately and thoughtfully directed me through every aspect of my degree, usually going far beyond the call of duty. As well as always giving me as much time as I needed, he was a constant source of encouragement. I am extremely fortunate to have been his student, and I shall always be grateful for the time he took to guide me through my studies.

I would like to thank Julian Shillcock, for coffee and endless discussions of physics. He carefully worked through details of many calculations with me, and patiently answered many of my questions on statistical mechanics.

The office staff were always kind and helpful, regardless of how stressed I was. They happily provided much of the technical support necessary to let me focus on my studies, and I thank them all. In reverse alphabetical order: Shauna, Sharon, Sada, Margaret, Julie, Edith and Audrey. I wish you all well.

My parents were extremely generous in their support: emotional, financial and nutritional.

My officemates and friends here and away provided me with laughter and perspective, and I could not have finished without them. I especially want to thank Jeff Rudd for wonderful conversations, and fabulous demos. He helped to revive my interest in physics whenever it waned (especially a demo of critical opalescence), and fed me far more cookies than I possibly deserved. And thanks to Andrew McConnell for far too many interesting conversations.

A big hug goes to Kevin Fleming, you were always there for me, no matter how far away

you were. I know that you never left me alone. May the angels take care of you.

Finally thanks to Guy Martel for always caring, especially through the last few months.

Contents

List of Tables

List of Figures

List of Symbols

a Constant.

a_0 Bond length of subsequent monomers on a polymer.

$\mathbf{a}$ Acceleration.

$\mathbf{a}_i$ Basis vectors with $i = x, y, z$.

a_{ij} Product of basis vectors, $a_{ij} = \mathbf{a}_i \cdot \mathbf{a}_j$.

A Arbitrary function.

A_c Arbitrary constant.

A_1 Anisotropy.

α Replica index.

$\mathbf{b}_j$ Average position of j-th monomer.

β Inverse of $k_B T$.

β_t Scaling exponent of elasticity with crosslink density.

β_q Scaling exponent of order parameter with crosslink density.

β_Q Scaling exponent of fraction of localized monomers with crosslink density.

β_ξ Scaling exponent of localization length with crosslink density.

b, b_M Constant involving number of monomers and bond length, and the specific value when there are M monomers per polymer.

$\mathbf{c}_j$ Dimensionless polymer position vector.

C_{ijlk} Elastic constant.

$C(t)$ Autocorrelation function.

c Concentration.

γ Scaling exponent for average size of finite clusters in the percolation model.

D Dimension of generalized membrane.

d Embedding dimension of membrane.

$d(t)$ Energy metric measured at time t.

E Shear modulus.

$E_{\mathbf{int}}$ Internal energy.

$E_j(t)$ Energy of particle j at time t.

$\epsilon_j(t)$ Normalized energy of particle j at time t.

$\epsilon_{aj}(t)$ Normalized energy of particle j at time t starting from initial state a.

ϵ Energy parameter in simulation potential.

ε A small number of crosslinks above the critical crosslink density.

F Free energy.

f Free energy in Goldbart's Theory.

$f^{\mathbf{var}}$ Variational free energy.

$\mathcal{F}_n$ Replica free energy.

$\mathbf{f}$ Force.

f_i Force per unit area in direction $i = x, y, z$.

f Fraction (of simulation box).

ζ Inverse square localization length.

$\hat{\zeta}$ Laplace transform of the inverse square localization length.

$g(c)$ Arbitrary function.

G_0 Plateau modulus.

$\mathcal{H}$ Hamiltonian.

H_1^E Edward's Hamiltonian.

$I_{\alpha\beta}$ Moment of inertia tensor.

$\mathbf{k}$ Vector in reciprocal space.

$\mathbf{k}_i$ Particular values of reciprocal space vectors, with $i = 1, 2$.

k Magnitude of vector in reciprocal space and parameter of energy in tethering potential.

k_B Boltzamann's constant.

κ Spring constant.

l Length scale of membrane or polymer.

L Size of simulation box or size of the membrane.

L_x, L_y, L_z Size of simulation box in each of the x, y, z directions.

L_p Length of polymer in Goldbart's theory.

L_1, L_2 Lengths of specific membranes.

l_p Persistence length.

dl Infinitesimal length change.

L_K Kuhn statistical length.

m Mass.

m_b Number of bonds in a polymer with M monomers.

M Number of monomers in a polymer.

M_{eff} Effective number of monomers in a polymer.

M_e Number of monomers in an entanglement length.

μ^2 Parameter that controls the crosslink density.

n Crosslink density.

n_c Critical crosslink density.

n_{cl} Number of crosslinks.

n_{sa} Number of self-avoiding particles in variable self-avoiding membranes.

$n_{sa}(c)$ Critical number of self-avoiding particles.

N Number of polymers.

N_M Number of polymers with M monomers.

$\mathcal{N}$ Total number of particles.

p Percolation probability.

p_c Critical percolation probability.

p_t Critical percolation probability necessary for rigidity.

P Pressure.

P_M Distribution of crosslinks.

P_i Pressure along the i-th axis.

$\mathcal{P}$ Probability that a walk from a chosen vertex is finite.

$P(\xi)$ Probability distribution of localization lengths.

$P(\mathcal{X})$ Probability distribution of the x-component of position.

$p(\zeta)$ Probability distribution of inverse square localization lengths.

$\hat{p}(\hat{\zeta})$ Laplace transform of probability distribution of inverse square localization lengths.

$\tilde{P}$ Probability that a walk from a given vertex is infinite.

$\pi(\vartheta)$ Scaled version of $p(\zeta)$.

$\hat{\pi}$ Laplace transform of $\pi(\vartheta)$.

$\rho(k)$ Fourier transform of the density function of a monomer.

q Order parameter.

q' Order parameter that depends on fraction of localized monomers.

q_j Order parameter for the monomer j.

$q(t)$ Order parameter as a function of time.

Q Fraction of localized monomers.

$Q_{\hat{k}}$ Replica version of fraction of localized monomers.

$\mathcal{Q}$ Probability that a walk in a given direction is finite.

$\mathbf{r}$ Position.

$\mathbf{r}_i$ Position of i-th particle.

r_{ij} Magnitude of the vector difference of the positions of particles i and j.

r_x Radius of circle used to look for potential crosslinks in the simulation.

$R_{\mathbf{ee}}$ End-to-end distance of a polymer.

R_{CM} Position of the centre of mass.

R_g Radius of gyration.

R_0 Maximum extension of tethered particles.

$\mathbf{R}_j$ Position of j-th monomer.

$\overline{\mathbf{R}}_j$ Average position of j-th monomer.

s Scaled position in Goldbart's theory.

s_p Distance between two segments on a polymer.

S_T Total number of monomers in a volume of size $\tilde{\xi}^3$.

S_F Total number of monomers in finite clusters in a volume of size $\tilde{\xi}^3$.

S_G Total number of monomers that belong to the infinite cluster in a volume of size $\tilde{\xi}^3$.

S Fraction of monomers in the infinite cluster (gel fraction).

$\mathcal{S}$ Entropy.

σ Size of particle.

σ_0 Fundamental unit of length in potential.

σ_c Critical diameter for variable self-avoiding membranes.

t, t' Time.

t_o Observation time.

t_s Simulation time.

t_i Tension per unit area in the i-th direction.

τ Dummy variable of time.

T Temperature.

δt Time step increment.

ϑ Scaled version of ζ.

ϑ' Dummy version of ζ.

θ Angle.

U, $U(\mathbf{r}_i - \mathbf{r}_j)$ Pair potential.

U_{nn} Nearest neighbour pair potential.

U_{LJ} Lennard-Jones pair potential.

v Excluded volume parameter.

$\mathbf{v}$ Velocity.

V Volume.

W Work.

w Dummy variable of integration.

x Monomer position in Goldbart's theory.

ξ Localization length.

$\overline{\xi}$ Average localization length.

ξ_{typ} Most probable value of localization length.

x_j Compenent of position of the j-th monomer along the x direction.

X Relative importance of fluctuations of the number of monomers in the infinite cluster.

$\tilde{\xi}$ Correlation length.

z, z^*, $z_{\hat{k}}$, $z^*_{\hat{k}}$ Variables of integration.

Z Partition function.

Z_c Average size of cluster in volume of size $\tilde{\xi}^3$.

$\phi(\mathbf{R}_j)$ Probability of finding monomer j at position $\mathbf{R}_j$.

λ_i Eigenvalue of the moment of inertia tensor.

λ Value of elongation.

ν_i Scaling exponent of the i-th eigenvalue of the moment of inertia tensor.

$\nu_{j,eff}$ Effective scaling exponent.

ϕ, ϕ_0, ϕ_n Replica free energy.

$\phi(a_i)$ Probability distribution of i-th bond.

$\Psi(R_{\mathbf{ee}}, m_b)$ Probability that a polymer m_b bonds has length R_{ee}.

η_{ij} Strain tensor.

Chapter 1

Introduction

1.1 Introduction

Polymers are long linear and highly flexible molecules. Their material attributes such as thermal, optical and elastic properties are very useful to chemists and materials scientists developing new compounds. Polymers attract the interest of biologists, since biopolymers such as DNA and RNA play a pivotal role in most biological processes. A polymer consists of a single unit or monomer repeated hundreds or thousands of times to form a long chain. The monomers can be quite simple molecules such as CH_2 or can be formed of tens or hundreds of atoms. The synthesis of the chains usually occurs by the addition of single monomer units or by short chains merging together. Simple linear polymers are not the only type of polymer available. Polymers can take on other shapes such as a comb formation, where there is a long backbone from which emanate many smaller chains, or polymer stars, where many long polymers meet at a central junction. In this thesis the discussion of polymers is limited to linear polymers.

Polymers do not follow the simple phase diagram of low-molecular-weight substances. A gas of polymers is difficult to obtain except in the most extreme experimental conditions. On the other hand a very dilute solution of polymer can be considered gaseous since the chains are far apart and practically non-interacting. As the concentration of polymers in solution is increased a semi-dilute melt is created. If the concentration of polymer is increased to the point of where there is solvent, then a pure polymer system or dense melt is created. A pure polymer system can exist in several phases, including crystalline, glassy and viscoelastic. The crystalline phase is similar to the low-molecular-weight crystal except that due to the

long chain nature of polymers defect-free crystals are impossible to obtain, and this phase is generally only partially crystalline. The glassy phase is actually a liquid but one with so large a viscosity that there is generally no observable flow during a reasonable period of observation. Many common plastics are really glassy polymers. The viscoelastic phase is very striking in its properties. This system is fluid but does not behave as a simple fluid. The long chains are highly entangled, which limits the motion of the polymers. This entanglement results in a behaviour which is a combination of liquid and solid, so that on appropriate timescales the melts have the viscosity of fluids and the elasticity of solids. For example, when a finite strain is imposed on a melt the initial deformation is that of a solid, but then the system continues to flow like a fluid. Alternatively, the stress required to keep the system at constant deformation diminishes with time.

A polymer network is a solid made from a dense melt of polymers by creating new chemical links between randomly chosen monomers. The links can be made by the addition of a chemical, for example, sulphur, that joins two units or by subjecting the melt to ionizing radiation. One example of such a network is vulcanized rubber. The addition of a few crosslinks traps the entanglements present in the melt while still leaving a lot of flexibility of the chains between the junction points. The most remarkable property of rubber is its elasticity. While a typical low-molecular-weight crystal has a maximum extensibility of less than 1%, most rubbers have extensibilities in the range of 500 - 1000%. Only a few links per chain are necessary to achieve this state. This means that between the crosslinks the chains are highly coiled and as entangled as in the melt. When a tensile force is applied the polymers become less coiled and are, thus, highly extensible. The elasticity of rubber is primarily entropic, depending on the number of configurations that the monomers of the chains can have for a particular end-to-end length of the polymer. On the other hand the elasticity of a crystal is due almost entirely to changes of internal energy, when the crystal is deformed.

1.2 Properties of Single Polymer Chains

The model of an ideal polymer melt is a useful simplification of a system of real polymers. In this model the intrachain repulsion that the monomers experience is screened by other polymer chains. In a melt the preferred conformation of a polymer is generally more coiled than if the polymer were stretched end-to-end. Thermal motion prevents the polymer

molecule from having an unchanging geometrical size. For this reason an average measure of size must be calculated, which can be considered to be the time average that would be obtained from the measurement of the size of the polymer at random times. One common measure is the mean square end-to-end length of the polymer $R_{\rm ee}^2$, which is the square of the straight line distance between the two ends of the molecule. To calculate $R_{\rm ee}^2$ we consider a very simple model of a polymer: a freely orienting chain. In this model each monomer is a fixed distance a_0 from its immediate neighbour on the chain, but the bonds are free to take any direction. The monomers have no excluded volume, which means that different parts of the chain can overlap, as in Fig. 1.1. The number of bonds is M, and the i-th bond is designated by a vector $\mathbf{a}_i$ which stretches from one monomer to its neighbour, and $|\mathbf{a}_i| = a_0$. The position of the i-th monomer $\mathbf{r}_i$ is simply the sum of all the vectors of the previous bonds: $\mathbf{r}_i = \sum_{j=1}^{i} \mathbf{a}_j$. The end-to-end length squared of the polymer is the sum of the square of the bond vectors taking one end of the polymer as the origin, and

$$\begin{aligned} \langle R_{\rm ee}^2 \rangle &= \langle (\mathbf{r}_M - \mathbf{r}_0)^2 \rangle \\ &= \sum_{i,j=1}^{M} \langle \mathbf{r}_i \cdot \mathbf{r}_j \rangle \\ &= \sum_{i}^{M} \langle \mathbf{r}_i^2 \rangle + 2 \sum_{i>j} \langle \mathbf{r}_i \cdot \mathbf{r}_j \rangle \\ &= M a_0^2 \end{aligned} \tag{1.1}$$

because, for $i \neq j$, $\langle \mathbf{r}_i \cdot \mathbf{r}_j \rangle = 0$. The result that $\sqrt{R_{\rm ee}^2} = \sqrt{M} a_0$ indicates that the polymer is quite crumpled compared to its fully stretched length $\sqrt{R_{\rm ee}^2} = M a_0$. A polymer is self-similar in the sense that a subsection of the chain is expected to behave in the same way as the whole chain.

One can then ask what is the probability distribution function of this polymer. Since each bond is a randomly oriented vector of length a_0 the probability distribution of each bond is

$$\psi(\mathbf{a}_i) = \frac{1}{4\pi a_0^2} \delta(|\mathbf{a}_i| - a_0), \tag{1.2}$$

where $\delta(|\mathbf{a}_i| - a_0)$ is a delta-function, and $\mathbf{a}_i$ is a vector describing the i-th bond. We want to find the probability distribution function that the end-to-end vector of a chain consisting of m_b bonds connecting M monomers is $R_{\rm ee}$, and we denote this function by Ψ. We get

$$\Psi(R_{\rm ee}, m_b) = \int d\mathbf{r}_1 \ldots \int d\mathbf{r}_{m_b} \, \delta \left(\mathbf{R}_{\rm ee} - \sum_{i=1}^{m_b} \mathbf{r}_i \right) \prod_{i=1}^{m_b} \psi(\mathbf{r}_i), \tag{1.3}$$

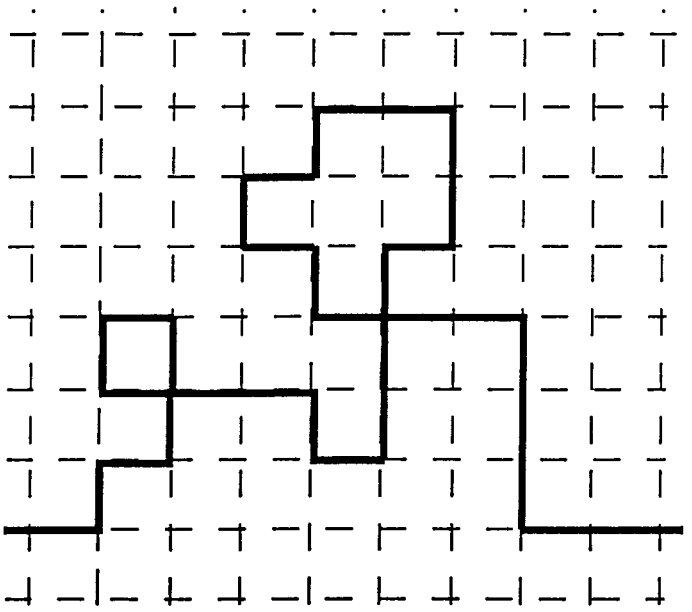

Figure 1.1: The random walk model of a polymer.

and we use the integral representation of the delta-function

$$\delta(\mathbf{r}) = \frac{1}{(2\pi)^3} \int d\mathbf{k} e^{i\mathbf{k}\cdot\mathbf{r}} \tag{1.4}$$

(1.3) becomes

$$\begin{aligned} \Psi(R_{\mathrm{ee}}, m_b) &= \frac{1}{(2\pi)^3} \int d\mathbf{r}_1 \ldots \int d\mathbf{r}_{m_b} \int d\mathbf{k}\, e^{i\mathbf{k}\cdot\mathbf{R}_{\mathrm{ee}}} \prod_{i=1}^{m_b} e^{-i\mathbf{k}\cdot\mathbf{r}_i} \psi(\mathbf{r}_i) \\ &= \frac{1}{(2\pi)^3} \int d\mathbf{k}\, e^{i\mathbf{k}\cdot\mathbf{R}_{\mathrm{ee}}} \left[\int d\mathbf{r}\, e^{-i\mathbf{k}\cdot\mathbf{r}} \psi(\mathbf{r}) \right]^{m_b}. \end{aligned} \tag{1.5}$$

Each of the integrals in the square bracket in the previous equation can be solved in a straightforward manner by transforming to spherical coordinates and results in a factor of $\sin(ka_0)/ka_0$. Substituting this in (1.5) we get

$$\Psi(R_{\mathrm{ee}}, m_b) = \frac{1}{(2\pi)^3} \int d\mathbf{k}\, e^{i\mathbf{k}\cdot\mathbf{R}_{\mathrm{ee}}} \left[\frac{\sin(ka_0)}{ka_0} \right]^{m_b} \tag{1.6}$$

where we use the large m_b approximation, so that $(\sin(ka_0)/ka_0)^{m_b}$ is small unless ka_0 is

small, so that

$$\left[\frac{\sin(ka_0)}{ka_0}\right]^{m_b} = \left[1-\frac{k^2a_0^2}{6}\right]^{m_b} \approx 1-\frac{m_b k^2 a_0^2}{6} \approx e^{-m_b k^2 a_0^2/6}. \quad (1.7)$$

This equation can now be substituted in (1.5), and the integral over $\mathbf{k}$ can be solved for each component by completing the square. The result of this is

$$\Psi(R_{ee}, m_b) = \left(\frac{3}{2m_b\pi a_0^2}\right)^{3/2} e^{-\frac{3}{2m_b a_0^2}\mathbf{R}_{ee}^2}. \quad (1.8)$$

Equation (1.8) gives the probability distribution function for a polymer of m_b bonds having end-to-end distance $\mathbf{R}_{ee}$.

This model is highly simplified in that all excluded volume effects are ignored, the neighbour distance is considered fixed and successive bond vectors are randomly oriented. More realistic models correct for some of these problems, for example, the freely rotating chain model is similar to the random flight model except that i-th bond is connected to the $i-1$-th bond with a fixed angle θ but is free to move about that angle. The end-to-end vector is found to be $R_{ee}^2 = Ma_0^2(1+\cos\theta)/(1-\cos\theta)$, which again shows that $R_{ee} \sim \sqrt{M}$. Another model is the Gaussian chain where the monomers are modelled as points connected by springs of average length a. In this case calculation of the end-to-end vector gives $R_{ee}^2 = Ma^2$. In each of these models, the monomer is not meant to represent a particular submolecule, but rather a group of them. The calculations are not sensitive to the exact number of submolecules in the group as long as the the number of such groups used to form the chain is $M \gg 1$.

Another measure of polymer size is the radius of gyration R_g^2. Qualitatively the radius of gyration measures the average distance of the mass of the polymer from the centre of mass,

$$R_g^2 \equiv \frac{1}{M}\sum_{i=1}^{M}(\mathbf{r}_i - \mathbf{R}_{CM})^2. \quad (1.9)$$

The calculation for the freely jointed chain proceeds in a manner similar to that of the end-to-end distance:

$$R_g^2 \equiv \frac{1}{2M^2}\sum_{i=1}^{M}\sum_{j=1}^{M}\langle(\mathbf{r}_i - \mathbf{r}_j)^2\rangle$$

$$= \frac{1}{2M^2}\sum_{i=1}^{M}\sum_{j=1}^{M}|i-j|a^2 \tag{1.10}$$

$$= \frac{a^2}{2M^2}\sum_{i=1}^{M} i\,(i+1)$$

$$= \frac{1}{6M^2}\left[M\,(M+1)\,(2M+1) - \frac{1}{2}M\,(M+1)\right] \tag{1.11}$$

$$= \frac{a^2}{6M}\left(M^2-1\right)$$

$$\sim \frac{a^2M}{6}. \tag{1.12}$$

Thus, we see the relationship

$$R_g^2 = R_{\text{ee}}^2/6 = \frac{a^2M}{6}. \tag{1.13}$$

For more realistic models of polymers, such as the freely rotating chain or Gaussian chain, the relationship (1.13) still holds but with the length of neighbouring bonds a_0 replaced by the average length of neighbouring bonds $\langle a_0 \rangle$. The relationship R_{ee}^2/Ma_0 is known as the Kuhn statistical length L_K and is one measure of the stiffness of the chain. Different polymers will be more or less flexible depending on their composition and on external parameters such as temperature. The degree of flexibility affects the various transport coefficients such as diffusion rate and viscosity of the polymer. For the freely orienting chain L_K is simply a_0, but it varies for other models. Its intuitive value is seen as this: if we know the length of the fully stretched polymer Ma_0, then we can treat a real polymer as if it consisted of $M_{eff} = Ma_0/L_K$ segments and the above calculations hold. It is related to the stiffness of the chain in the sense that the stiffness will determine how entangled the polymer can become, and hence the value of L_K [1].

A related quantity is known as the persistence length l_p. It is the length over which the polymer remains relatively straight on a microscopic level, i.e., length over which the chain remembers its direction. This length is related to the flexibility or energy required to bend the chain [2]. Chain segments with length l_p can be regarded as practically stiff since their end-to-end distance is approximately l_p. A more precise definition of persistence length can be obtained by considering segments of the chain. For many polymer models two successive segments of the chain are correlated. Considering two randomly chosen segments of the chain a distance s_p apart we can define $\langle \cos\theta(s_p) \rangle$ as the mean cosine of the angle between the chain segments. The persistence length defines the degree of correlation of the

segments through the relation $\langle \cos\theta(s_p)\rangle = \exp(-s_p/l_p)$. Thus the persistence length has a clear microscopic meaning whereas the Kuhn statistical length is more easily obtained experimentally [1]. Both quantities measure the degree of flexibility of the real polymer.

1.3 Tethered Membranes

Although polymers have a very rich phase diagram and many interesting properties, there is even more diversity in the properties of membranes. These objects are topologically two-dimensional. Most membranes are fluid, which is a phase inaccessible to linear objects. One example of such a fluid membrane is a lipid bilayer. The lipid bilayer can be thought of as a highly simplified model for many complex biological structures, and one example is a red blood cell. In the laboratory it is possible to make a model for a red blood cell by dispersing amiphiphilic lipids in aqueous solution. The lipids spontaneously form closed spherical shells known as vesicles. The two-dimensional system is fluid in the sense that the molecules can diffuse in the plane and there is no resistance to shear deformations. The shape of the overall membrane is primarily governed by its bending rigidity and has large out-of-plane fluctuations. Experiments show that the vesicles have a rich variety of shapes and phase transitions.

More closely related to the linear polymers described above are tethered membranes. In this case there is an underlying lattice structure to the arrangement of monomers, so that the nearest neighbours of a given particle are fixed. Thus the monomers are no longer free to diffuse in the plane, and the membrane has a non-zero shear modulus. The network structure means that in-plane strains caused by out-of-plane undulations are suppressed, giving the membrane a large entropic bending rigidity. Experimental realizations of tethered membranes are difficult to create, but some examples are the spectrin network of red blood cells' cytoskeleton, polymers of chiral precursors [3], and sheets of graphite oxide (GO) [4]. Graphite oxide membranes are sheets of micron size that are formed by exfoliating carbon with an oxidizing agent. The latest experiment [4] indicates that these membranes are flat, but with large fluctuations near the edges of the membrane. Nevertheless, if these sheets are suspended in a 'poor' solvent is some long-range attraction between the monomers creates a highly compact configuration, as is seen in some computer simulations [5] and in experiments [4, 6].

1.4 Organization of the Thesis

This thesis is structured as follows. In the next chapter computer simulations of tethered membranes are discussed. The membranes are embedded in $d = 4, 5$ dimensions and the role of this embedding dimension is explored. Monomer size is varied for fully self-avoiding membranes in both embedding dimensions. As well, for $d = 4$, the effect of self-avoidance is investigated through a model which varies both the size of the monomer and the degree of self-avoidance. In Chapter 3 the classical theory of vulcanization is described, and then a new theory is discussed. The latter incorporates the ideas of quenched random variables into the semi-microscopic treatment of randomly crosslinked polymer systems. An order parameter capable of distinguishing liquid, crystal and amorphous solid is presented. It is found that the amorphous solid state is characterized by the fraction of localized monomers and the distribution of the monomers' localization lengths. The results of an extensive set of simulations on randomly crosslinked polymers are presented in Chapter 4. Starting from equilibrated melts, crosslinks are imposed between randomly chosen monomers. Some properties of the melt and the crosslinking procedure are discussed. Results of the calculation of the order parameter as well as the localization of the monomers and scaling exponents are discussed. In Chapter 5 calculations of the shear modulus of the randomly crosslinked polymers are presented. The analytical theory of the shear modulus for a polymer network is reviewed. The results of a series of simulations on randomly crosslinked polymer networks is presented.

Chapter 2

Tethered Membranes

2.1 Introduction

A natural generalization of a one-dimensional polymer is a two-dimensional membrane. Just as linear polymers are formed by connecting a large number of monomers in a linear structure, a membrane is formed by connecting monomers in a planar structure. In other words, if the bonds between monomers are fully stretched, one could map the structure of a membrane onto a plane. There are many examples of this straightforward structure. For example, a simple model of a red blood cell is a spherical shell consisting of a lipid bilayer. Bilayers can be prepared artificially in the laboratory and can exhibit a variety of phases. At low temperatures the bilayer can be in a crystalline or hexatic phase, whereas at higher temperature the molecules diffuse freely in the plane with zero shear modulus. If the internal structure of the membrane is fixed, that is, the nearest neighbours are fixed, the membrane becomes a polymerized membrane. An example of this is the cytoskeleton network found under the bilayers of cells, or sheets of graphite oxide [4].

The work in this thesis is restricted to the *tethered membrane* model, introduced by Kantor *et al* [7]. In this model the connectivity of the monomers is fixed. Most of the existing work has focused on the shapes that tethered membranes can take on. Although a fully stretched membrane is a planar object, when embedded in a dimension d where $d > D = 2$ and allowed to fluctuate, it can take on a variety of conformations.

The simplest version of a tethered membrane is one where the only interaction between particles is that of nearest-neighbour (nn) attraction to enforce the connectivity constraint. Since there is no energy cost to monomers overlapping, this model is called a phantom

membrane. In this approximation the Hamiltonian is

$$\mathcal{H} = \sum_{i,j(nn)} U(|\mathbf{r}_i - \mathbf{r}_j|) = \sum_{i,j(nn)} U(r_{i,j}), \tag{2.1}$$

where U is the interaction potential, $\mathbf{r}_i$ is the position of the ith monomer in d-space. In analogy to ideal polymers, U is chosen to be a spring potential, $U(r_{i,j}) = \kappa r_{i,j}^2/2$. In this case (2.1) becomes

$$\mathcal{H} = \frac{1}{2} \sum_{i,j(nn)} \kappa(\mathbf{r}_i - \mathbf{r}_j)^2. \tag{2.2}$$

In the continuum limit, for a D-dimensional network,

$$\mathcal{H} = \frac{1}{2}\kappa \int d^D x (\nabla r)^2, \tag{2.3}$$

where x denotes the internal space of the D-dimensional membrane, and ∇r is the derivative of r with respect to x (in D dimensions).

A more realistic model that restricts the monomers from overlapping is the generalized version of the Edwards model [7]:

$$\mathcal{H} = \frac{1}{2}\kappa \int d^D x (\nabla r)^2 + \frac{1}{2} v \int \int_{|x_1 - x_2| \geq a} d^D x_1 d^D x_2 \delta^d[r(x_1) - r(x_2)]. \tag{2.4}$$

Here v represents the strength of the two-body interaction. Dimensional analysis can be performed on this equation, where the variable x of the internal space is rescaled by length l as $x' = x/l$. If the membrane is isotropic $r(x)$ is then rescaled as $r' = r/l^\nu$, where ν is the exponent characterizing the scaling behaviour of the membrane in the embedding space. With these substitutions, (2.4) becomes

$$\mathcal{H} = \frac{1}{2}\kappa l^{D-2+2\nu} \int d^D x (\nabla r)^2 + \frac{1}{2} v l^{2D-d\nu} \int \int_{x_1 - x_2 \geq a} d^D x_1 d^D x_2 \delta^d[r(x_1) - r(x_2)]. \tag{2.5}$$

By using a scheme devised by Flory to find the scaling behaviour of a chain, we balance the Gaussian and the excluded volume terms in (2.5). We require that both terms scale in the same way with l, and obtain

$$l^{D-2+2\nu} \sim l^{2D-d\nu}, \tag{2.6}$$

or $D-2+2\nu = 2D-d\nu$, and $\nu = \frac{D+2}{d+2}$. For a two-dimensional network in three dimensional space this predicts $\nu = 4/5$. If the upper critical dimension is defined as the embedding dimension where the self-avoidance no longer plays a role, then we must have $2D - d\nu = 0$, or substituting for ν, $d = \frac{2D}{2-D}$. Thus, self-avoidance should be relevant in any embedding

dimension for $D = 2$. We also note that if $v = 0$ scale invariance produces $\nu = \frac{2-D}{2}$ for the Gaussian model a result that can also be easily derived by direct calculation [7].

The thermodynamic phases of the membrane can be partially characterized by the shape of the membrane in the thermodynamic limit $L \to \infty$, where L is a characteristic linear size of the membrane. To describe this shape we use the moment of inertia tensor,

$$I_{\alpha\beta} = \frac{1}{\mathcal{N}} \sum_i (r_{i\alpha} - \bar{r}_{i\alpha})(r_{i\beta} - \bar{r}_{i\beta}), \tag{2.7}$$

where $r_{i\alpha}$ is the α-component of the position vector of the i-th particle, α, β run over the dimension of the embedding space, and $\mathcal{N}$ is the number of particles in the membrane. The eigenvalues λ_α of the matrix $I_{\alpha\beta}$ are the principal moments of inertia. We order those eigenvalues in the following way: $\lambda_\alpha \leq \lambda_\beta$ when $\alpha < \beta$. The radius of gyration R_g is the sum of the eigenvalues:

$$R_g^2 = \sum_i \lambda_i. \tag{2.8}$$

The scaling of the radius of gyration and the eigenvalues of the inertia tensor with linear size L of the membrane provides information about the shape of the membrane. The relations

$$\lambda_i \sim L^{2\nu_i}, \tag{2.9}$$

$$R_g^2 \sim L^{2\nu}, \tag{2.10}$$

define the scaling exponents ν_i and ν. The range of ν is restricted by some straightforward geometrical constraints: $0 \leq \nu \leq 1$, where $\nu = 1$ holds when the membrane is fully stretched. A self-avoiding membrane has a further constraint due to the volume of the particles. When the membrane has the most compact conformation in d-space, its mass occupies a volume proportional to R_g^d in the embedding space; thus $L^D \sim R_g^d$ and $R_g \sim L^{D/d}$, which gives $D/d \leq \nu$.

The phases of the membrane, or its conformation in the embedding space, can be determined by the scaling behaviour of λ_i with L. The two phases that are of interest in this work are flat and crumpled. In the flat phase the scaling exponents vary as

$$\begin{aligned} \nu_d = \nu_{d-1} = \ldots = \nu_{d-D+1} = 1 & \\ \nu_i < 1, \qquad i \leq d - D, & \end{aligned} \tag{2.11}$$

while in the isotropically crumpled phase they are identical,

$$\nu_d = \nu_{d-1} = \ldots = \nu_1 < 1. \tag{2.12}$$

In the case of phantom membranes $\nu_i = 0$, $i = 1, \ldots, d$. Thus phantom membranes increase in size with L more slowly than any power.

Assuming only nearest neighbour interactions as in (2.2), Kantor *et al* [7] were able to predict that the radius of gyration R_g increases as $(\ln L)^{1/2}$ for a phantom membrane embedded in $d \geq 3$. In the presence of only excluded volume interactions, they found that $R_g \sim L^{\nu}, \nu = 0.8$ for $d = 3$. They attempted to verify these predictions with Monte Carlo simulations of a system in which the particles interacted via an infinite square well potential. That is, for the particles to be closer than the hard-core size, or farther than the maximum tether length cost an infinite amount of energy; any other distance had no energy cost associated with it. These simulations, for rather small systems, seemed to be consistent with the theoretical predictions. Despite this promising start, later simulations [8, 9, 10, 11] on larger membranes with full self-avoidance showed conclusively that such membranes are flat: $\nu_3 = \nu_2 = 1$, $\nu_1 \approx 0.7$.

One possible explanation for this unexpected flat state [12] is the presence of an "implicit bending rigidity." This rigidity is not explicit in the microscopic Hamiltonian but rather is generated through self-avoidance. It is expected to be related to the size of the particles. The idea that an explicit bending rigidity by itself could cause a membrane to remain flat was tested for phantom membranes. The Hamiltonian consisted of the tethering potential, with an added bending rigidity term. The membranes showed a transition from a phantom state to a flat state [13, 14] for large enough bending rigidity. A similar transition was obtained for a membrane with a slightly different model [12]. In this case the potential describing the monomers had a self-avoiding constraint for first and second neighbours only, and the length of the tethering potential was systematically shortened. A transition occurred from a crumpled state with a long tether to a flat state with a short tether length.

This last study indicates that entropic bending rigidity drives the system toward the flat phase for short enough tether lengths in a membrane with limited self-avoidance. Conversely, in a membrane with full self-avoidance it is possible that the crumpled state may be recovered if the size of the particles were small compared to the tether length. Computer simulations with variable sized hard cores so far have failed to find a crumpled state for non-zero hard core [9]. It has been conjectured that, at least for $d = 3$, there is a single fixed point which controls the large scale behaviour of the membrane for any non-zero hard core.

If an entropic bending rigidity induces the membranes to remain flat, it is possible that increased entropy causes the membranes to crumple. One way to increase the entropy is

to remove some fraction of the monomers. In this case, the connectivity of the lattice is still fixed, but the lattice contains some defects. A study done on site-diluted membranes [15] indicated that the membranes are flat above the percolation threshold. A related study on bond-diluted membranes [16] indicated that membranes also are flat above the bond-percolation threshold. Another way to reduce excluded volume effects is to reduce the number of self-avoiding interactions that any given monomer has. This was studied for a variable number of such self-avoiding interactions [17]. These authors estimated the "critical value of the hard-core size" as a function of the number of self-avoiding interactions. They found that the critical value of the hard-core size was zero for a fully self-avoiding membrane, indicating that any non-zero size of particle would stabilize the membrane to remain flat.

Theoretical work on tethered membranes yields conflicting predictions about the dimension in which these membranes should crumple. Renormalization-group calculations [7, 18, 19, 20] and ϵ-expansions [21] suggest that the flat phase is unstable in $d = 3$, although later work using a gaussian variational approximation [22] indicates that the membranes are flat below $d = 4$. As well, $1/d$-expansion that include self-avoidance also predict that the membranes are flat until $d = 4$ [23].

Prior to the work reported here, there were two simulation studies done on membranes embedded in dimensions greater than three. The first study found that membranes in $d = 4, 5$ were asymptotically flat [10]. The second study found that membranes were flat for $d = 4$, and crumpled for $d \geq 5$ [24]. The first study was limited to relatively small membranes, while the latter used a tethering potential that might cause a rather rigid membrane, and hence increase the effective bending ridigity.

Most computer simulations have been carried out for models in which the interactions between particles are short ranged. This is not necessarily the most appropriate model. If membranes immersed in solvent behave as polymers do , the type of solvent that the membrane is immersed in will have some effect. In analogy to polymers, the monomers of membranes immersed in poor solvents are expected to attract at long distances. Models where only nearest neighbours attract are related to experiments on membranes in good solvents [25]. As well, most simulations have been done for open topologies. However, one recent study done on tethered membranes in the shape of closed spherical shells [26] indicated that the membranes remain flat in the sense that $R_g^2 \sim \mathcal{N}$, with $\mathcal{N}$ particles on the shells.

The rest of this chapter is organized as follows: in the next section I describe the

model and the general molecular dynamics technique used. In the subsequent two sections I describe the results of the simulations in $d = 5$ and $d = 4$, respectively.

2.2 Method and Model

The technique used to do all the studies reported in this thesis is constant-energy molecular dynamics, which is described in detail below. This type of simulation samples points from a microcanonical ensemble. Since the microcanonical ensemble has constant volume, energy and number of particles, a straighforward way to implement the dynamics is to integrate forward in time Newton's equations of motion. The numerical integration can be done in several ways, including predictor-corrector methods and Verlet schemes, [27]. The canonical ensemble, where temperature instead of energy is kept constant, can be sampled using different molecular dynamics techniques. A direct, but time consuming, method to keep the temperature constant is to rescale the velocities every time the equations of motion are integrated forward. A more sophisticated way to generate the canonical ensemble is to couple the system to a heat bath. One way to implement this coupling is to cause a collision between a randomly selected particle and an imaginary heat-bath particle. In practice this is done by changing the velocity of the particle to a value chosen from a Maxwell-Boltzmann distribution, which causes the system to jump from one constant-energy surface to another. A second way to generate a constant temperature is the Nosé-Hoover [28] dynamics scheme, which couples the system directly to a heat bath. A new degree of freedom which represents the thermal resevoir is included and associated with it is a conjugate momentum which relates to the velocities of the real particles, and extra terms are included in the potential energy. A comparison of elastic constants generated from traditional molecular dynamics and constant temperature molecular dynamics found that both methods efficiently generated elastic constants, although the results from the constant-energy calculations more closely matched those from Monte Carlo methods [29].

In a constant-energy molecular dynamics simulation the classical equations of motion are integrated forward in time to produce successive values of the positions and velocities of the particles. If $U(|\mathbf{r}_i - \mathbf{r}_j|)$ is the potential describing the interaction between particles i and j then the force acting on particle i due to this interaction is

$$\mathbf{f}_i = -\nabla_{\mathbf{r}_i} U(|\mathbf{r}_i - \mathbf{r}_j|) \tag{2.13}$$

where

$$\nabla_{\mathbf{r}_i} \equiv (\frac{\partial}{\partial x_i}, \frac{\partial}{\partial y_i}, \frac{\partial}{\partial z_i}). \tag{2.14}$$

The total force on particle i is found by summing over all the particles in the system that i interacts with,

$$\mathbf{f}_i = -\nabla_{\mathbf{r}_i} \sum_j U(|\mathbf{r}_i - \mathbf{r}_j|). \tag{2.15}$$

Once the initial positions of particles and their velocities are chosen, the system is integrated forward in time according to the velocity Verlet [27] method:

$$\begin{aligned} \mathbf{r}_i(t+\delta t) &= \mathbf{r}_i(t) + \delta t \mathbf{v}_i(t) + \frac{1}{2}(\delta t)^2 \mathbf{a}_i(t) \\ \mathbf{v}_i(t+\delta t) &= \mathbf{v}_i(t) + \frac{1}{2}\delta t[\mathbf{a}_i(t) + \mathbf{a}_i(t+\delta t)] \\ \mathbf{a}_i(t) &= \mathbf{f}_i(t)/m, \end{aligned} \tag{2.16}$$

where $\mathbf{f}_i(t)$ is the total force acting on particle i, and m is its mass. At this stage there are new particle positions and velocities, new forces can be calculated, and the whole procedure is repeated. In doing the simulation, care must be taken in choosing the integration parameter δt. If δt is chosen to be too small, a great deal of computer time will be required to advance the positions and velocities of the system to equilibrium values; if it is too large, particles will violate the tethering or self-avoiding constraints and energy will not be adequately conserved. To find the optimal values I started out with larger values of δt, and gradually chose smaller ones until the particles no longer violated the constraints of the potential in a simulation run.

In implementing such a scheme the system evolves through phase space. The ergodic hypothesis states that an ensemble average is equal to a time average over a given trajectory, but there is no guarantee that a system started from an arbitrary non-equilibrium point in phase space will reach an equilibrium state during the length of a simulation, i.e., it is possible that the system can be trapped in a subspace of the constant energy surface. To avoid this one can do several repetitions with different initial conditions. The system then traces different paths through phase space, and, presumably, not all of these paths confine the system to a particular region. Furthermore, there must be sufficient time for the system to evolve to equilibrium. Equilibrium is determined by monitoring some representative quantity A of the system as a function of time. Since the integration parameter δt is small,

successive values of the positions and velocities of equation (2.16) are highly correlated. If A is sampled every few time steps and plotted as a function of the number of time steps, then typical behaviour of A is shown in Fig. 2.1: A decays from its initial value to an equilibrium value about which it fluctuates normally. The data acquired during the non-equilibrium period are discarded when analyzing A.

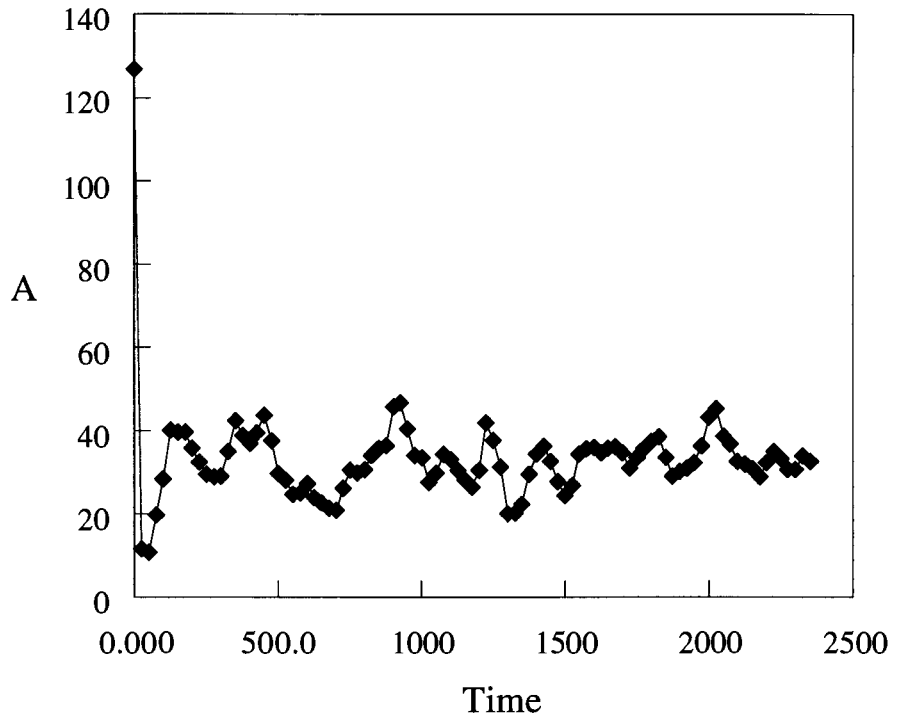

Figure 2.1: Typical behaviour of a system quantity, in this case the largest eigenvalue of the inertia tensor of a membrane with $\sigma = 1.2\sigma_0$ and $L = 41$. There is a very fast decay of the eigenvalue from its initial to its equilibrium value.

The potential used to describe the particle interactions is similar in form to that used in [24]. Nearest neighbours are tethered by the attractive potential,

$$U_{nn}(r_{ij}) = \begin{cases} -\frac{1}{2}kR_0^2 \ln\left[1 - \left(\frac{r_{ij}}{R_0}\right)^2\right] & r_{ij} < R_0 \\ \infty & r_{ij} \geq R_0, \end{cases} \tag{2.17}$$

which has the virtue that it is not necessary to compute a square root when calculating the

force between the particles. Self-avoidance is imposed by the repulsive potential

$$U_{LJ}(r_{ij}) = \begin{cases} 4\epsilon\left[\left(\frac{\sigma}{r_{ij}}\right)^{12} - \left(\frac{\sigma}{r_{ij}}\right)^{6} + \frac{1}{4}\right] & r_{ij} < 2^{1/6}\sigma \\ 0 & r_{ij} \geq 2^{1/6}\sigma\,, \end{cases} \tag{2.18}$$

where the maximum extension of nearest neighbours R_0 and the measure of size of each particle σ are measured in units of σ_0 which is a unit of length.

The membrane is a hexagonal section of a triangular lattice with the number of particles $\mathcal{N}$ related to the longest diagonal through $\mathcal{N} = (3L^2 + 1)/4$. The initial conformation of the membrane was a flat, nearly stretched, configuration. Although starting far from the equilibrium shape increases the running time, the initial configuration does not determine the final shape of the membrane. Numerical studies [10, 12] have shown that the eventual equilibrium shape of the membrane is independent of the initial configuration. The initial configurations tested in these studies were flat, collapsed, folded and crumpled.

As mentioned above, the starting configuration used is a flat, nearly stretched one, and the monomers were given random velocities such that the initial temperature

$$k_B T/\epsilon = \frac{1}{\mathcal{N}d}\frac{m}{\epsilon}\sum_{i=1}^{\mathcal{N}} \mathbf{v}_i^2 = 1. \tag{2.19}$$

During the first phase of a run, the velocities were periodically rescaled to this temperature to remove some of the effects of the potentially atypical starting configuration. After this transient the kinetic energy fluctuated about this mean value. The time step used for the integration was $\delta t = 0.01\sigma_0\sqrt{m/\epsilon}$, which is small enough to ensure energy conservation to one part in 10^4 even for a very long run. The centre of mass velocity and angular momentum were set to zero at the beginning of each simulation, and periodically reset to zero during long simulations to correct for accumulated numerical roundoff errors. We monitored the potential and total energies and the eigenvalues of the moment of inertia tensor,

$$I_{\alpha\beta} = \frac{1}{\mathcal{N}}\sum_i (r_{i\alpha} - \bar{r}_{i\alpha})(r_{i\beta} - \bar{r}_{i\beta}), \tag{2.20}$$

every 200-300 time steps. To determine when equilibrium was reached, a time series of the eigenvalues was taken. The eigenvalues are expected to decay to their equilibrium values and then to oscillate normally about those mean values. Once the equilibrium values were believed to have been reached, the autocorrelation function $C(t)$ was examined. For a

quantity A, where A is a measurable system quantity such as the radius of gyration, $C(t)$ is defined as

$$C(t) = \frac{\langle [A(t) - \langle A \rangle] [A(0) - \langle A \rangle] \rangle}{\langle [A(t) - \langle A \rangle]^2 \rangle}, \tag{2.21}$$

where the angular brackets denote a local time average of the samples. Successive configurations are highly correlated and the autocorrelation function determines the number of molecular dynamics steps or, equivalently, the length of time between independent configurations (Fig. 2.2).

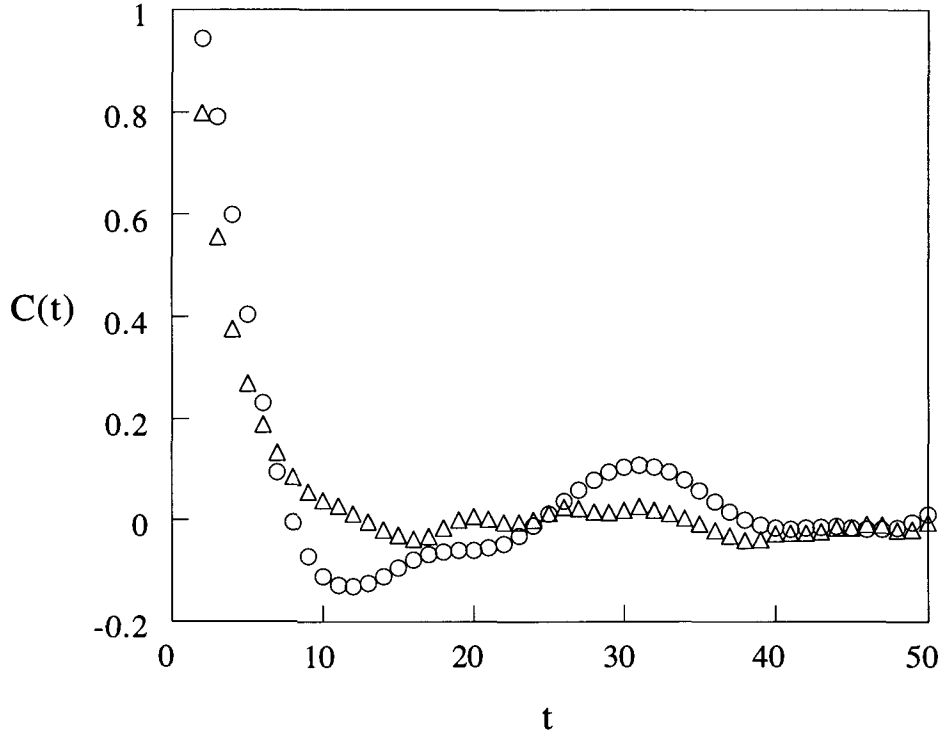

Figure 2.2: The autocorrelation function $C(t)$ of the largest and smallest eigenvalues of the system $L = 7$, $\sigma/\sigma_0 = 1.0$ for a membrane in $d = 5$. The '$\triangle$' symbol corresponds to λ_1 and the '$\circ$' to λ_5.

As mentioned in the introduction, one way to describe the shape of the membrane is to determine how the eigenvalues λ_j scale with the linear size of the membrane L, namely $\lambda_j \sim L^{2\nu_j}$. The most straightforward way is to plot $\lambda_j = aL^{2\nu_j}$ for different system sizes

and to do a least squares fit to find ν_j. This method treats equally the data points from membranes of different sizes. The results from larger systems are expected to have smaller finite size effects and thus be more representative of the thermodynamic limit. In an attempt to minimize some of the finite-size effects, one can calculate the effective exponents, $\nu_{j,eff}$. These are defined as the scaling exponents between two successive values of L,

$$\nu_{j,eff}(L_1, L_2) = \frac{1}{2}\frac{\ln(\lambda_j(L_2)/\lambda_j(L_1))}{\ln(L_2/L_1)}. \tag{2.22}$$

Taking $L_2 > L_1$, one then plots $\nu_{j,eff}$ versus L_2^{-1} and extrapolates to $L_2^{-1} = 0$.

In addition to examining the scaling properties of the eigenvalues, one can look at the shape anisotropy. This function is defined as the ratio of the smallest eigenvalue to the largest,

$$A_1 = \langle \lambda_1/\lambda_d \rangle. \tag{2.23}$$

The anisotropy reflects the shape in the following way: In the thermodynamic limit, if $A_1 \to 0$, then the membrane is flat, since the largest eigenvalue increases at a greater rate than the smallest one; otherwise, if the limit is a non-zero constant, then the membrane is considered to be crumpled, since both eigenvalues increase at a comparable rate. These methods are used to analyze the results for the simulations done in embedding dimensions $d = 4, 5$.

2.3 Five Dimensions

In $d = 5$, the parameters used in equations (2.17) and (2.18) were $R_0/\sigma_0 = 1.5$, $k\sigma_0^2/\epsilon = 4.0$, $\sigma/\sigma_0 = 0.4 - 1.3$ and the simulations were done for system sizes of length $L = 7, 11, 21, 41$, and for the cases of $\sigma/\sigma_0 = 0.4, 1.0$, $L = 71$. I will illustrate the methods of extracting the scaling exponents for the case of $\sigma/\sigma_0 = 1.0$ and will report the results for the other parameters. The equilibrium values for the eigenvalues were found from analyzing the time series of the data, as described in the previous section.

For most of the range σ/σ_0 and $L \leq 71$ several different computer runs were done. For given parameter values, each simulation had different values of initial velocity and some had slightly different values of initial position. From each simulation a value of the uncertainty of λ_i can be found by plotting λ_i versus time and doing a least-squares fit to λ_i once equilibrium is reached. The quoted uncertainties of the eigenvalues are a weighted average of the errors

found from least squares fit for the different runs. When only one simulation was done, the uncertainty of λ_i was due solely to the least-squares fit.

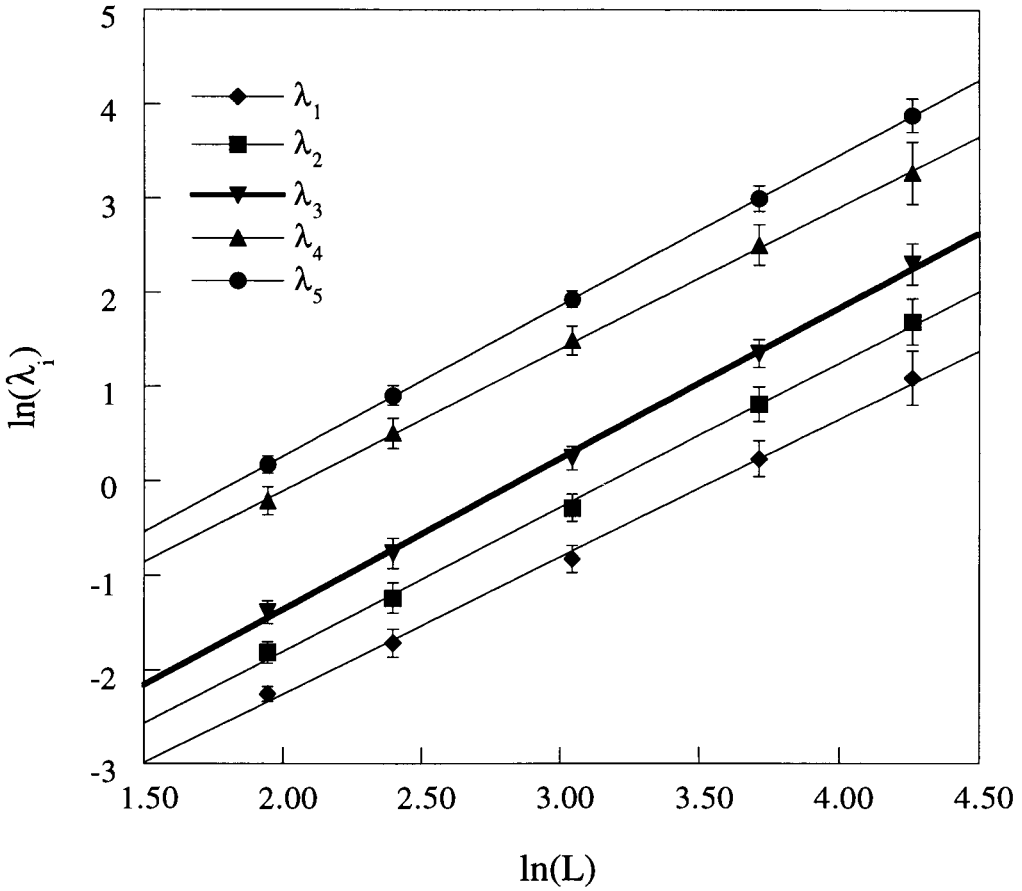

Figure 2.3: Eigenvalues of the moment of inertia tensor as a function of L for $\sigma/\sigma_0 = 1.0$ in $d = 5$. The slopes of the straight lines are the scaling exponents 2ν.

To determine the scaling exponents ν_i, we assume a functional form $\lambda_i = aL^{2\nu_i}$ and do a least-squares fit to find ν_i. Fig. 2.3 shows a plot of $\ln \lambda_i$ versus $\ln L$. This figure provides initial evidence that the membrane is crumpled, since the scaling exponents, which are the slopes of straight lines, are roughly equal. A least-squares fit of the data leads to the exponents shown in Table 2.1.

The anisotropy factor A is shown in Fig. 2.4. It is clear from this figure that for large L, A tends to a non-zero constant. This means that the largest and smallest eigenvalues

are increasing at the same rate, indicating that the membrane is crumpled. As well, this figure gives some indication of the finite-size effects: The anisotropy of the smallest system is significantly different from that of the larger ones. The finite-size effects are emphasized by examining the effective exponents, shown in Fig. 2.5. Only the smallest and largest eigenvalues are shown, for clarity. This figure suggests that ν_1 and ν_5 approach the same limit as $L \to \infty$.

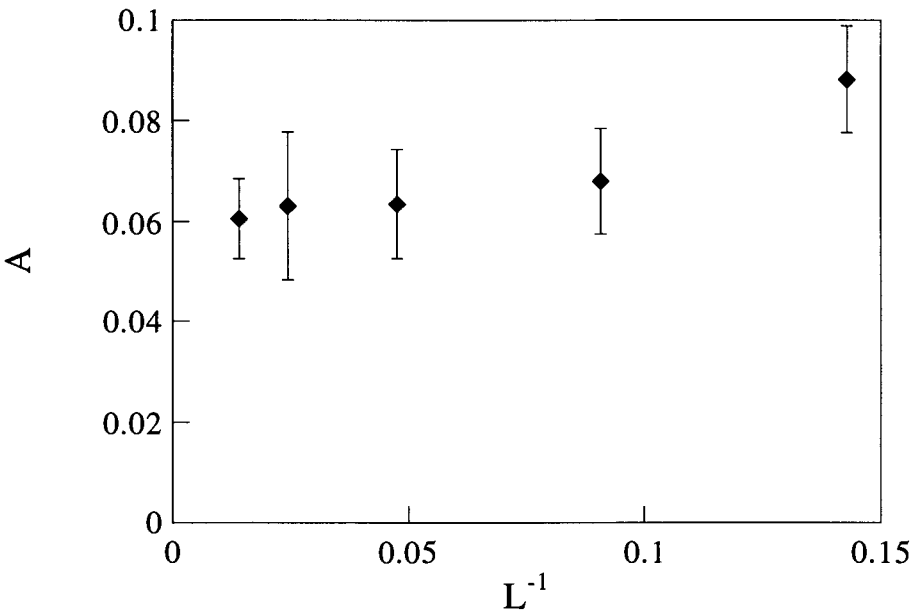

Figure 2.4: Anisotropy λ_1/λ_5 for $\sigma/\sigma_0 = 1.0$ in $d = 5$. A tends toward a non-zero constant for large L.

The results for the scaling exponents of all the parameters are shown in Table 2.1. The results are consistent with a crumpled membrane and $\nu_i = \nu = 0.80 \pm 0.05$ for $i = 1 \ldots 5$. There is no evidence for a flat phase, even when the particle size is almost 90% the size of the maximum tether length. This result is in agreement with one previous simulation [24] in which it was found that $\nu = 0.85 \pm 0.05$, and with recent analytical calculations [23, 22]

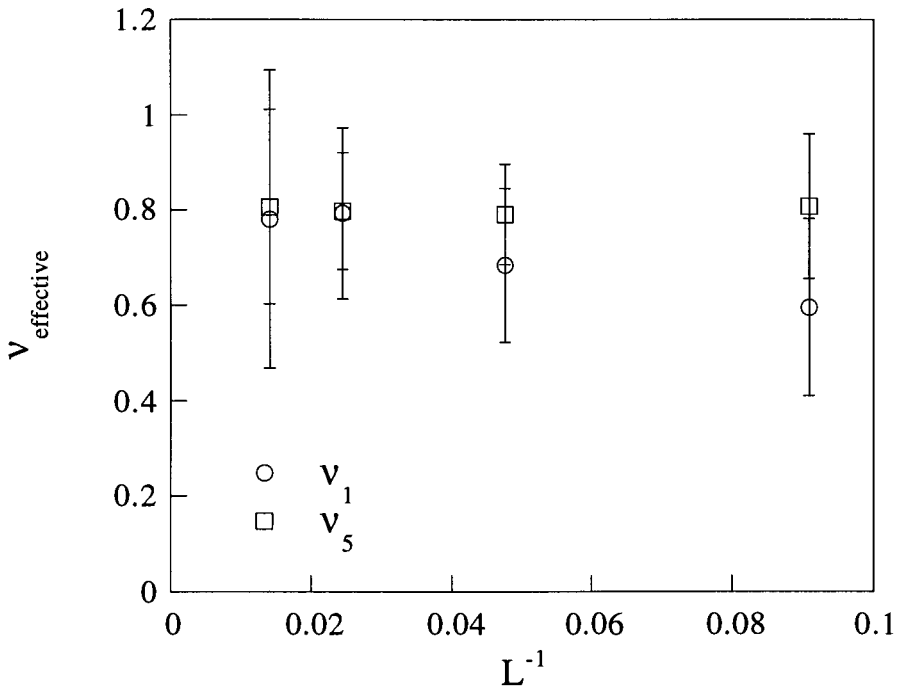

Figure 2.5: The effective exponents of the smallest and largest eigenvalues for $\sigma/\sigma_0 = 1.0$ in $d = 5$. The remaining exponents are not shown, for clarity.

that indicate $\nu \approx 0.8$.

σ/σ_0	$2\nu_1$	$2\nu_2$	$2\nu_3$	$2\nu_4$	$2\nu_5$
0.4	1.4 ± 0.1	1.4 ± 0.1	1.5 ± 0.1	1.5 ± 0.1	1.5 ± 0.1
0.6	1.4 ± 0.1	1.4 ± 0.1	1.4 ± 0.1	1.5 ± 0.1	1.5 ± 0.1
0.8	1.4 ± 0.1	1.4 ± 0.1	1.5 ± 0.1	1.5 ± 0.1	1.6 ± 0.1
1.0	1.5 ± 0.1	1.5 ± 0.1	1.6 ± 0.1	1.6 ± 0.2	1.6 ± 0.1
1.2	1.4 ± 0.1	1.6 ± 0.1	1.7 ± 0.1	1.6 ± 0.1	1.6 ± 0.2
1.3	1.4 ± 0.1	1.5 ± 0.1	1.6 ± 0.1	1.7 ± 0.2	1.7 ± 0.2

Table 2.1: 2ν and σ/σ_0 for membranes in $d = 5$.

2.4 Four Dimensions

Two previous studies [10, 24] of membranes embedded in $d = 4$ have indicated that membranes are flat. Both studies used parameters that might lead to fairly stiff membranes and, hence, favour the flat phase. We simulated fully self-avoiding membranes with a range of particle sizes so as to examine the effects of variable stiffness on the membranes. The model and methods of equilibration and analysis of the eigenvalues are the same as described in the previous two sections. The parameters used in equations (2.17), (2.18) were: $R_0/\sigma_0 = 4.0$, $k/\epsilon = 4.0$ and $\sigma/\sigma_0 = 0.1, 0.2, 1.0$. Both the parameters of the potential and the range of particle sizes lead to a much more flexible membrane than ones previously studied [24]. The sizes of the longest diameter of the membrane were $L = 7, 11, 21, 41, 71$.

For $\sigma/\sigma_0 = 0.2$ a plot of the eigenvalues as a function of membrane size is shown in Fig. 2.6. Despite some curvature for small size, the plot shows that the two smallest and the two largest eigenvalues increase at different rates. The difference in scaling exponents indicates that the membrane is not isotropically crumpled but rather is flat. A similar plot for $\sigma/\sigma_0 = 1.0$ is shown in Fig. 2.7. Again, there is curvature in the data but $\nu_{3,4} = 0.98 \pm 0.05$ and $\nu_{1,2} = 0.81 \pm 0.05$ provide reasonable fits, especially for large L.

The curvature is emphasized by examining the effective exponents, Fig. 2.8. This plot clearly shows the change in exponents with system size. As well, it indicates that extracting the scaling exponents by merely doing a linear regression of $\ln(\lambda_i)$ and $\ln(L)$ may not give the correct values for the exponents. Since the regression treats all point equally, it would

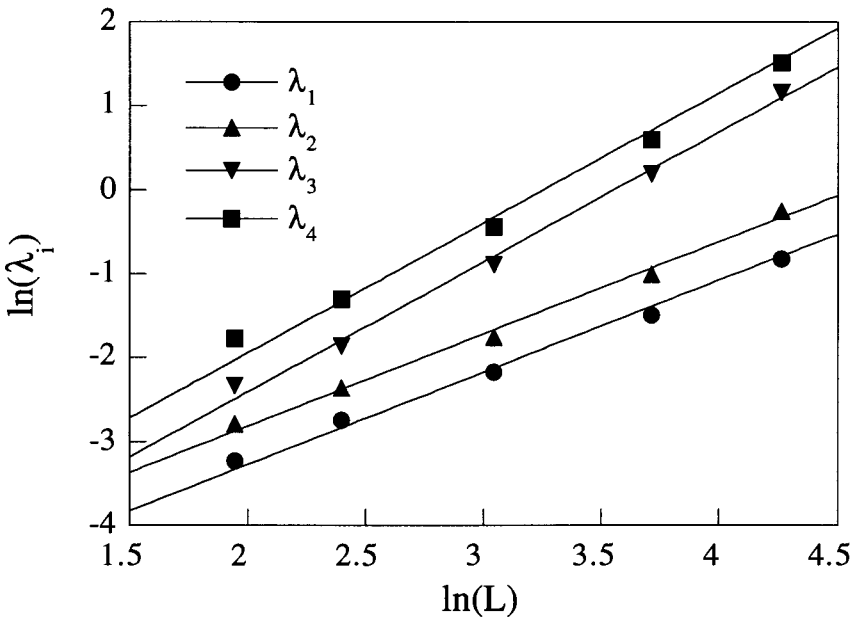

Figure 2.6: The eigenvalues of the moment of inertia tensor as a function of L for $\sigma/\sigma_0 = 0.2$ in $d = 4$. The eigenvalues are fit to the lines $\lambda_{1,2} \sim L^{1.1}$, $\lambda_{3,4} \sim L^{1.6}$. The error bars are not shown but are smaller than the symbol size.

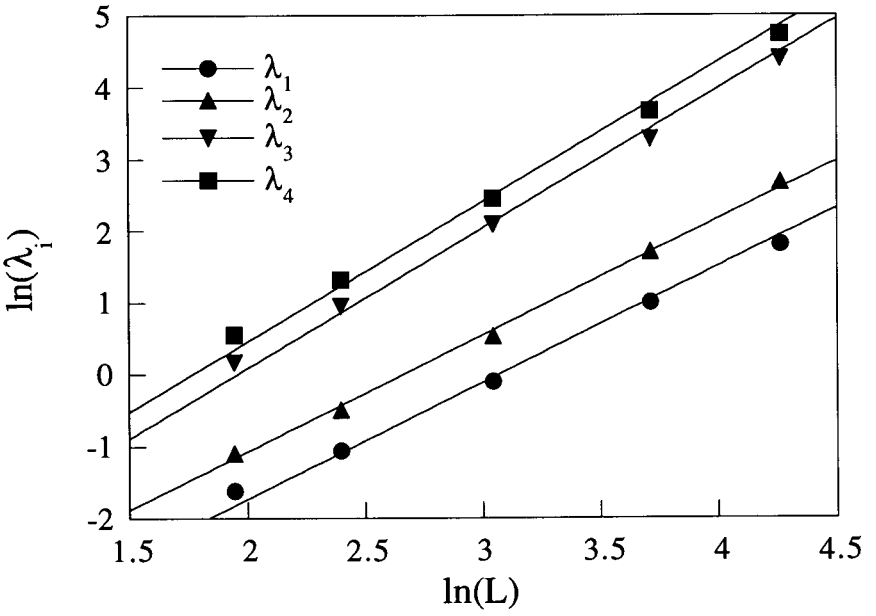

Figure 2.7: Eigenvalues of the moment of inertia tensor as a function L for $\sigma/\sigma_0 = 1.0$ in $d = 4$. As before, the error bars are smaller than the symbol size. The eigenvalues are fit to the lines $\lambda_{1,2} \sim L^{1.62}$, $\lambda_{3,4} \sim L^{1.95}$.

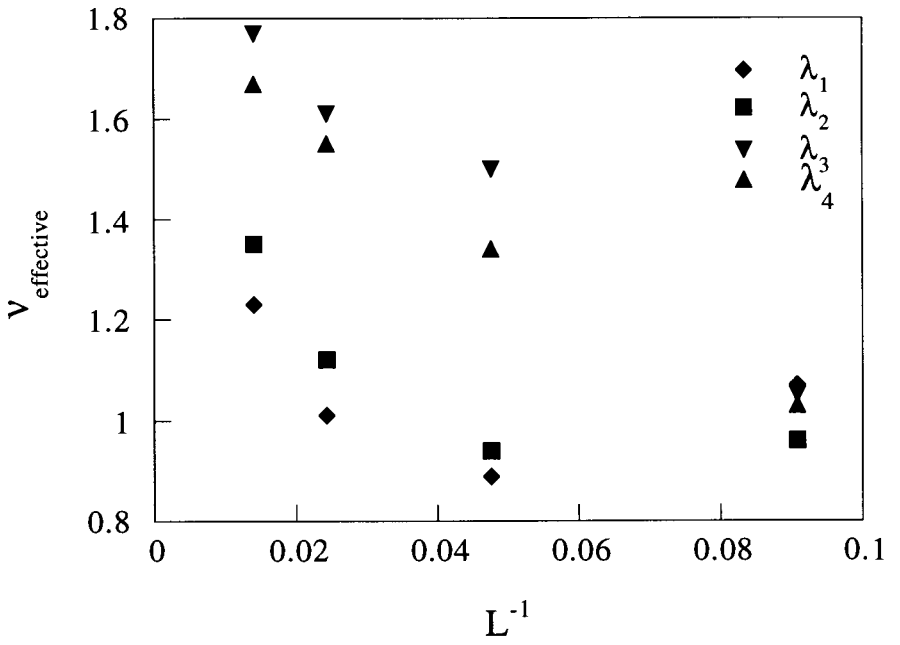

Figure 2.8: Effective exponents for $\sigma/\sigma_0 = 0.2$ in $d = 4$. The exponents are in two different groups. The extrapolated limits are $2\nu_{1,2} = 1.6 \pm 0.1$, $2\nu_{3,4} = 1.9 \pm 0.1$

be biased by the smaller system sizes, which are more sensitive to finite size effects. In contrast to what happens in $d = 5$, the larger and smaller effective exponents extrapolate to different limits, which suggests that the membrane is in a flat state.

Further evidence that the membrane is flat is obtained by examining the anisotropy parameter A_1 in Fig. 2.9. Except for the smallest system there is a clear decrease of A_1 with system size. This again suggests that the largest eigenvalue is increasing at a much faster rate than the smallest one, supporting the conclusion that the membrane is flat.

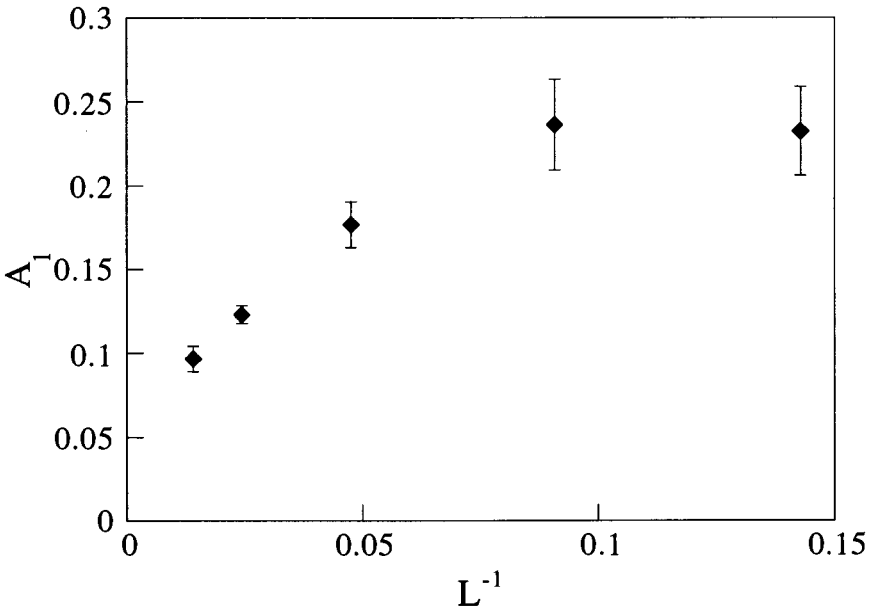

Figure 2.9: Anisotropy of the membrane in $d = 4$ for $\sigma/\sigma_0 = 0.2$. There is a clear decrease of A_1 with system size, except for the smallest system $L = 7$. This is indicative of a flat membrane.

The data for the scaling exponents are summarized in Table 2.2 for the particle diameters studied. All the data indicate that the membrane embedded in $d = 4$ is flat even for very small particle diameter. The largest two scaling exponents are clearly different from the smallest two, even for a small value of the particle diameter, and this is characteristic of the

flat phase. This suggests that a bending rigidity proportional to the amount of excluded volume is not responsible for the flat phase but that a non-phantom membrane is always flat in $d = 4$. As mentioned at the beginning of this section, two previous studies done on membranes embedded in $d = 4$ found that such membranes were flat. These results are in agreement with a more recent theoretical prediction [22] that membranes remain flat for $d \leq 4$.

σ/σ_0	$2\nu_1$	$2\nu_2$	$2\nu_3$	$2\nu_4$
0.1	1.1 ± 0.1	1.1 ± 0.1	1.8 ± 0.1	1.8 ± 0.1
0.2	1.6 ± 0.1	1.6 ± 0.1	1.9 ± 0.1	1.9 ± 0.1
1.0	1.65 ± 0.1	1.65 ± 0.1	1.95 ± 0.1	1.95 ± 0.1

Table 2.2: The scaling exponents 2ν for the different particle sizes σ/σ_0 studied in $d = 4$.

Although the three cases of particle size studied lead to asymptotically flat membranes, this does not mean that particle size has no effect on the calculation of the scaling exponents for finite membranes. As can be seen from a comparison of Figs. 2.6 and 2.7, the simulations with the value of $\sigma/\sigma_0 = 1.0$ attain the thermodynamic value of the scaling exponent at a smaller membrane size L than those of $\sigma/\sigma_0 = 0.2$. The observation that the particle diameter had a role to play in the simulations provided the motivation to conduct a study of how the size of the particle and the degree of self-avoidance affect the phase of the membrane. To this end we adapted a method introduced by Kantor and Kremer [17] where the self-avoidance is limited to a fixed distance about each particle. They used this method of limited self-avoidance to estimate the size of particle necessary for a transition to an apparent crumpled phase in $d = 3$. This method and the results of simulations done in $d = 4$ are reported in this section.

As mentioned above, this model restricts the self-avoidance experienced by any given particle i. When a hexagonal membrane is stretched the six nearest neighbours of any given particle are a fixed distance away. One can characterize the nearest neighbours by this distance, or by the number of particles enclosed in the hexagon bounded by these six neighbours[1], which is $n_{sa} = 7$. Similarly the 6 next-nearest-neighbours can be characterized by their distance away from the central particle, or by the $n_{sa} = 13$ particles enclosed in

[1]Note that the degree of self-avoidance n_{sa} is denoted by n in ref.[17].

the shape bounded by the next-nearest neighbours, Fig. 2.10. Then, for each particle i the repulsive interaction is restricted to a neighbourhood about i characterized by n_{sa}. In the thermodynamic limit any membrane would behave as a phantom membrane for fixed n_{sa}. The goal of this analysis is to examine how the size of the particle σ and the strength of the purely local repulsive interaction characterized by n_{sa} determine the point at which crossover to the large L limit sets in. In particular, it is known that for $\sigma = 0$ or equivalently $n = 1$ the membrane behaves as a phantom, that is, $R_g \sim \sqrt{\ln(L)}$. Conversely, for a fully self-avoiding membrane and a relatively large value of σ all the simulation evidence indicates that the membrane is flat $R_g \sim L$.

The parameter values in equations (2.17) and (2.18) were: $\sigma/\sigma_0 = 0.1, 1.0, 2.0, 3.0$, $k/\epsilon = 4$ and $R_0/\sigma_0 = 4$. The range of self-avoidance measured by n_{sa} is $7 \leq n_{sa} \leq 91$. The linear sizes of the membranes were $L = 7, 11, 21, 41$. The equilibration and determination of the eigenvalues and scaling exponents were the same as described in previous sections.

For each value of σ/σ_0 the membranes behaved as phantom membranes for small n_{sa} and as flat membranes for large n_{sa}, Fig. 2.11. For intermediate values of n_{sa} the largest two scaling exponents $\nu_{3,4} < 1$, but they were clearly different from the smallest exponents and increased with increasing n_{sa}. For a given value of σ/σ_0 and size L, R_g increased with increasing n_{sa}. In order to obtain a relationship between σ/σ_0, n and the crossover point a critical diameter $\sigma_c(n_{sa}(c))$ was defined. In our analysis $\sigma_c(n_{sa}(c))$ is the value of σ and n_{sa} such that for $n_{sa} < n_{sa}(c)$ the membrane is phantom in the sense that $R_g < L^{0.5}$, and for $n_{sa} > n_{sa}(c)$ $R_g \sim L^{\nu}$, with $\nu > 0.5$. This criterion does not distinguish an isotropically crumpled phase from a flat phase. A plot $\sigma_c(n_{sa})$ versus n_{sa} is shown in Fig. 2.12. This plot shows that as n_{sa} increases the value of σ/σ_0 needed to make the membrane phantom decreases. One cannot draw any firm conclusion from this analysis, other than that the rate of decrease of σ/σ_0 is rapid, and an extrapolated limit of $\sigma/\sigma_0 \approx 0$ for $n_{sa} \to \infty$, indicating that the membrane may be flat for any non-zero value of σ/σ_0. As well, it should be noted that, for intermediate values of n_{sa}, no isotropically crumpled phase was found: As the value of n_{sa} was increased the membrane changed from a phantom-crumpled phase to a phase where $\nu_{3,4} > \nu_{1,2}$. There was no range of n_{sa} for which the four scaling exponents were equal. This data seems to suggest that there is no isotropically crumpled phase in $d = 4$ even for small but finite particle size.

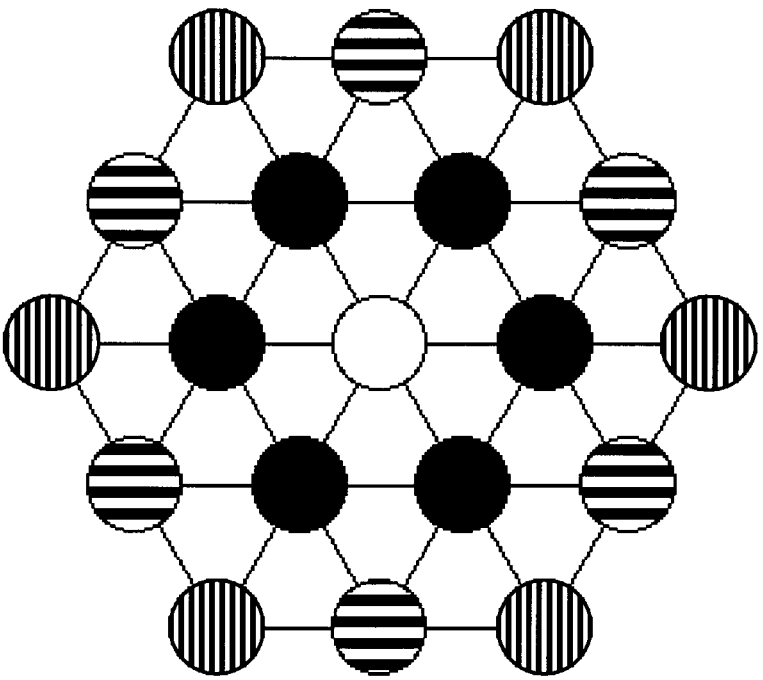

Figure 2.10: For the central particle, the solid particles are nearest neighbours $n_{sa} = 7$, the horizontally striped particles next-nearest-neighbhours $n_{sa} = 13$, and the vertically striped particles are the third nearest neighbours $n_{sa} = 19$.

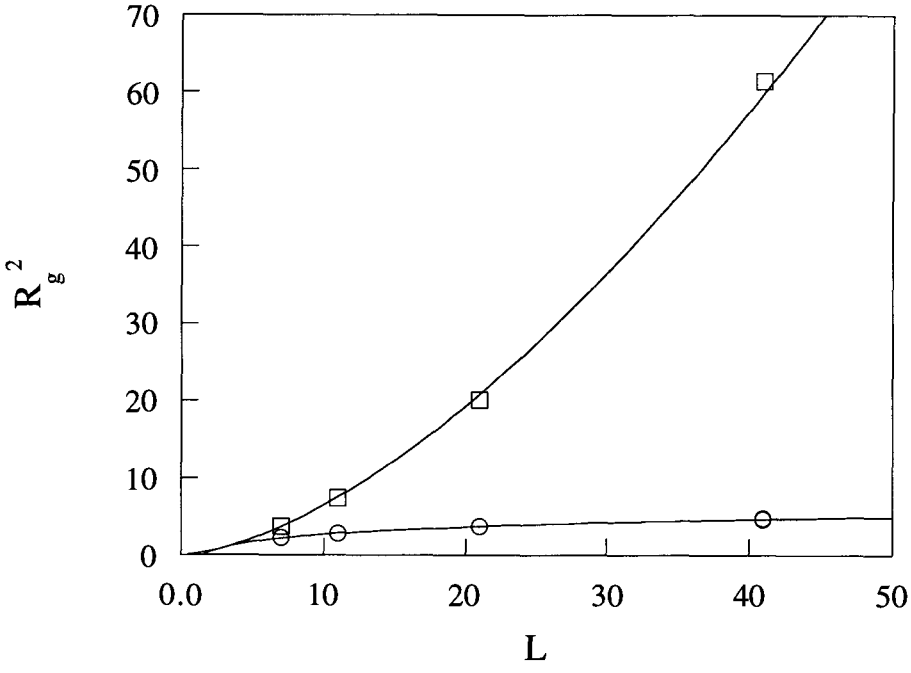

Figure 2.11: Variation of R_g^2 with the degree of self-avoidance n_{sa}. The upper plot shows the typical behaviour of the membrane with $n_{sa} = 91$, the curve is a power-law with scaling exponent $\nu = 0.8$. The lower curve is typical of phantom membranes: $R_g^2 \sim \ln(L)$, $n_{sa} = 13$. Both curves are for $\sigma/\sigma_0 = 1$.

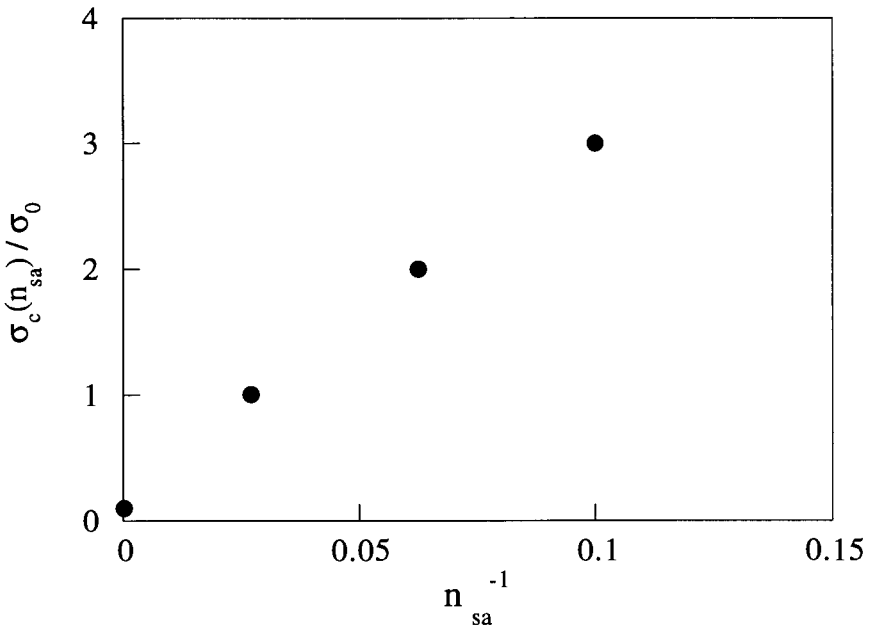

Figure 2.12: The variation of σ_c/σ_0 with n_{sa}.

2.5 Conclusions

Extensive molecular dynamics simulations on tethered membranes in $d = 4$ and $d = 5$ have been done [30]. In $d = 5$ it was found that regardless of the size of the monomer the membrane is always crumpled with $R_g \sim L^{\nu}$, with $\nu = 0.80 \pm 0.05$. There was no evidence to suggest that the membranes would be flat, even for very large hard-core repulsion.

In $d = 4$ a study was done on the relationship between the degree of self-avoidance, the size of the monomer, and the thermodynamic phase. For the sizes of monomer studied, the membrane was always flat with a large degree of self-avoidance, $R_g \sim L$. For a membrane with only partial self-avoidance, a parameter that determines the crossover from phantom to flat behaviour was calculated. Extrapolating to the thermodynamic limit indicates that all membranes in $d = 4$ will be flat, regardless of the size of hard-core repulsion. Both the four- and five-dimensional results are consistent with the predictions of recent analytical work [22, 23].

Chapter 3

Theory of Polymer Networks

3.1 Introduction

The vulcanization of rubber is a transition from a liquid to a solid of a dense melt of linear polymers. It occurs when chemical bonds which create links between monomers that were not previously attached to one another are added to the melt. The bonds or crosslinks are generally created by the addition of chemical agents, typically sulphur, or by using ionizing radiation to, for example, a melt of polyisoprene. In either case the effect is to link two randomly chosen monomers in a permanent way. This means that there is no restriction placed on whether the monomers belong to different polymers. The crosslinks are not truly permanent but the bonds are usually as strong as the intrapolymer bonds that link one monomer to the next along the polymer and are not broken by thermal fluctuations. The crosslinks have the same effect as the intrapolymer bonds in that crosslinked monomers are constrained to be close to each other, although the pair can move about in the system.

The addition of a small number of crosslinks to a melt of polymers creates clusters of different sizes but does not solidify the system. The system as a whole still behaves as a liquid with finite viscosity and no shear modulus. As more crosslinks are added the clusters become larger and eventually most polymers are connected to one large cluster. At this extreme the system acts like a solid with an infinite viscosity and a finite shear modulus. This transition as a function of the number of crosslinks occurs even if not all polymers are attached to the large cluster.

The rest of this chapter is as follows: I will review the classical theory of vulcanization in the next section. Then I will discuss a new theory of vulcanization incorporating replica

methods.

3.2 Classical Theory

The classical theory of vulcanization [31] is based on a 'tree' approximation, Fig. 3.1. Each monomer is assumed to have the same number of potential links z_t. Closed loops are not allowed to form, only new branches can emanate from the tree. The branches occur freely, never limited in their growth by the presence of other branches, which means that excluded volume effects are ignored. This model is precisely percolation on a Bethe lattice and is at the level of a mean field theory. An important assumption in this theory is that percolation coincides with the acquisition of a non-zero shear modulus or rigidity. Thus, to find when the liquid-solid transition occurs as a function of the number of crosslinks, it suffices to find when the system percolates.

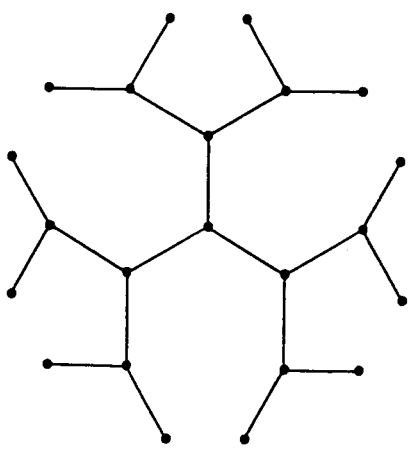

Figure 3.1: The tree approximation where each monomer has $z_t = 3$ neighbours.

Each vertex on the tree is occupied by a monomer, but the bonds between neighbouring monomers are formed with a probability p. For small p there are a large number of small clusters, but for large enough p there will be a single cluster spanning the entire network

and a few unconnected small clusters. This value is known as the percolation probability p_c, and as stated above it is assumed that solidification coincides with p_c.

The derivation of the percolation probability follows that of Essam [32]. To find p_c we assume that neighbouring monomers in the tree are linked with probability p. The probability of no bond is $1-p$. The probability that a walk from a chosen vertex is infinite is $\tilde{P}$, and the probability that the walk from a chosen vertex is finite is $\mathcal{P} = 1 - \tilde{P}$. The probability that the walk in a given direction is finite is denoted by $\mathcal{Q}$. It is evident that $\mathcal{P} = \mathcal{Q}^{z_t}$ and thus $\tilde{P} = 1 - \mathcal{Q}^{z_t}$. Therefore $\mathcal{Q}$ satisfies the following equation

$$\mathcal{Q} = 1 - p + p\mathcal{Q}^{z_t - 1}. \tag{3.1}$$

This recurrence relationship is straightforward: starting from a particular monomer either there is no bond with the next monomer in a given direction with probability $1-p$, or there is a bond with probability p but the walk terminates with probability $\mathcal{Q}^{z_t-1}$. This equation always has the solution $\mathcal{Q} = 1$ which corresponds to no spanning cluster, which is true for small p. As p becomes large another solution emerges continuously from $\mathcal{Q} = 1$. In general there are $z_t - 1$ solutions to this equation but the one describing the infinite cluster is the one that emerges continuously from $\mathcal{Q} = 1$.

To solve (3.1) the equation is rewritten as $A = 1 - p + p\mathcal{Q}^{z_t-1} - \mathcal{Q}$. The implicit function theorem [33] can now be applied. It states that if $\partial A/\partial \mathcal{Q} \neq 0$ at a point $(\mathcal{Q}_0, p_0)$ then there is a unique solution for $\mathcal{Q}(p)$. Since we are looking for a second solution we set $\partial A/\partial \mathcal{Q} = 0$.

$$\begin{aligned} \partial A/\partial \mathcal{Q} = \quad 0 \quad &= p\,(z_t - 1)\,\mathcal{Q}^{z_t-2} - 1 \\ &= p_c\,(z_t - 1) - 1 \end{aligned}$$

and $p_c = 1/(z_t - 1)$ where $\mathcal{Q} = 1$. To examine the behaviour just above the critical point $p > p_c$, we can do a Taylor expansion of A around $\mathcal{Q} = 1$. Keeping only the first two terms, we get

$$\mathcal{Q} = 1 - \frac{2(1 - p_c/p)}{z_t - 2}. \tag{3.2}$$

Then the probability of an infinite walk is

$$\begin{aligned} \tilde{P} &= 1 - \mathcal{Q}_t^z \\ &= 1 - [1 - \frac{2(1 - p_c/p)}{z_t - 2}]^{z_t} \end{aligned}$$

$$= z_t \frac{2(1-p_c/p)}{z_t - 2}$$
$$\approx (1-p_c/p).$$

Thus $\tilde{P}$ increases linearly with p_c/p near the transition, so $P \sim (1-p_c/p)^1$. Other critical exponents are [31]: the 'gel' fraction i.e., the fraction of monomers belonging to the infinite cluster $S \sim (1-p_c/p)^1$; the correlation length $\tilde{\xi} \sim (1-p_c/p)^{-1/2}$; the shear modulus $E \sim (1-p_c/p)^3$. An important aspect of this theory is that the number of potential neighbours z_t increases with the length of the polymer.

Although these results are based on mean field theory, deGennes [34] argued that the classical exponents should be valid everywhere except in a narrow range around p_c. For a value of p is just above threshold $p > p_c$, he examined the fluctuations of the gel fraction δS in a volume of size $\tilde{\xi}^3$, which is large compared to the size of a monomer. In this volume there are a total of S_T monomers, where $S_T = c\tilde{\xi}^3$ and c is the concentration. Of this total, the number of monomers belonging to the infinite cluster (gel fraction) is S_G, and the remainder S_F belong to finite-sized clusters. In terms of the gel fraction S, the number of monomers in the gel fraction can be written $S_F = S \cdot S_T$. The fluctuation of the total number of monomers in this volume is negligible, and so the fluctuations of the number of monomers in the infinite and finite clusters are related by $\delta S_G + \delta S_F = 0$. If the S_F are found in clusters of average size Z_c, then we use a Ginzburg criterion to estimate the fluctuations of S_F and find $(\delta S_F)^2 \sim S_F Z_c$. Since the percolation probability is just above the critical value, very few of the monomers in the volume belong to the infinite cluster, and $S_F \approx S_T$. The relative importance of the fluctuations of the infinite cluster is denoted X and is defined as

$$X = \frac{(\delta S_G)^2}{S_G^2} = \frac{(\delta S_F)^2}{S_G^2} = \frac{S_T Z_c}{S_G^2} = \frac{Z_c}{S^2 c\tilde{\xi}^3}. \tag{3.4}$$

Using the classical values of the scaling exponents, deGennes found that $X \sim M^{-1/2}(p_c/(p-p_c))^{3/2}$, where M is the length of the polymer. For small X the fluctuations are small and so the classical exponents are valid. The classical exponents no longer apply when X is large which occurs when $p - p_c \sim p_c M^{-1/3}$. For example, if the system is composed of polymers of size $M = 1000$ units, the classical exponents are valid everywhere except when $p \sim 1.1p_c$.

The shear modulus E is not proportional to the gel fraction, because the gel fraction includes many dangling ends, which do not contribute to the shear modulus. If the dangling ends are removed from the system the remaining chains are said to be elastically active, because they form the backbone of the spanning cluster and are thought to give rise to the

shear modulus. De Gennes [35] argued that the conduction of random resistors is analogous to the elasticity and, by using this analogy he derived the scaling law for the shear modulus. He based his calculation on the number of active network chains per monomer and derived the elasticity as a function of this number. This yields the result $E \sim (p - p_t)^{\beta_t}$ with $\beta_t = 1.7$, a number that is known from computer simulations of random resistor networks, and p_t denotes the critical probability for rigidity. As pointed out by Feng and Sen [36], DeGennes' argument strictly holds only if the potential between the neighbours on a lattice is "separable", for example, a Hookean spring $U(r_{ij}) = 1/2\kappa(\mathbf{r}_i - \mathbf{r}_j)^2$. For more general central force fields it is not possible to map the force balance equations onto Kirchoffs laws for circuits. Besides calling into question the connection between the exponents of the resistor network and the rigidity, Feng and Sen also raised the issue of whether or not rigidity sets in at the percolation threshold. Indeed, computer simulations indicate that in general rigidity does not set in at the percolation concentration but rather at a separate, larger rigidity percolation concentration for both triangular and fcc lattices with central forces between the particles [36, 37, 38]. An explanation for this is that although a single line of connected bonds can carry all the current in the random resistor, more connections need to be made for rigidity to occur.

Although the tree theory provides a good starting point for an understanding of the vulcanization transition, it is not descriptive of the experimental process. The simplifying assumptions of no loops and no self-avoidance are unrealistic. Finally, it is not a theory that lends itself to calculating a partition function or thermal averages.

3.3 Replica Theory of Vulcanization

Building on the work of Deam and Edwards [40], Goldbart *et al.* [39] have devised a mean field theory of vulcanization from microscopic principles. In their theory, as the density n of crosslinks in a melt of polymers is increased beyond some critical density n_c, there is a second-order transition from a liquid to an amorphous solid. This theory merges the spin-glass techniques of Edwards and Anderson with the polymer theory of Deam and Edwards. It attempts to reproduce the experimental situation more accurately than the classical theory. In the liquid state all the monomers may explore any position in the system, whereas in the amorphous solid state it is expected that a non-zero fraction of the monomers are localized about positions that are randomly distributed in the volume occupied by the solid. The

fraction of localized monomers depends on the number of crosslinks.

The crosslinks act as quenched random variables, analogous to the random exchange interactions of spin glasses. That they are quenched variables means that the system cannot change the monomers chosen for the crosslinks or the polymers they link in order to reduce the free energy. The set of pairs of linked monomers alone is not sufficient to describe the new state of the system. Polymers are not able to pass through each other and so merely listing the linked monomers does not completely characterize the topology. Fig. 3.2 illustrates this: the monomers linked in (a) and (b) are identical, yet the resulting topology is quite different. Not only do the crosslinks restrict the phase space available to the system, but so does the particular topology. There can be two systems of identical crosslinks, but different topologies that are mutually inaccessible in phase space. The complications due to the different topologies will not be dealt with in the analytic theory as there is at present no means to incorporate this into the semi-microscopic treatment presented here. An inherent feature of the incorporation of crosslinks is broken ergodicity. Different sets of crosslinks restrict the evolution of the system in configuration space. The configuration space that is accessible to the system as a liquid is broken into disjoint regions once the crosslinks are imposed.

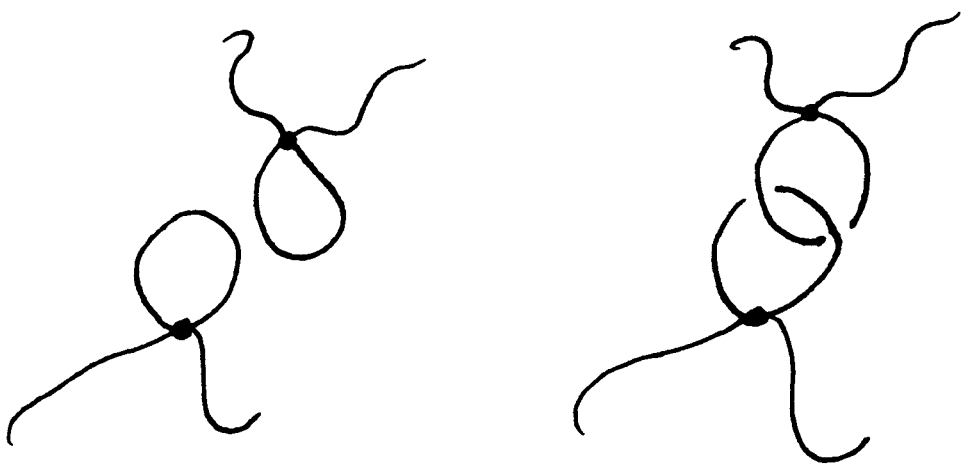

Figure 3.2: As this picture shows, merely knowing the position of the links isn't sufficient to determine the topology of the system.

The aim of this section is to give an overview of the methods that Goldbart *et al* used in their calculations. Details of the calculations and the work which do not directly relate to the simulations discussed in the next chapter are not included. The order parameter that distinguishes liquid from solid, the fraction of localized monomers, and the distribution of localization lengths in the solid state are the main points of interest.

The general scheme of the method used by Goldbart *et al.* is as follows. Initially a Hamiltonian that describes the polymer melt is defined. This Hamiltonian is used to construct the partition function of the crosslinked system. The partition function is used in turn to define the probability of a particular realization of crosslinks. Before the statistical mechanics is tackled, an order parameter is defined. This order parameter is capable of distinguishing three different states: liquid, crystalline and amorphous solid. It is a straightforward quantity depending only on how the monomers are localized. A more detailed order parameter can be defined which utilizes only the fraction of localized monomers and the distribution of localization lengths. The statistical mechanics focuses mainly on calculating the free energy. Firstly the quenched random variables are eliminated using the replica method. The price for this elimination is the introduction of an effective coupling between the replicated polymers. The replicated polymers are treated in a field-theoretic description by the introduction of stochastic fields. The polymers interact indirectly at this point - only through the fields. The average of the free energy is approximated in a mean-field way using the saddle point method. Within this approximation the free energy is found to have only a single solution below a critical density of crosslinks. This describes the liquid state. At the critical density of crosslinks a second solution continuously emerges - that of amorphous solid. The probability distribution of localization lengths is found within this saddle point approximation.

Model

The model of the polymer melt consists of N identical polymers in a cubical volume V. Each of the polymers is characterized by a length L_p and persistence length l, so that the effective number of independent segments on each polymer is $L_p/l \gg 1$. A version of the Edward's Hamiltonian is used to describe this melt:

$$H_1^E = \frac{1}{2}\sum_{i=1}^{N}\int_0^{L_p}\frac{dx}{l}\left|\frac{d}{dx}\mathbf{R}_i(x)\right|^2 + \frac{v}{2}\sum_{i,i'=1}^{N}\int_0^{L_p}\frac{dx}{l}\int_0^{L_p}\frac{dx'}{l}\delta[\mathbf{R}_i(x)-\mathbf{R}_{i'}(x')]. \qquad (3.5)$$

In this equation x labels the distance of a monomer from one end of the polymer, $\mathbf{R}_i(x) = \mathbf{R}_i$ is the position of the monomer at x of polymer i in d-dimensional space. v is the excluded

volume parameter and i, i' are polymer labels. The δ-function in the excluded volume part is understood to be a d-dimensional δ-function. Using this Hamiltonian, expectation values are defined in the usual way,

$$\langle A \rangle = \frac{\int d\mathbf{R}\, e^{-\beta H_1^E} A}{\int d\mathbf{R}\, e^{-\beta H_1^E}}, \tag{3.6}$$

where A is an arbitrary function.

If M crosslinks are simultaneously and instantaneously imposed, the partition function of that crosslinked system relative to that of the melt is

$$Z = \langle \prod_{e=1}^{M} \delta(\mathbf{R}_{ie}(x) - \mathbf{R}_{i'e}(x')) \rangle. \tag{3.7}$$

The δ-function implements the crosslinks: the e-crosslink constrains monomer x of polymer i to be at the same place as monomer x' of polymer i'. Defining the partition function relative to that of the melt means that the free energy calculated from this partition function is the increase of free energy due to the crosslinks. This partition function, as defined, is not the true partition function. In the melt there are N indistinguishable polymers, leading to a factor of $N!$ in the partition function describing the melt. This is no longer true once the crosslinks are imposed. The numerical factor required for the crosslinked system involves the product of the factorials of the number of all the segments of identical chain length. Since the difference between (3.7) and the true partition function is merely a numerical factor it only adds a constant to the calculation of the free energy and is not relevant to the ideas presented below.

The partition function is defined for one particular realization of crosslinks. It is of greater interest to develop a method that predicts typical properties of vulcanized systems, instead of the properties of one given crosslink distribution. To do this a probability distribution that assigns a sensible statistical weight to each possible realization of M is required. This distribution of crosslinks is due to Deam and Edwards [40],

$$P_M = \frac{(\mu^2 V/2N)^M Z}{M! < \exp(\frac{\mu^2 V}{2N} \sum_{i,i'=1}^{N} \int_0^{L_p} \frac{dx}{l} \int_0^{L_p} \frac{dx'}{l} \delta[\mathbf{R}_i(x) - \mathbf{R}_{i'}(x')]) >}, \tag{3.8}$$

where μ^2 is a parameter that controls the crosslink density. The average density of crosslinks M/N is a smooth, increasing function of $\mu^2[M/N]$. In principle it is possible to calculate μ^2 from this equation, but it is sufficient to know that μ^2 is a monotonically increasing function of M/N. It is important to note that the probability distribution for the crosslinks M is

itself dependent upon the partition function and hence the polymer melt so the correlations of this probability distribution incorporate the correlations of the melt itself. In particular, different realizations of crosslinks only acquire an appreciable statistical weight if they are compatible with a reasonably probable configuration of the liquid.

Order Parameter

For a specific crosslink realization one can define the quantity,

$$q = \frac{1}{N}\sum_{j=1}^{N}\int_0^{L_p}\frac{dx}{l}\langle\, e^{i\mathbf{k}_1\cdot\mathbf{R}_j(x)}\rangle\ \langle\, e^{i\mathbf{k}_2\cdot\mathbf{R}_j(x)}\rangle, \tag{3.9}$$

where $\mathbf{k}_{1,2}$ are non-zero $\mathbf{k}$-space vectors and $< e^{i\mathbf{k}\cdot\mathbf{R}_j(x)} >$ is the Fourier transform of the static density $< \delta(\mathbf{r}-\mathbf{R}_j(x)) >$. Furthermore, if a given monomer is localized near a position $\mathbf{b}_j$, then

$$\langle\, e^{i\mathbf{k}\cdot\mathbf{R}_j(x)}\rangle\ = e^{i\mathbf{k}\cdot\mathbf{b}_j}\rho(k), \tag{3.10}$$

where $\rho(k)$ is the Fourier transform of the density profile of a monomer localized near the origin. To see that this order parameter distinguishes liquid, amorphous and crystalline solid, we examine how the order parameter behaves in the different cases.

For a liquid no monomer is localized about a particular position in the system. That is, each monomer is free to explore the entire configuration space so that each monomer is localized, but only within the volume of the system. The density is

$$\langle\, \delta(\mathbf{r}-\mathbf{R}_j(x))\rangle\ \sim \frac{1}{V}. \tag{3.11}$$

The only term that survives in the Fourier transform is the $\mathbf{k}=\mathbf{0}$ term, and

$$q \sim \delta_{\mathbf{k}_1,\mathbf{0}}\ \delta_{\mathbf{k}_2,\mathbf{0}}. \tag{3.12}$$

Therefore, for a liquid $q=0$, unless both $\mathbf{k_1}$ and $\mathbf{k_2}$ are zero. For a solid

$$q = \frac{1}{N}\sum_{j=1}^{N}\int_0^{L_p}\frac{dx}{l}\, e^{i(\mathbf{k}_1+\mathbf{k}_2)\cdot\mathbf{b}_j}\,\rho(k_1)\rho(k_2). \tag{3.13}$$

In a crystal the mean positions of the particles $\mathbf{b}_j$ are periodically spaced and q is non-zero when $\mathbf{k}_1+\mathbf{k}_2 \in \mathbf{G}$, where $\mathbf{G}$ is the reciprocal lattice. For an amorphous solid, where the particles are localized but their positions are randomly distributed through the system the order parameter is non-zero only when $\mathbf{k}_1+\mathbf{k}_2=\mathbf{0}$. Even if not all the particles are localized, this is an effective order parameter: In that case the only non-zero contributions

come from the localized particles; the delocalized particles contribute nothing to the sum. Thus, knowing for which values of $\mathbf{k}$ q is non-zero, we can distinguish between liquid, crystal and amorphous solid.

A more sophisticated measure of the degree of localization is found, if we assume that Q monomers are localized about their mean positions and $(1-Q)$ monomers are delocalized. Furthermore, we assume that each localized monomer is characterized by a Gaussian distribution about its mean position. In this case the localization length ξ is easily defined. The square of the localization length is $\xi^2 = \xi_x^2 + \xi_y^2 + \xi_z^2$, where ξ_x^2 is the variance of the distribution of positions in the x direction. The inverse of the square of the localization length[1] is $\zeta = 1/\xi^2$. The order parameter can be written

$$\begin{aligned} q' &= (1-Q)\delta_{\mathbf{k}_1,0}\delta_{\mathbf{k}_2,0} + Q\delta_{\mathbf{k}_1+\mathbf{k}_2,0}\int_0^\infty d\frac{1}{\xi^2}\,P\left(\frac{1}{\xi^2}\right)e^{-\frac{(k_1^2+k_2^2)\xi^2}{2}} \\ &= (1-Q)\delta_{\mathbf{k}_1,0}\delta_{\mathbf{k}_2,0} + Q\delta_{\mathbf{k}_1+\mathbf{k}_2,0}\int_0^\infty d\zeta\,P(\zeta)\,e^{-\frac{(k_1^2+k_2^2)}{2\zeta}} \end{aligned} \tag{3.14}$$

where $P(\zeta)$ is the distribution of inverse-square localization lengths. Note that this distribution explicitly excludes all delocalized monomers.

Free Energy

The evaluation of the free energy proceeds in a manner similar to that for spin-glasses. The probability distribution (3.8) is summed over the quenched random variables to give the total free energy. If f is the free energy, then

$$f = \sum_M P_M f(M) = -\sum_M P_M \ln(Z(M)), \tag{3.15}$$

where $f(M)$ is the free energy and $Z(M)$, the partition function of a system with M crosslinks. To evaluate this we use the standard replica trick: $\ln(Z) = \lim_{n\to 0}(Z^n - 1)/n$. We will concentrate on the factor $\sum_M P_M Z^n$. Then

$$\sum_M P_M Z^n = \sum_M \frac{(\mu^2 V/2N)^M Z^{n+1}}{M! < \exp(\sum_{i,i'=1}^N \int_0^{L_p}\frac{dx}{l}\int_0^{L_p}\frac{dx'}{l}\,\delta[\mathbf{R}_i(x) - \mathbf{R}_{i'}(x')]) >}. \tag{3.16}$$

Using dimensionless variables, $s = x/l$ and $\mathbf{c} = \mathbf{R}/\sqrt{lL_p}$, and suppressing the arguments of $\mathbf{c}_i(s) = \mathbf{c}_i$ and $\mathbf{c}_{i'}(s) = \mathbf{c}_{i'}$, the $n+1$ factors of Z can written as:

$$Z^{n+1} = \langle \prod_{e=1}^{M} \delta[\mathbf{c}_{ie} - \mathbf{c}_{i'e}]\rangle^{n+1}$$

[1]Note that the inverse square localization length ζ is denoted by τ in ref.[39].

$$
\begin{aligned}
&= \langle \prod_{e=1}^{M} \delta[\mathbf{c}_{ie}^{0} - \mathbf{c}_{i'e}^{0}] \rangle \\
&= \langle \prod_{e=1}^{M} \delta[\mathbf{c}_{ie}^{1} - \mathbf{c}_{i'e}^{1}] \rangle \ldots \langle \prod_{e=1}^{M} \delta[\mathbf{c}_{ie}^{n} - \mathbf{c}_{i'e}^{n}] \rangle \\
&= < \prod_{e=1}^{M} \prod_{\alpha=0}^{n} \delta[\mathbf{c}_{ie}^{\alpha} - \mathbf{c}_{i'e}^{\alpha}] > \\
&= \langle \prod_{\alpha=0}^{n} \delta[\mathbf{c}_{i}^{\alpha} - \mathbf{c}_{i'}^{\alpha}] \rangle^{M}, \qquad (3.17)
\end{aligned}
$$

where the $n+1$ factors of the partition function have been written in terms of a new variable $\mathbf{c}^{\alpha}$, where α ranges over $\{0, \ldots, n\}$. Each element of $\mathbf{c}^{\alpha}$ is a different replica of the position vector $\mathbf{c}$. Using (3.17), the sum over M in (3.16) is now seen to be the expansion of an exponential:

$$
P_M Z^n = \frac{\langle \exp(\frac{\mu^2 V}{2N} \sum_{i,i'=1}^{N} \int_0^1 ds \int_0^1 ds' \sum_{\alpha=0}^{n} \delta[\mathbf{c}_i^{\alpha} - \mathbf{c}_{i'}^{\alpha}]) \rangle}{\langle \exp(\frac{\mu^2 V}{2N} \sum_{i,i'=1}^{N} \int_0^1 ds \int_0^1 ds' \delta[\mathbf{c}_i - \mathbf{c}_{i'}]) \rangle}. \qquad (3.18)
$$

The numerator and denominator of this expression contain similar expressions, the difference being that the numerator contains an interaction (via product and sum) of the replicated position variables $\mathbf{c}^{\alpha}$, whereas the denominator contains a single (i.e., non-replicated) variable $\mathbf{c}$. We recognize that this expression can be written as: $e^{-n\phi}/e^{-n\phi_0}$, where ϕ_0 indicates that the expression does not include any replicas. If $e^{-n\phi}/e^{-n\phi_0} = \sum_M P_M Z^n$, then

$$
\begin{aligned}
f &= -\lim_{n \to 0} (\sum_{M} P_M Z^n - 1)/n \\
&= -\lim_{n \to 0} (e^{-n(\phi - \phi_0)} - 1)/n \\
&= -\lim_{n \to 0} \frac{1 - n(\phi - \phi_0) + \mathcal{O}(n^2) - 1}{n} \\
&= (\phi - \phi_0).
\end{aligned}
$$

This allows us to focus on the factor $e^{-n\phi}$ i.e., the numerator of (3.18), to find the free energy.

At this stage we have managed to write the products of Z in terms of a new variable $\mathbf{c}^{\alpha}$. As well, we have removed the explicit interaction of the quenched variables which has reappeared as an exponential of products of δ-functions of the new variable $\mathbf{c}^{\alpha}$. Note that in this case all the replicas interact simultaneously (sum over all the replicas), whereas in spin glass models the replicas interact pairwise.

The next step in this process is to write the δ-functions in terms of their Fourier transforms. The following identity is useful:

$$\begin{aligned}\prod_{\alpha=0}^{n}\delta(\mathbf{x}^{\alpha}) &= \delta^{n+1}(x)\\ &= (\frac{1}{V}\sum_{\mathbf{k}}e^{i\mathbf{k}\cdot\mathbf{x}})^{(n+1)}\\ &= \frac{1}{V^{(n+1)}}\sum_{\mathbf{k}_0\ldots\mathbf{k}_n}e^{i\sum_{\alpha=0}^{n}\mathbf{k}^{\alpha}\cdot\mathbf{x}^{\alpha}}\\ &= \frac{1}{V^{(n+1)}}\sum_{\hat{k}}e^{i\hat{k}\cdot\hat{x}}\end{aligned} \tag{3.19}$$

where $\hat{k}=\{\mathbf{k}_0,\mathbf{k}_1,\ldots,\mathbf{k}_n\}$. The sum over $\hat{k}$ ranges over all possible values of each of the vectors $\mathbf{k}^{\alpha}$. We now define the function

$$Q_{\hat{k}}=\frac{1}{N}\sum_{j=1}^{N}\int_0^1 ds\, e^{i\hat{k}\cdot\hat{x}_j} \tag{3.20}$$

and apply these results to the δ-functions that appear in (3.18). The result is

$$\begin{aligned}\sum_{i,i'=1}^{N}\int_0^1 ds\int_0^1 ds'\prod_{\alpha=0}^{n}\delta[\mathbf{c}_i^{\alpha}-\mathbf{c}_{i'}^{\alpha}] &= \frac{N^2}{V^{n+1}}\sum_{\hat{k}}\left|\frac{1}{N}\sum_{j=1}^{N}\int_0^1 ds\, e^{i\hat{k}\cdot\hat{c}_j}\right|^2\\ &= \frac{N^2}{V^{n+1}}\sum_{\hat{k}}|Q_{\hat{k}}|^2.\end{aligned}$$

The free energy can now be written as

$$\exp(-n\phi_n) = \langle\,\exp(\frac{\mu^2N}{2V^n}\sum_{\hat{k}}|Q_{\hat{k}}|^2)\rangle\ . \tag{3.21}$$

The sum over pairs of polymers has been eliminated at the expense of the introduction of a new variable $Q_{\hat{k}}$, which implicitly sums over all polymers. The sum over all the polymers is eliminated by again introducing a new variable z. The following identity is useful

$$e^{a|w|^2}=\frac{a}{\pi}\int d(\mathrm{Re}\,z)\,d(\mathrm{Im}\,z)\,e^{-a|z|^2}e^{2a\,\mathrm{Re}(z^*w)} \tag{3.22}$$

where z^* is the complex conjugate of z, and a is a constant.

An integral of this type is included for each factor of $Q_{\hat{k}}$. If $\mathcal{D}z$ is defined so that

$$\int\mathcal{D}z\,e^{\frac{-\mu^2N}{2V^n}\sum_{\hat{k}}|z_{\hat{k}}|^2}=1 \tag{3.23}$$

then (3.21) becomes

$$e^{-n\phi_n} = \int \mathcal{D}z\, e^{\frac{-\mu^2 N}{2V^n}\sum_{\hat{k}}|z_{\hat{k}}|^2} \langle e^{\frac{\mu^2 N}{2V^n}\sum_{\hat{k}} \mathrm{Re}(z_{\hat{k}}^* Q_{\hat{k}})} \rangle. \tag{3.24}$$

Now the N replicated polymers have been decoupled: There is only the sum over all the polymers, implicit in the factor $Q_{\hat{k}}$. This sum is eliminated by use of the following identity [41]

$$\langle e^{\sum_{i=1}^{N} g(c_i)} \rangle = e^{N \ln(\exp(g(c)))}, \tag{3.25}$$

where g is an arbitrary function of the monomer position c_i, and c is the position of a single monomer. Applying (3.25) to $Q_{\hat{k}}$ of (3.24), we get

$$e^{-n\phi_n} = \int \mathcal{D}z\, e^{-nN\mathcal{F}_n} \tag{3.26}$$

where

$$\mathcal{F}_n = \frac{\mu^2}{2V^n}\sum_{\hat{k}}|z_{\hat{k}}|^2 - \ln\langle e^{\frac{-\mu^2}{V^n}\sum_{\hat{k}} \mathrm{Re}(z_{\hat{k}}^* \int_0^1 ds \exp(i\hat{k}\cdot\hat{c}))} \rangle. \tag{3.27}$$

A mean-field approximation is now made. This is done by replacing the functional integral of (3.24) by the value of the integrand which is stationary with respect to variations of $z_{\hat{k}}$. Fluctuations and correlations of the fields $z_{\hat{k}}$ are ignored. One consequence of this is that the excluded-volume parameter does not appear explicitly in any of the equations, but is implicit through the expectation values. Treating the fluctuations and the excluded volume properly means that the tendency for molecules to avoid each other would be incorporated and, thus, the topologically distinct character of the quenched random variables would be described.

The value of $z_{\hat{k}}$ which makes (3.24) stationary is

$$z_{\hat{k}} = Q\delta_{\hat{k},0}\int_0^\infty d\zeta\, p(\zeta)\, e^{-\frac{\hat{k}^2}{2\zeta}} \tag{3.28}$$

where Q is the fraction of localized monomers.

A variational free energy is defined as

$$f = \lim_{n\to 0}\phi_n \approx \min_{Q,p(\zeta)} f^{\mathrm{var}}. \tag{3.29}$$

If the density of crosslinks is just above the transition value, then we can write $\mu^2 = 1 + \varepsilon/3$ with ε a parameter that is small. One result of the stationarity condition is that $Q = 2\varepsilon/3$. This allows the replacement of both parameters μ^2 and Q by functions of ε. Now we can

focus on how $f^{\rm var}$ depends on the distribution of localization lengths $p(\zeta)$. The following assumptions are made: only crosslink densities in the vicinity of the transition will be considered, i.e., $\varepsilon \ll 1$, with $\overline{\zeta}$ of order ε. Since the inverse square localization lengths ζ are small, this means that the localization lengths $\xi = 1/\sqrt{\zeta}$ are large compared to the size of a free polymer.

These assumptions and substitutions are used and the integrals in (3.27) are performed. The resultant equation is Laplace transformed and then $f^{\rm var}$ is made stationary with respect to $\hat{p}(\hat{\zeta})$, which is the Laplace transform of $p(\zeta)$. The result is a differential equation for $\hat{p}(\hat{\zeta})$,

$$\hat{\zeta}\frac{d^2\hat{p}}{d\hat{\zeta}^2} = \varepsilon\,\hat{p}(\hat{\zeta})\,(1-\hat{p}(\hat{\zeta})). \tag{3.30}$$

To solve this nonlinear differential equation, it is easier to rewrite (3.30) in terms of scaled variables: $\vartheta = 2\zeta/\varepsilon$ and $\pi(\vartheta) = \varepsilon\, p(\zeta)$. This replacement allows both variables ε and ζ to be combined into a single scaled variable ϑ. The differential equation satisfied by $\hat{\pi}(\hat{\vartheta})$, which is the Laplace transform of $\pi(\vartheta)$, becomes

$$\hat{\vartheta}\frac{d^2\hat{\pi}}{d\hat{\vartheta}^2} = 2\hat{\pi}(1-\hat{\pi}). \tag{3.31}$$

No analytic solution has been found to this equation. Instead the inverse Laplace transform is taken to obtain the equation,

$$\frac{\vartheta^2}{2}\frac{d\pi}{d\vartheta} = (1-\vartheta)\pi(\vartheta) - \int_0^\infty d\vartheta'\,\pi(\vartheta')\,\pi(\vartheta-\vartheta'), \tag{3.32}$$

subject to the normalization $\int_0^\infty d\vartheta\pi(\vartheta) = 1$. This equation can be solved numerically, but the asymptotic properties can be found analytically. For $\vartheta \ll 1$ we find $\pi(\vartheta) \sim \vartheta^{-2}e^{-2/\vartheta}$ by neglecting the the second term in (3.32). When $\vartheta \gg 1$ we solve (3.31) approximately near the value of $\hat{\vartheta}$ at which $\hat{\pi}$ diverges. The inverse Laplace transform is taken and the asymptotic form $\pi(\vartheta) \sim (\vartheta - 3/5)e^{-\vartheta}$ is obtained. The distribution of scaled localization lengths can be found numerically from the solution of (3.32) and is shown in Fig. 3.3. In this graph the localization length ξ is scaled by the value of the average localization length $\overline{\xi}$. There is a single maximum of the scaled localization length which can be associated with the most probable value of the localization lengths ξ_{typ}.

As a final note it should be added that some of the density fluctuations have been taken into consideration. The effect of the 1-replica sector gaussian density fluctuations is to simply renormalize a coefficient in the variational free energy. In particular, the behaviour

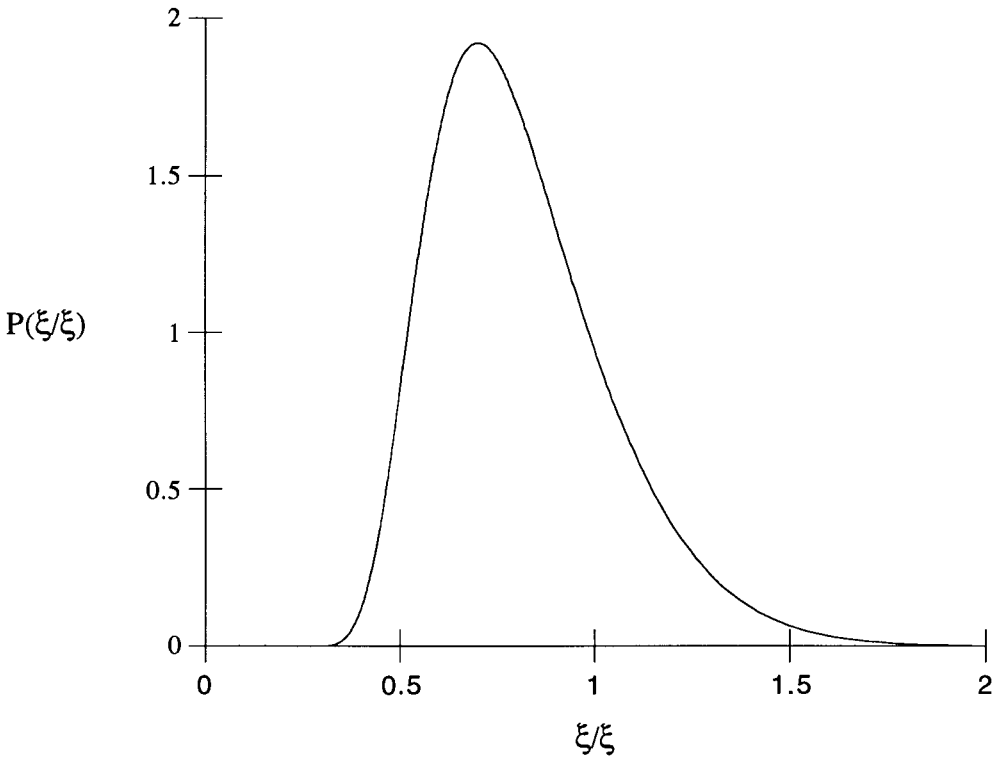

Figure 3.3: The distribution of scaled localization lengths $\xi/\overline{\xi}$ is shown.

of the fraction of localized monomers Q and the crosslink density at the transition ($\mu^2 = 1$) are unchanged. The distribution of localization lengths is changed by the renormalization of the factor $\varepsilon' = \varepsilon/(1+\varepsilon)$. This renormalization is finite and does not change the form of the scaling function.

In summary, the liquid to solid transition of a system of randomly crosslinked polymers occurs when the density of crosslinks M/N exceeds a critical value. The critical value corresponds to $\mu^2 \sim 1$, or about one crosslink per polymer. The solid state can be described by a fraction of localized monomers or gel fraction Q. The gel fraction grows with a classical exponent $\beta = 1$ or $Q \sim \mu^2 - 1$. The solid state is also characterized by a statistical distribution of localization lengths. In the vicinity of the transition this distribution can be rewritten in terms of scaled variables $\pi(\vartheta)$, valid for all near-critical crosslink densities. Since this distribution has a single maximum, one can define a typical localization length, ξ_{typ}. This length obeys the scaling relation $\xi_{typ} \sim (\mu^2 - 1)^{-1/2}$.

Chapter 4

Localization and Ergodicity Breaking

The main focus of this chapter is a set of simulations of the vulcanization transition based on the theory presented in Chapter 3. The starting point of the simulations is a well equilibrated polymer melt, and this chapter begins by a description of various properties of such melts. I then discuss the microscopic model used in the study of this transition before describing the results for the order parameter and the distribution of localization lengths. As well, the issue of broken ergodicity is discussed, and I present evidence that, at least according to one criterion, ergodicity is not broken in these systems except when crosslinks are imposed.

4.1 Properties of Polymer Melts

There is a significant body of work pertaining to various properties of polymer melts and vulcanized rubber. In this section I will describe various properties of the polymer melts that the simulations were based on, since an equilibrated polymer melt is the basis for vulcanization.

A dense melt of linear polymers is ideal in the sense that the polymers obey random walk statistics for the end-to-end vector and for the radius of gyration, as discussed in Chapter 1. The dynamics of polymers are typically described in terms of the Rouse and reptation models which are discussed in turn. The Rouse model neglects entanglements. It is useful

for describing the dynamics on short timescales when topological constraints are not felt, or for short polymers where entanglements do not play a dominant role. The model consists of a Gaussian polymer which experiences a local viscosity. Each monomer on the polymer is described as a bead connected by springs to its neighbours. The rest of the polymers and solvent are modelled as random thermal noise, so that the monomers of the test polymer feel a random force of zero average. The Rouse model is useful when the polymer is making small enough displacements so that the rest of the monomers in the melt can be characterized by a local viscosity.

When the length M of the polymer exceeds some length M_e for a given density, then the polymer is likely to become intertwined with other polymers. These other polymers prevent Brownian motion of the centre of mass that the Rouse model describes. In the reptation model, the monomers not belonging to the test polymer are pictured as being fixed constraints, Fig. 4.1. The test polymer then moves along its own contour where the shape of this contour is determined by the positions of the surrounding polymers. If the polymer were to move perpendicular to its contour many other polymers would have to be displaced at a tremendous cost in energy. While this is a more sophisticated model than the Rouse model it does not take into consideration that the background chains themselves are moving so that on a long enough time scale the constraints are not fixed but continually reform. One limitation of both models is that they are single chain models, where a test chain moves through an idealized background.

The most comprehensive computer simulation of dense melts of which I am aware was done by Kremer and Grest [42]. They had a large range of number of monomers per polymer $5 \leq M \leq 400$. The model they used is described in the next section. One quantity of interest is the entanglement length M_e which roughly corresponds to the number of monomers per chain necessary to achieve a sufficiently entangled system that reptation dynamics apply. They used two methods to estimate M_e. A direct method involves monitoring the motion of the centre of mass of each polymer R_{CM}. In the Rouse picture the mean square displacement of R_{CM} from its original position $\langle\, R_{CM}(t) - R_{CM}(0))^2$ follows the standard $t^{1/2}$ law of diffusion. In the reptation model the dynamics are slowed down because the entanglements limit the motion and $\langle\, R_{CM}(t) - R_{CM}(0))^2$ follows a characteristic $t^{1/4}$ law. By noting which length of chain reached the $t^{1/4}$ regime they were able to estimate that the entanglement length was $M_e \approx 35$ monomers. This estimate was consistent for all chains $50 \leq M \leq 200$. A second estimate of the entanglement length can be deduced from an 'effective' shear

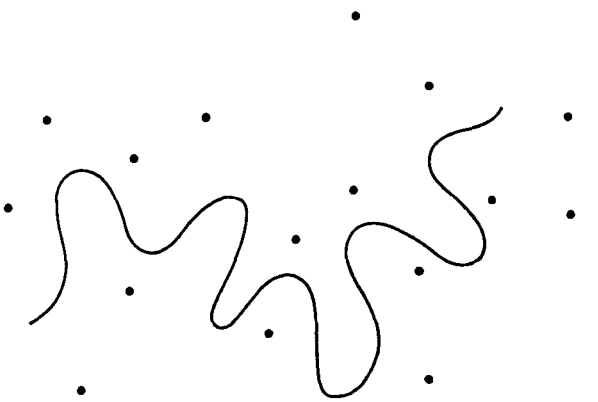

Figure 4.1: A model of the chain in the reptation mode. A single chain encounters fixed constraints which are the other polymers in the melt, modelled here by thick dots.

modulus, the plateau modulus G_0[1]. The characteristic decay of G_0 for viscoelastic materials differentiates Rouse dynamics from reptation, and based on this an estimate of $20 \leq M_e \leq 60$ was obtained. They concluded that $M_e = 35$ is a reasonable estimate of the entanglement length for their system of polymers. This number is noted here, since our simulations use the same model for polymers and the same density of melt.

While polymer melts are relatively well understood there are no models for the dynamics of vulcanized melts. The hypothesis of Goldbart *et al.* [39] is that there are a certain fraction of monomers Q that will be localized about mean positions and $1-Q$ delocalized monomers. On very short time scales each segment of chain between crosslinks probably behaves as a Rouse chain, feeling just random noise from the rest of the polymers. On longer timescales it is possible that the crosslinks act as fixed constraints envisioned by the reptation picture, except that reptation is also inhibited.

[1]For a polymeric liquid the shear modulus eventually decays to zero, as for a typical fluid. However, because the entanglements in a melt of polymers can act as constraints, the time to reach $G_0 = 0$ is characteristic of the polymeric liquid and is different for the Rouse and reptation models [2, 44].

4.2 Microscopic Model

As before, we denote the number of polymers by N and the number of monomers per chain by M. The systems studied were $M = 10$ monomers on $N = 25, 100$ chains, $M = 20$ monomers on $N = 30, 100$ chains and one larger system with $M = 50$, $N = 60$. The potential describing the interaction between the monomers is similar to that used in Ch.2. Successive monomers on the chain were tethered by the attractive potential,

$$U_{nn}(r_{ij}) = \begin{cases} -\frac{1}{2}kR_0^2 \ln\left[1 - \left(\frac{r_{ij}}{R_0}\right)^2\right] & r_{ij} < R_0 \\ \infty & r_{ij} \geq R_0. \end{cases} \tag{4.1}$$

Self-avoidance was imposed by the repulsive potential,

$$U_{LJ}(r_{ij}) = \begin{cases} 4\epsilon\left[\left(\frac{\sigma}{r_{ij}}\right)^{12} - \left(\frac{\sigma}{r_{ij}}\right)^{6} + \frac{1}{4}\right] & r_{ij} < 2^{1/6}\sigma \\ 0 & r_{ij} \geq 2^{1/6}\sigma \end{cases} \tag{4.2}$$

which acted between all monomers. The parameters chosen for this simulation were $R_0 = 1.5\sigma_0$ as the maximum extension of tethered particles, the 'size' of each particle is $\sigma = 1.0\sigma_0$, where σ_0 is the basic unit of length, and the strength of the potential was $k = 30.0\epsilon$. These parameters are the same as those used in the simulations of Kremer and Grest [42] and do not allow chains to pass through each other.

The simulations were constant energy molecular dynamics with the equations of motion integrated forward in time with a standard velocity Verlet algorithm, as was described previously. The time step was chosen to be $\delta t = 0.01\sigma_0\sqrt{m/\epsilon}$ which was sufficient to keep the energy constant to one part in 10^4 for the length of a run and at average temperature of $k_BT = \epsilon$. To achieve the proper density of the melt, the chains are initially placed in a very large cubical box which is slowly compressed until the density of $\mathcal{N}\sigma_0^3/V = 0.85$ is reached, where $\mathcal{N} = N \cdot M$ is the total number of particles, and V is the volume of the box. The melts were further equilibrated for up to 1.2×10^7 integration steps. For these parameters there are data available with which to compare the properties of the melts. Quantities such as the end-to-end distance of the polymer, the radius of gyration and the eigenvalues of the moment of inertia tensor were consistent with expected values [42, 45] (see Table 4.1).

Once the melts were sufficiently equilibrated, crosslinks were imposed between monomers in the following manner. A monomer was chosen at random, and all monomers within a radius of $r_x = 1.25\sigma_0$ were enumerated. This radius is roughly the persistence length of the

M/N	R^2_{ee}	R^2_g	$\lambda_1^2 : \lambda_2^2 : \lambda_3^2$
10/25	12.8	2.14	1.0 : 2.94 : 13.88
10/25 (*)	13.1	2.2	1.0 : 3.0 : 14.3
20/30	28.5	4.78	1.0 : 2.81 : 12.53
20/30 (*)	29.7	5.0	1.0 : 2.9 : 13.4
10/100	13.0	2.19	1.0 : 2.90 : 13.41
20/100	30.4	5.02	1.0 : 2.87 : 13.42

Table 4.1: A table of the values of some polymer properties of the melt in units of σ_0^2. The starred data (*) is from [42]. A previous simulation [45] of very long random walks has given the ratio of eigenvalues as 1.0 : 2.69 : 11.80.

systems, calculated using $R^2_{ee} = \langle a_0 \rangle^2 l_p^2 (M-1)$, where $\langle a_0 \rangle$ is the average distance between successive monomers on a polymer. A monomer at random was chosen from this list and the link was made by enforcing the attractive potential (4.1). A link was not allowed if there already existed a link between the two chosen monomers, which could arise from previous crosslinking or if the two particles were successive monomers in a chain. This procedure was repeated until the desired number of crosslinks had been attained. The crosslinks formed in this way are identical in all respects to the binding of nearest neighbours. The number of crosslinks per particle was in principle restricted to be less than or equal to six, but in practice this restriction did not come into effect. Even in the heavily crosslinked regime a particle rarely had more than two links, excluding links to nearest neighbours. This method of crosslinking is most similar to irradiation crosslinking, where the crosslinks are formed rapidly.

The method described above is adapted from studies done by Grest and Kremer [46, 47]. These are the only previous studies of which I am aware that have considered fully self avoiding dense melts with randomly crosslinked monomers. Using a melt of similar density $\rho = 0.85/\sigma_0^3$ they added random crosslinks in the manner described above. They did a thorough investigation of the crosslinked melt and found that, if they imposed a density of crosslinks $n = n_{cl}/N$ on the melt, where n_{cl} is the number of crosslinks then the resulting distribution of crosslinks per chain is normal. The distribution is centred on the average number of crosslinks per chain and becomes more symmetric as the number of crosslinks increases. This result, although not surprising, indicates that the crosslinking procedure is reasonable. They found that the strand length, that is, the number of monomers between

crosslinks on a polymer, follows an exponential curve when plotted as a function of n. This distribution of lengths holds for a large range of crosslink densities but can only be defined on a given polymer when there are at least two crosslinks. The above results were found to be insensitive to the radius r_x used when making the crosslinks. These properties of the crosslinked melt were also found to hold when the density of the melt was reduced to $\rho = 0.40/\sigma_0^3$, or when the analysis was done on a system of random walks of density $\rho = 0.85/\sigma_0^3$. They also did a study on the percolation probability of the melt [47]. In this study they found that the density of crosslinks required to make one cluster percolate from one side of the box to the other was $p_c = 0.77$. This number decreased to $p_c = 0.60$ when they allowed only different polymers to link. The percolation probability was calculated for our melts. We found for the systems of $N = 100$ polymers and $M = 10, 20$ monomers per polymer $p_c = 0.7$, and for a system of $N = 60$ polymers and $M = 50$ monomers per polymer $p_c = 0.75$. These figures are only rough estimates, as the systems studied are too small to arrive at precise estimates of p_c. Nevertheless, classical exponents were found for the increase in cluster size with crosslink probability, Fig. 4.2.

4.3 Order Parameter

After the imposition of crosslinks the order parameter was calculated as follows. The average temperature was raised from $T = \epsilon/k_B$ to between $4\epsilon/k_B$ and $6\epsilon/k_B$. Although a smaller time step of $\delta t = .006\sigma_0\sqrt{m/\epsilon}$ was required to guarantee energy conservation, the sampling of configuration space was speeded up. From (3.9) the order parameter can be written as

$$q = \frac{1}{N}\sum_{j=1}^{N}\langle e^{i\mathbf{k}_1\cdot\mathbf{R}_j}\rangle\langle e^{i\mathbf{k}_2\cdot\mathbf{R}_j}\rangle \tag{4.3}$$

where $\mathbf{R}_j$ is the position vector of the j-th monomer and $\mathbf{k}_1 = -\mathbf{k}_2$ for an amorphous solid. We can define a value of q for each particle j in the system, so that $q = \sum_j q_j$. Then the equation for q_j becomes

$$q_j = \left|\langle e^{i\mathbf{k}\cdot\mathbf{R}_j}\rangle\right|^2, \tag{4.4}$$

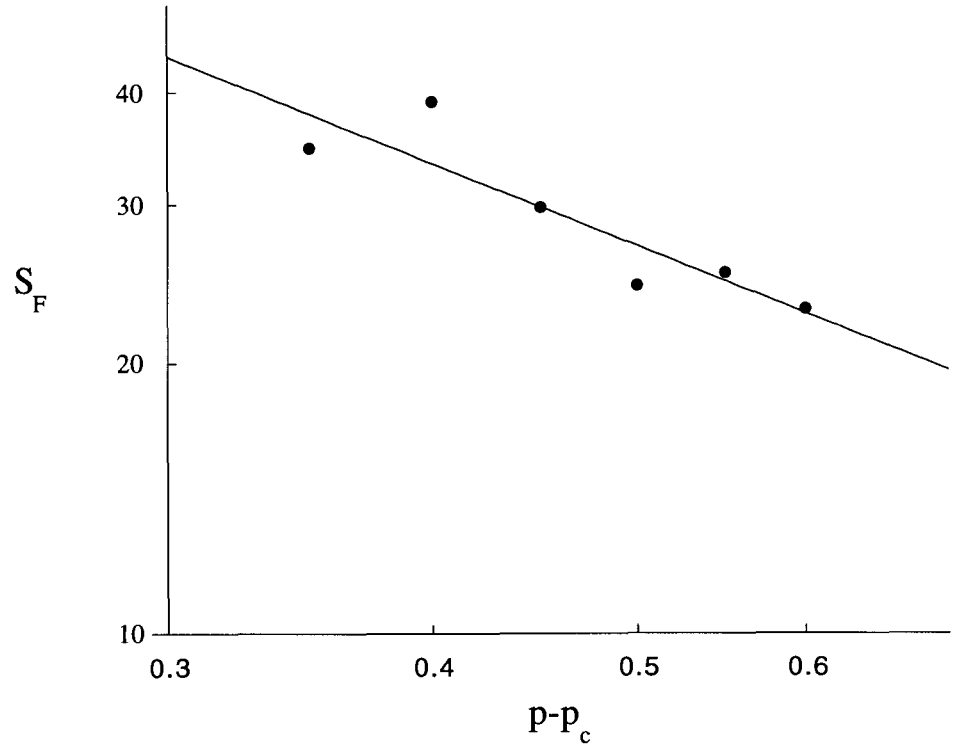

Figure 4.2: The average size of the clusters S_F excluding the largest one. The slope of the line is -0.95 consistent with the classical exponent $\gamma = -1$.

where the smallest k-vector $\mathbf{k} = 2\pi\,(1/L_x, 1/L_y, 1/L_z)$ appropriate to the box size was used. During the simulation the value of q_j was recorded as a function of time,

$$q_j(t_s) = \left| \frac{1}{t_s} \left(\sum_{t=1}^{t_s} \exp^{i\mathbf{k}\cdot\mathbf{R}_j(t)} \right) \right|^2 , \tag{4.5}$$

where $\mathbf{R}_j(t)$ is the position of the j-th monomer at time t. By construction $q_j(t_s = 1) = 1$ and so $q_j(t_s)$ decreases as a function of time (Fig. 4.3). At each time step the terms $\cos(\mathbf{k}\cdot\mathbf{R}_j)$ and $\sin(\mathbf{k}\cdot\mathbf{R}_j)$ were recorded for each monomer j. The value of $q(t_s)$ was found by periodically summing all the values for $q_j(t_s)$. The simulations ran for a finite amount of time, typically on the order of $100000t_s$ where t_s is the number of time steps used in the calculation of q or the number of elements in the sum of (4.5). For most of the range of crosslink density this time was not sufficient to reach equilibrium values of q. By plotting $q(t_s)$ versus $t_s^{-1/2}$, (Fig. 4.4) an extrapolation can be made to $t_s \to \infty$ after disregarding an initial transient period. This is the method used to estimate the value of q. In several cases the simulations were carried out for up to four times the standard length of run to ensure that the extrapolation procedure was an adequate way of finding the equilibrium values of q. This empirical method of extrapolation slightly underestimates the equilibrium value of q, and the underestimate is worse for highly crosslinked systems. When the systems were highly crosslinked the terminal value of q was reached, and the extrapolation procedure was not used, rather the value of q was estimated by a least-squares fit to a straight line over the portion of data that remained unchanged in time. The value of $q(t_s)$ as a function of $t_s^{-1/2}$ is shown in Fig. 4.5 for three different values of crosslink density n.

When random crosslinks are incorporated into a system, the actual location of those crosslinks has a bearing on the resultant value of q. Two possible extremes of this effect are polymers linked only internally when the crosslinks are introduced, and links only between different polymers. These two situations should produce different values of q. It was thus necessary to calculate q from up to fifteen different realizations of the same number of crosslinks in a given system. The value $q(t_s)$ is shown in Fig. 4.6 for two different realizations of the same number of crosslinks. To ensure that the realizations of crosslinks were not unduly influenced by the underlying melt a second melt was created. The new melt was made from the original by integrating forward in time the equations of motion for $t_s = 1.5 \times 10^6$ time steps. During this time each polymer moved an average of $2.4R_g$ from its original position. There was no significant difference in the values of q obtained from the two melts

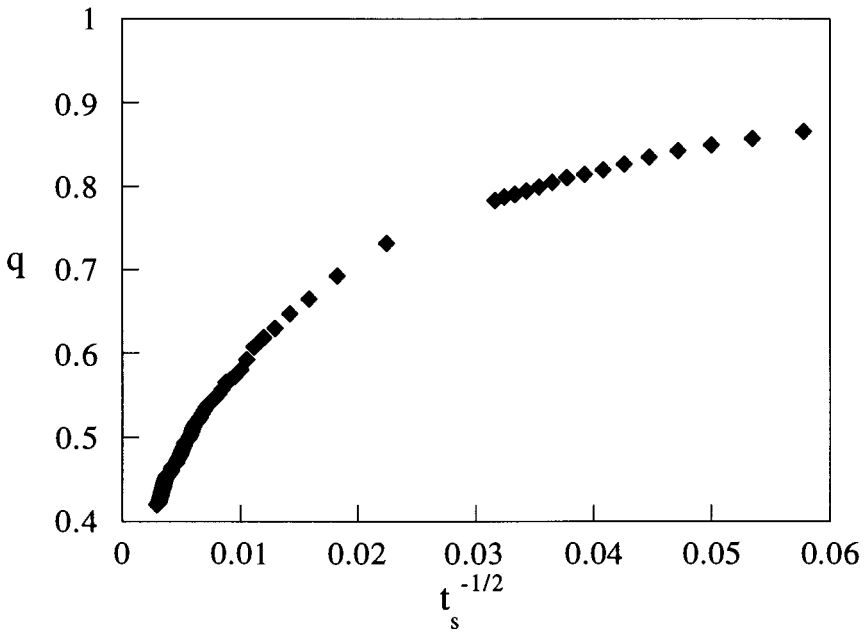

Figure 4.3: The value of the order parameter q as a function of $t_s^{-1/2}$. This value is for the system of $N = 100$ polymers with $M = 20$ monomers per polymer. The number of crosslinks in the system is 170 and the simulation time is $t_s \leq 121000$.

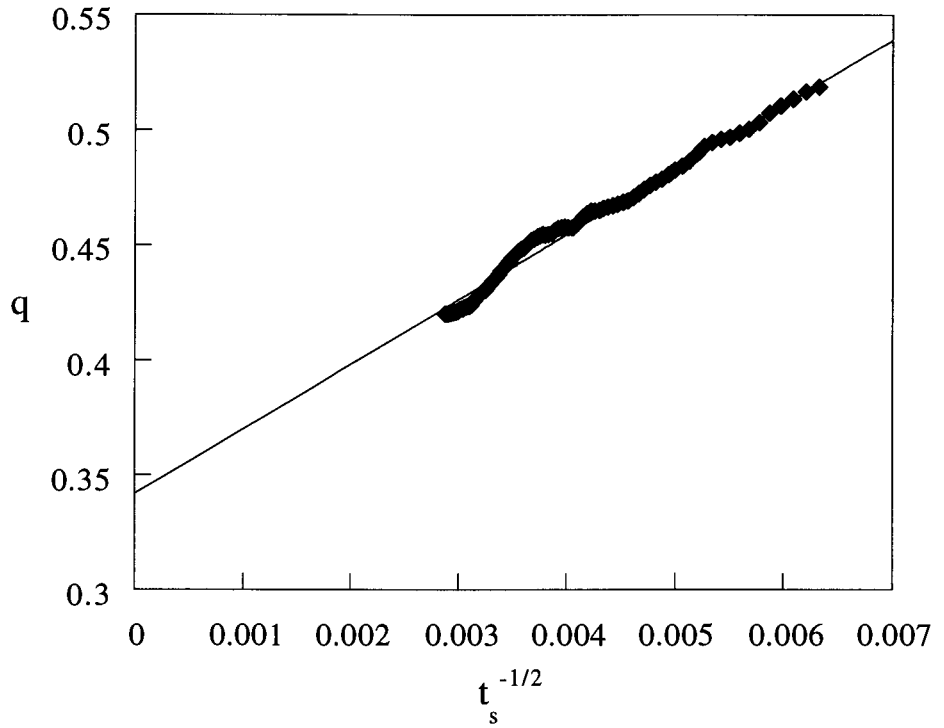

Figure 4.4: The value of the order parameter q as a function of $t_s^{-1/2}$. This extrapolation is shown for the same system shown in Fig. 4.3. The time frame used in the extrapolation was $25000 \leq t_s \leq 121000$, a least squares fit to the data gives a value of $q(t_s = \infty) = 0.338 \pm 0.002$.

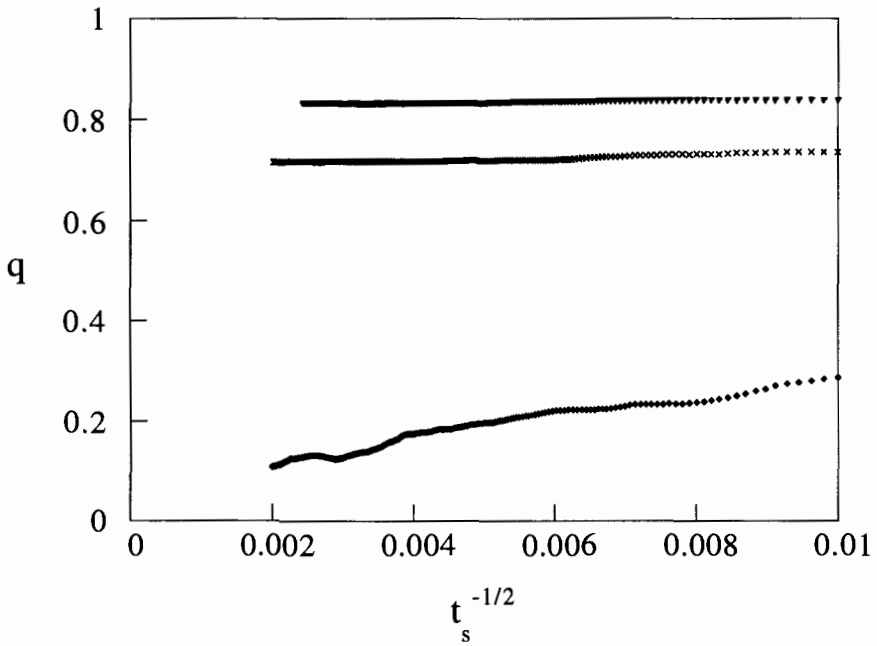

Figure 4.5: The value of q as a function of $t_s^{-1/2}$ for three different crosslink densities. The number of polymers is $N = 30$ with $M = 20$ monomers per polymer. The upper curve is for 180 crosslinks at a maximum time of $t_s = 170000$, the middle curve for 135 crosslinks for a maximum time of $t_s = 250000$, and the lower curve for 55 crosslinks for a maximum time of $t_s = 250000$.

as shown in Table 4.2. The properties of crosslinked melts including the value of q quoted henceforth are the combination of q from the two melts.

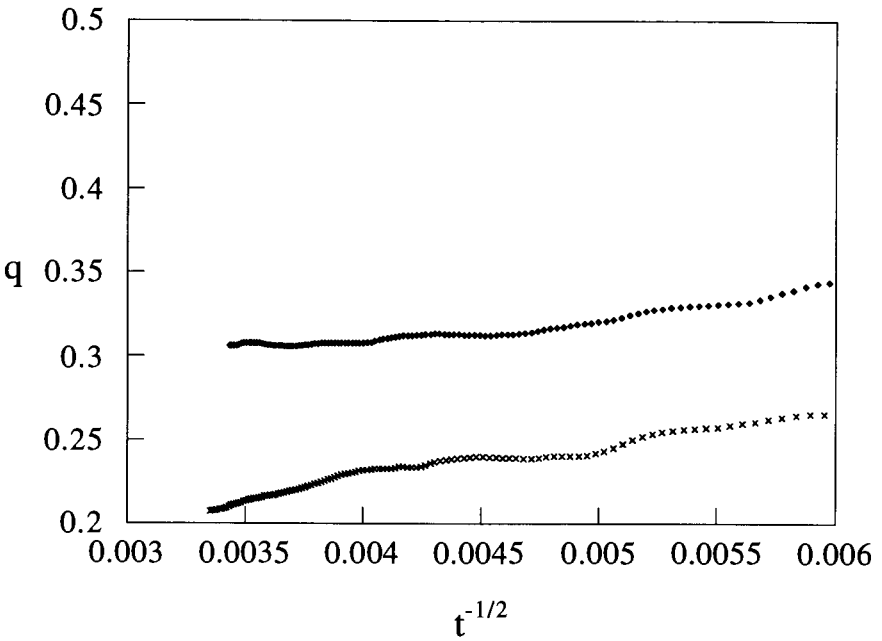

Figure 4.6: The value of the order parameter q as a function of $t_s^{-1/2}$ for two different realizations of the same number of crosslinks in the same melt. The system shown has $N = 100$ polymers $M = 10$ monomers per polymer and 130 crosslinks.

$M = 20$, $N = 30$	$n_{cl} = 60$	$n_{cl} = 75$	$n_{cl} = 90$
(a)	$.22 \pm .11$	$.36 \pm .04$	$.49 \pm .01$
(b)	$.23 \pm .09$	$.39 \pm .05$	$.48 \pm .05$
$M = 10$, $N = 100$	$n_{cl} = 130$	$n_{cl} = 140$	$n_{cl} = 160$
(a)	$.13 \pm .06$	$.20 \pm .06$	$.39 \pm .05$
(b)	$.16 \pm .06$	$.19 \pm .06$	$.38 \pm .02$

Table 4.2: A table of a selection of the values of q derived from two different melts.

As noted previously, to speed up the calculations of the order parameter, the temperature

of the system was raised. The order parameter was also evaluated for the temperature of $k_BT/\epsilon = 1$, although there were fewer realizations for each value of crosslink density. Results for both high and low temperature calculations are shown in Table 4.3.

$M = 10,\ N = 100$	$n_{cl} = 130$	$n_{cl} = 140$	$n_{cl} = 170$
$k_BT/\epsilon = 1$	.15	.21	.41
$k_BT/\epsilon = 6$	$.15 \pm .06$	$.19 \pm .05$	$.44 \pm .04$
$M = 20,\ N = 100$	$n_{cl} = 120$	$n_{cl} = 150$	$n_{cl} = 200$
$k_BT/\epsilon = 1$	.11	.20	.49
$k_BT/\epsilon = 6$	$.10 \pm .04$	$.21 \pm .02$	$.48 \pm .04$

Table 4.3: A comparison of q for different values of temperature. The data for $k_BT/\epsilon = 1$ do not have uncertainties quoted because there were too few realizations to accurately determine the standard deviation.

A final variation of some of the parameters was done. In select systems, when the crosslinks were imposed on the melt, a radius of $r_x = 1.35\sigma_0$ was used, instead of $r_x = 1.25\sigma_0$, used until this point. The method of imposing the crosslinks and of evaluating q for the larger value of r_x remained identical to the method used with the smaller radius r_x. The results are compared in Table 4.4. As was found previously by Grest and Kremer [47] for other properties of the system, there is no significant difference in the estimated value of q for a larger value of crosslinking radius.

$M = 20,\ N = 30$	$n_{cl} = 75$	$n_{cl} = 90$	$n_{cl} = 135$
$r_x/\sigma_0 = 1.25$	0.38 ± 0.04	0.48 ± 0.03	0.72 ± 0.01
$r_x/\sigma_0 = 1.35$	0.35	0.50	0.74

Table 4.4: A table of the values q for systems made with different crosslinking radii. The uncertainties are not quoted as there are too few realizations with $r_x/\sigma_0 = 1.35$ to get a reliable estimate of the standard deviation.

The results for q as a function of the number of crosslinks n for the different systems studied are shown in Figs. 4.7-4.8. In each case the data are fit to the equation $q = A_c\,(n - n_c)^{\beta_q}$ where A_c is a constant, and n_c is the critical number of crosslinks necessary to solidify the melt. A striking feature of the data is the system-size dependence for both the

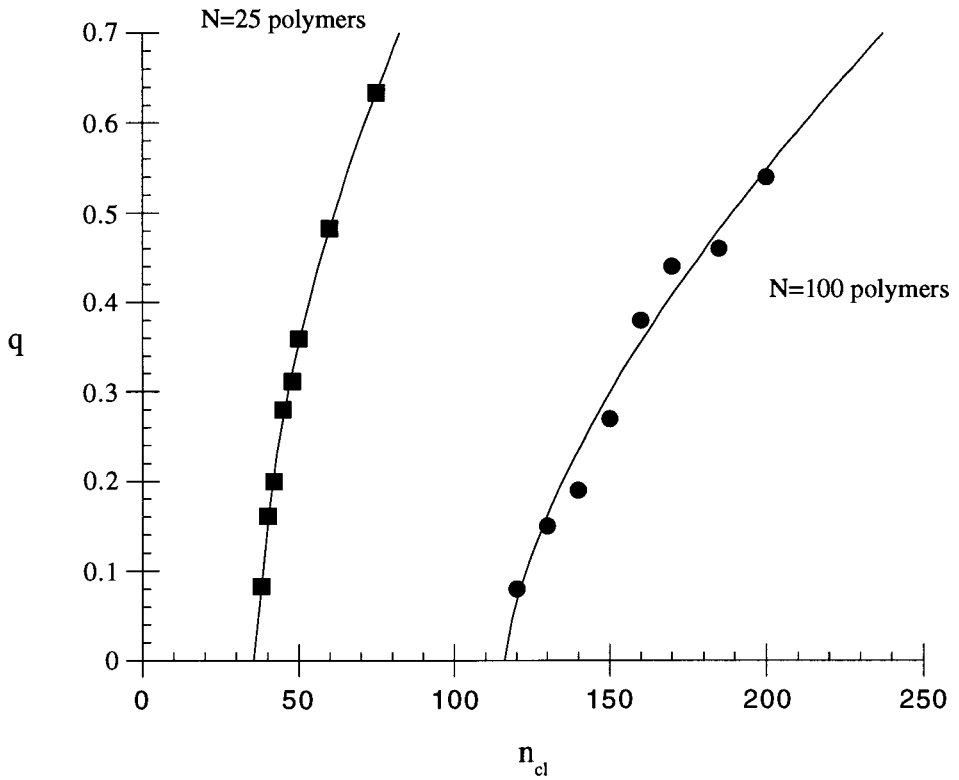

Figure 4.7: For $M = 10$ monomers per polymer the value of q is shown for the two systems studied. The critical number of crosslinks is 37 for $N = 25$ and 117 for $N = 100$. The exponent β_q is 0.54 for $N = 25$ and 0.66 for $N = 100$

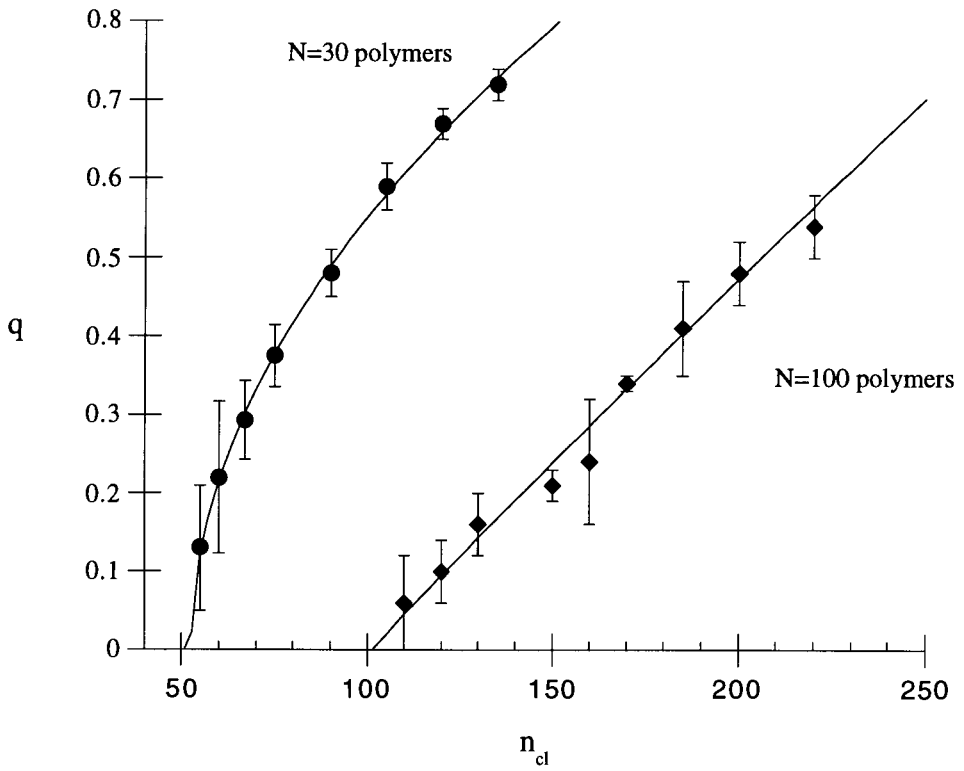

Figure 4.8: For $M = 20$ monomers per polymer the value of q is shown for the two systems studied. The critical number of crosslinks is 52 for $N = 30$ and 101 for $N = 100$. The exponent β_q is 0.50 for $N = 30$ and 0.96 for $N = 100$.

exponent β_q and n_c. For systems with $M = 10$ the exponent increases from 0.54 ± 0.02 to $0.66 \pm .17$ when N increases from 25 to 100, while n_c decreases from 1.48 ± 0.01 to 1.17 ± 0.6. When there are 20 monomers per polymer the changes are even more evident: β_q increased from 0.50 ± 0.08 to 0.96 ± 0.22 for N increasing from 30 to 100 while n_c decreases from 1.7 ± 0.1 to 1.01 ± 0.13. The trend is similar as the number of monomers per polymer is increased. It is difficult to estimate the actual value of β_q and n_c due to these strong finite-size effects. It is important to note that the systems that we have simulated are not in the range of validity of the theory of reference [39]. In this theory the density of crosslinks in the amorphous solid state is $n - 1 = n_{cl}/N - 1 \ll 1$. Thus, the results presented here serve only to show that the order parameter q as envisioned by [39] is a good measure of localization in the solid state and that their predicted critical density of crosslinks $n_c = 1$ cannot be excluded.

4.4 Localization Lengths

A second important prediction of Goldbart *et al.* [39] is the distribution of localization lengths of the localized monomers. It was assumed in their theory that the localized particles were distributed around their average positions according to a Gaussian distribution. This hypothesis was verified for our crosslinked melts for selected particles and for a wide range of crosslink densities. A normal distribution of monomer positions gives the probability of finding the monomer j at position $\mathbf{R}_j$ to be

$$\phi(\mathbf{R}_j) = \frac{1}{\pi^{3/2}\xi_j^3} e^{-(\mathbf{R}_j - \overline{\mathbf{R}}_j)^2/\xi_j^2} \tag{4.6}$$

where $\overline{\mathbf{R}}_j$ is the mean position of monomer j and ξ_j is the standard deviation of the distribution or the localization length of monomer j. The order parameter q_j as defined in (4.5) becomes

$$\frac{1}{t_s}\sum_{t=1}^{t_s} \exp^{i\mathbf{k}\cdot\mathbf{R}_j(t)} = \frac{\xi_j^3}{\pi^{3/2}} \int d\mathbf{R}_j \, e^{i\mathbf{k}\cdot\mathbf{R}_j} \, e^{-(\mathbf{R}_j - \overline{\mathbf{R}}_j)^2/\xi_j^2} \tag{4.7}$$

$$\tag{4.8}$$

This integral can be calculated by completing the square in $\mathbf{R}_j$ and results in

$$q_j = e^{-k^2\xi_j^2/2}, \tag{4.9}$$

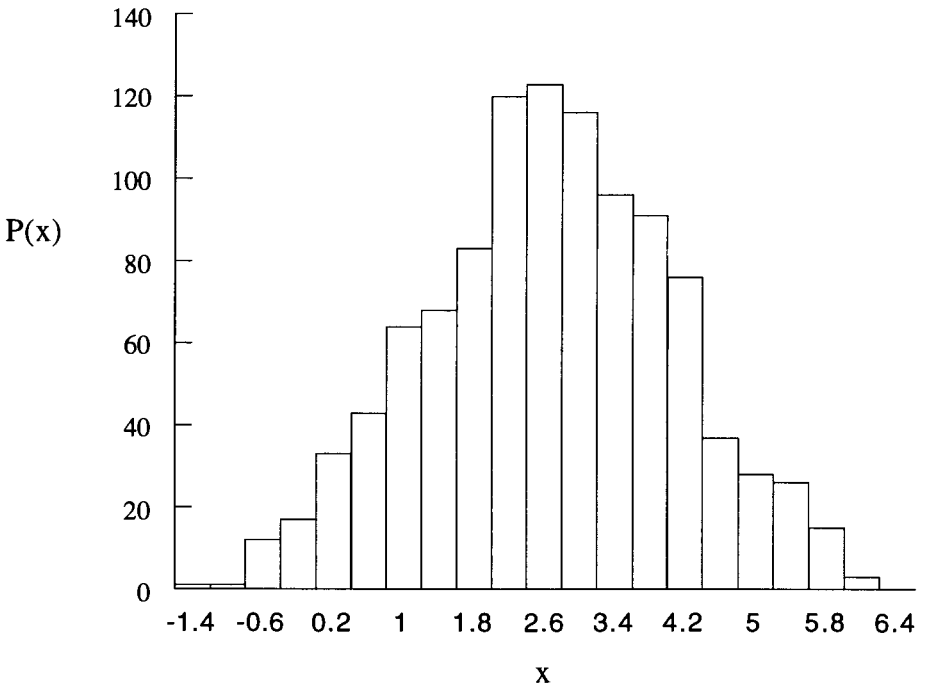

Figure 4.9: For a particular monomer j, we find the probability distribution $P(x_j)$ of the x component of position $\mathbf{r}_j$ is gaussian. This figure illustrates the distribution of x_j where $-L \leq x_j \leq L$ for a monomer in the box.

so that the localization length is

$$\xi_j = \sqrt{\frac{-\ln(q_j)}{2\pi^2}} L, \tag{4.10}$$

where the substitution $k = 2\pi/L$ was made.

The localization length of each monomer was calculated from the data kept in the calculation of the order parameter. To find the distribution $P(\xi)$ for each system the localization lengths were binned, after having been scaled by the average localization length. Generally 70 bins were used, but the overall results are insensitive to the exact number of bins used in the range $50 - 100$ bins. In the highly crosslinked regime the distribution of localization lengths does not change much over the course of a simulation run as illustrated in Fig. 4.10. Results for a moderate to high density of crosslinks are shown in Figs. 4.11 and 4.12.

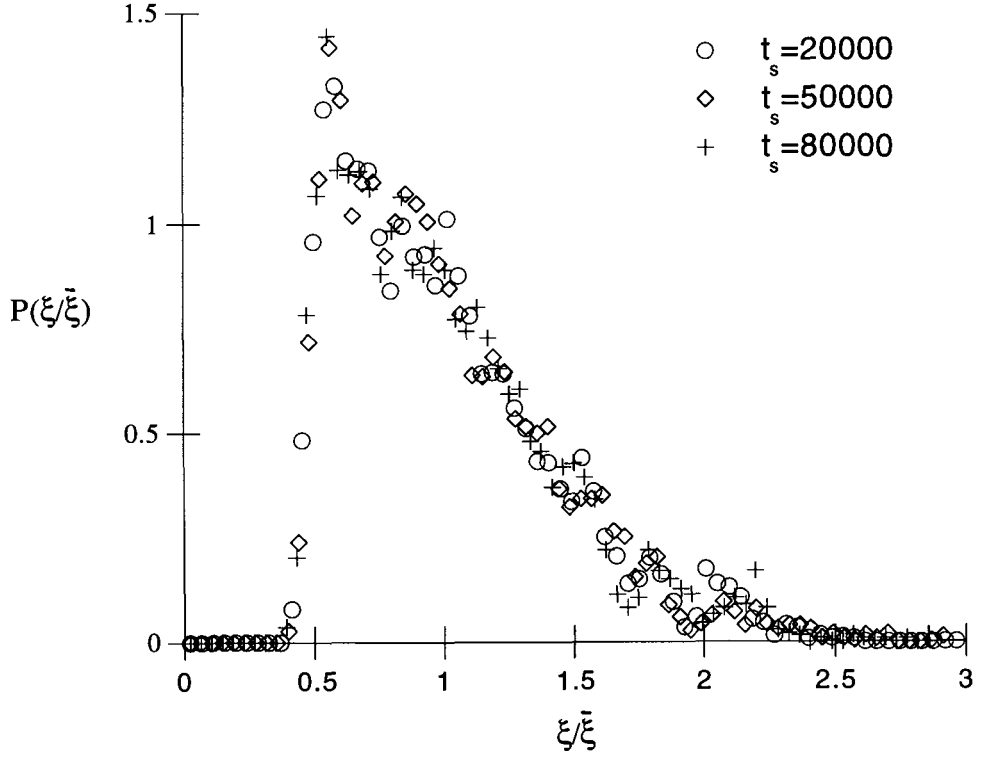

Figure 4.10: The distribution of localization lengths for three different simulation times of a system of $M = 20$, $N = 100$ with $n_{cl} = 170$ crosslinks.

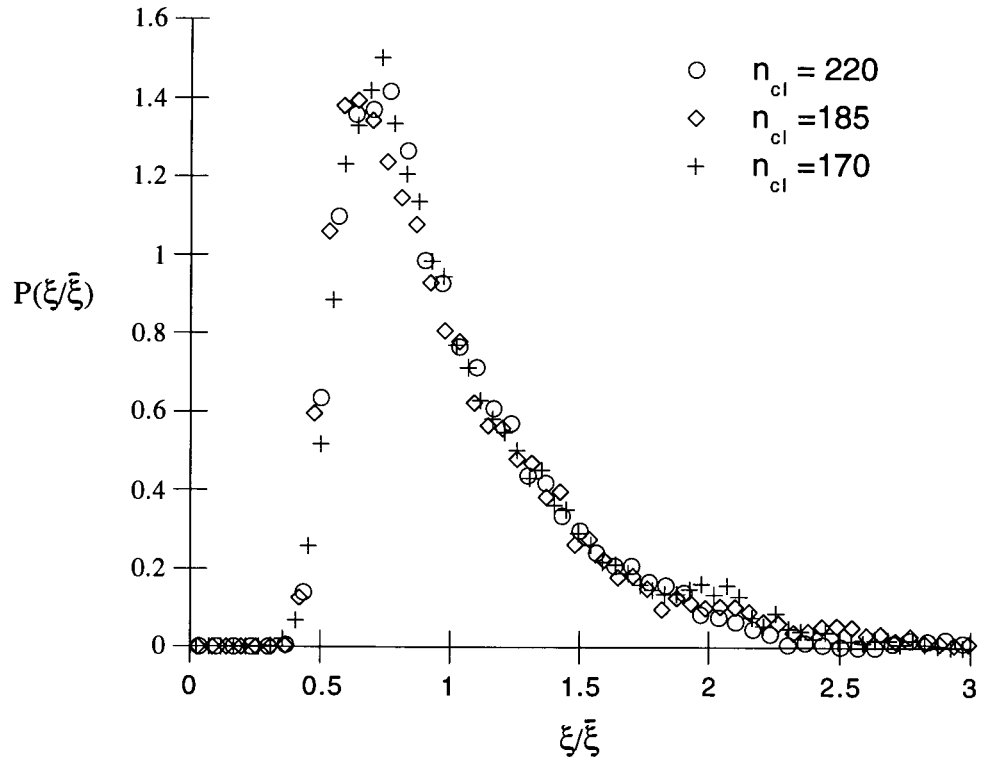

Figure 4.11: The distribution of localization lengths for a system of $M = 10$, $N = 100$ for the number of crosslinks in the range $170 < n_{cl} < 220$.

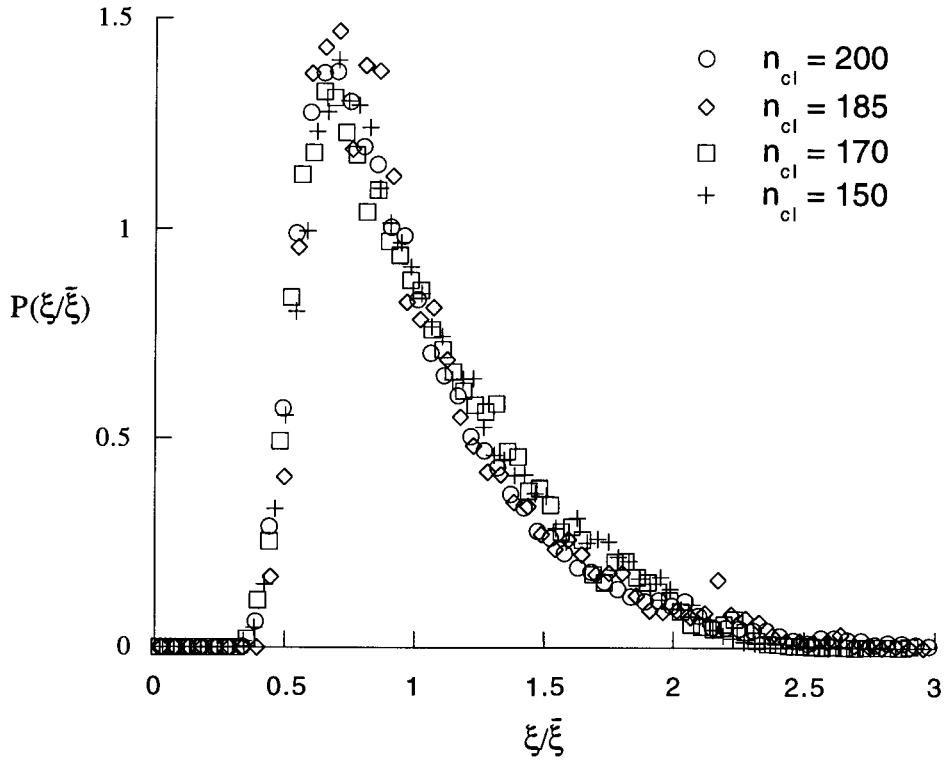

Figure 4.12: The distribution of localization lengths for a system of $M = 20$, $N = 100$ for the number of crosslinks in the range $150 < n_{cl} < 200$.

The form of the curve for $P(\xi)$ as a function of ξ changes character as the number of crosslinks is increased starting from the fluid regime. The distribution of localization lengths is much broader and the primary peak is lower, while a secondary peak is more prominent in the fluid compared to the moderately crosslinked state. This variation is shown in Fig. 4.13.

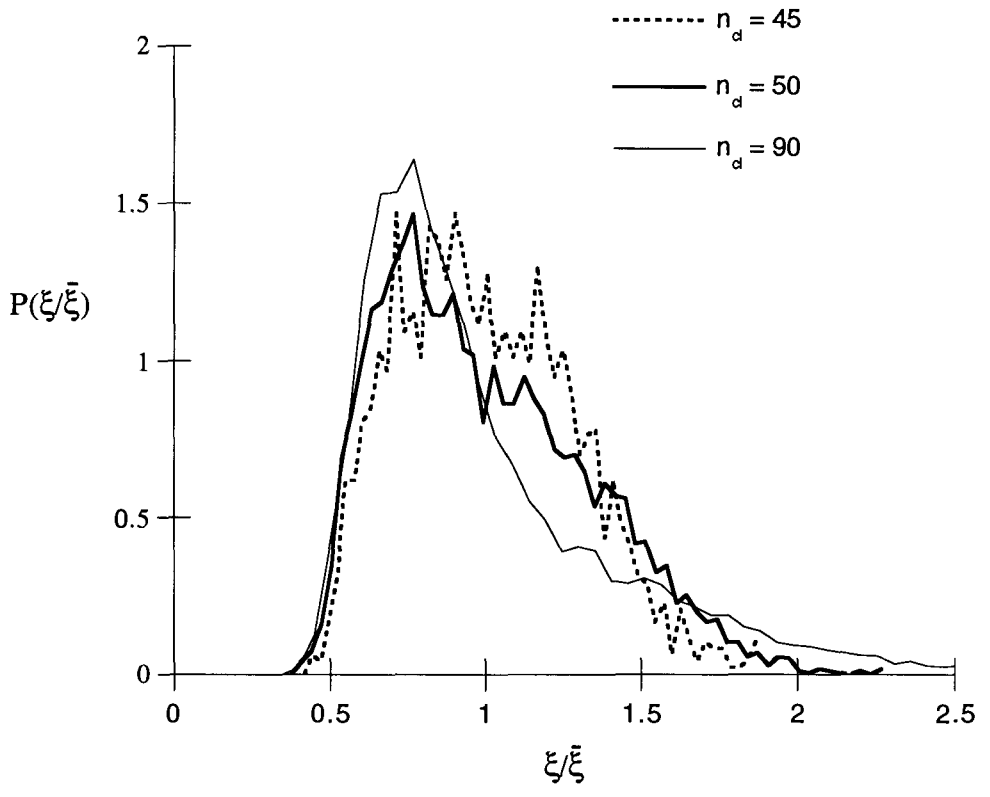

Figure 4.13: The distribution of localization lengths for three different densities of crosslinks, for the system $M = 20$, $N = 30$. When there are fewer crosslinks the distribution becomes wider, as expected, since we cannot clearly distinguish the localized and delocalized particles.

The calculation of $P(\xi)$ is different from that envisioned by Goldbart *et al.* [39]. In their formalism only the fraction Q of localized particles contribute to $P(\xi)$, and there should be a second peak of weight $1 - Q$ at $\xi = \infty$. For simulations of finite duration it is impossible to clearly distinguish the localized from the delocalized monomers. Very close to the critical crosslink density $P(\xi)$ develops a small secondary peak at large ξ. This is presumably due to the delocalized particles which will eventually sample the entire computational box. If

the data were extensive enough we could attempt to subtract the secondary peak from the distribution and obtain a function more closely related to that of [39].

Goldbart *et al.* predict that there is a single universal curve for the distribution of localization lengths. In Fig. 4.14 $P(\xi)$ is plotted as a function of ξ for several different systems. This graph clearly shows that the data collapse to a single curve. However, as is

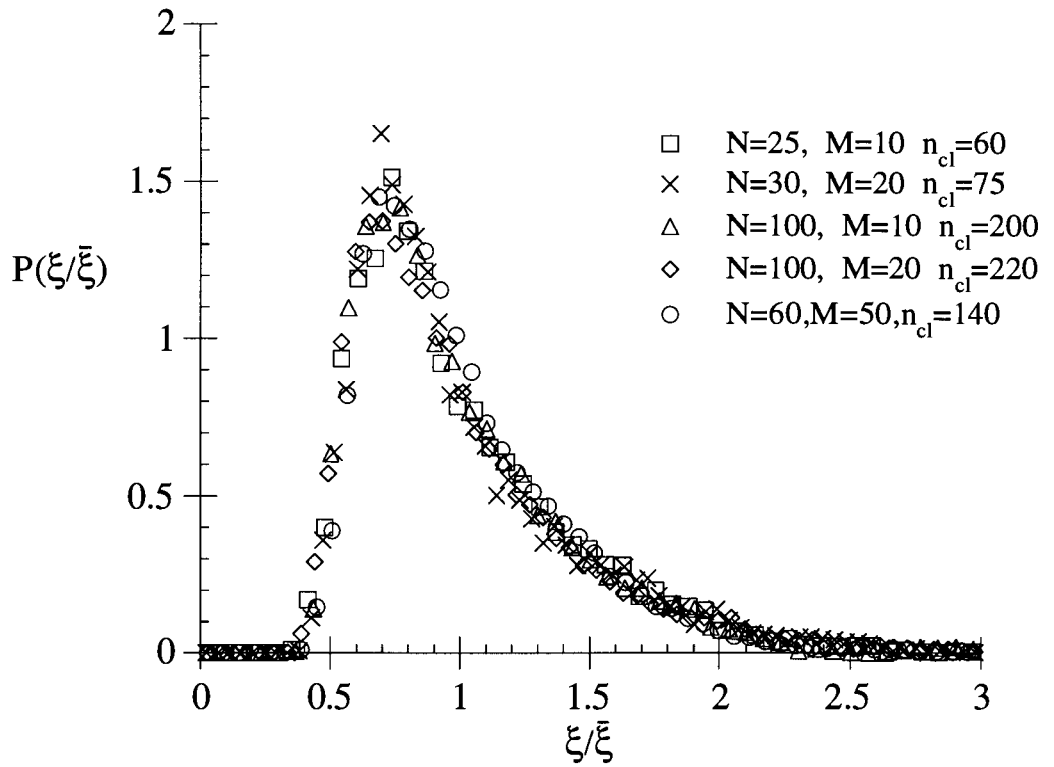

Figure 4.14: The distribution of localization lengths is plotted for one crosslink density for each of the different system sizes studied. All the data collapse to a single curve.

shown in Fig. 4.15, the curve that is predicted by Goldbart *et al.* is quite different than the curve we find.

A plot of the average localization length $\overline{\xi}$ as a function of crosslink density is shown in Fig. 4.16. The theory predicts the dependence of average localization length on crosslink density to be $\overline{\xi} \sim (n/n_c - 1)^{-1/2}$. From the data the results are that for $M = 20$, $N = 30$ the exponent $\beta_\xi = -0.24 \pm 0.03$; for $M = 10$, $N = 100$ then $\beta_\xi = -0.24 \pm 0.03$; and for

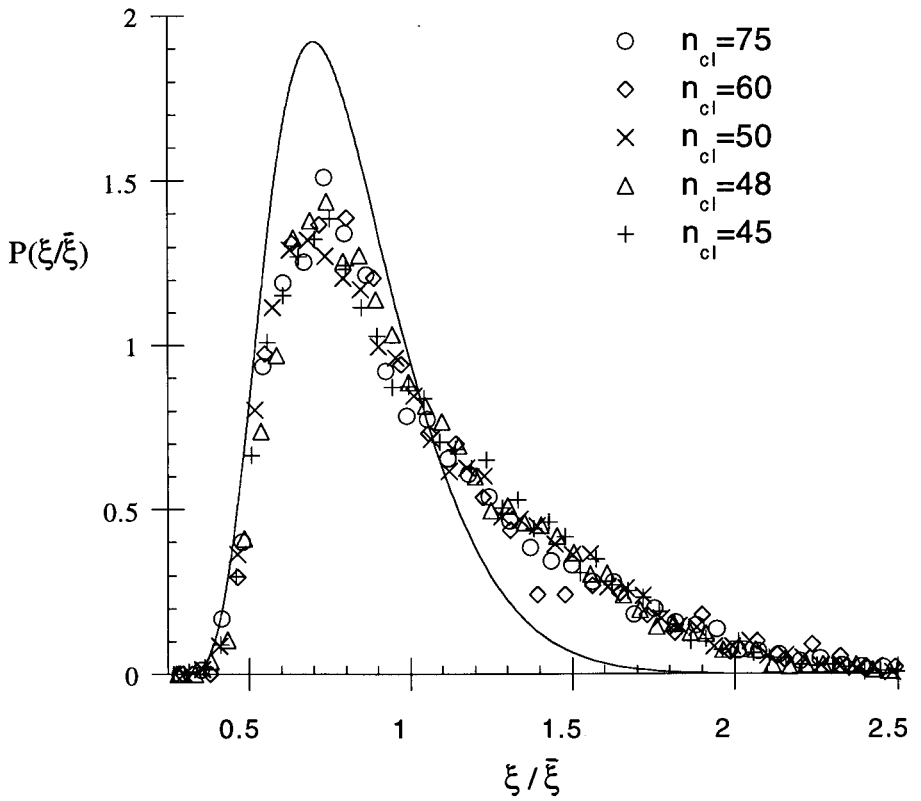

Figure 4.15: The universal curve predicted by Goldbart is plotted with the distribution of localization lengths for the system of $N = 25$ polymers and $M = 10$ monomers.

$M = 20$, $N = 100$ $\beta_\xi = -0.22 \pm 0.03$. If fewer data points are used, to be closer to the regime appropriate to the theory, then the exponents actually increase to $\beta_\xi = -0.13 \pm 0.05$ and $\beta_\xi = -0.17 \pm 0.04$ for the larger two systems, respectively. For the systems simulated the largest localization length found corresponds to $\xi \leq 1.9 R_g$. In the calculation of $P(\xi)$ in reference [39], it is assumed that $\bar{\xi} \gg R_g$, i.e., the polymers have a great deal of mobility, although the system is rigid. It will be very difficult to access this regime in simulations and certainly the present ones do not do so. Nevertheless, the universal nature of $P(\xi)$ somewhat away from the transition point seems well established by the results presented here.

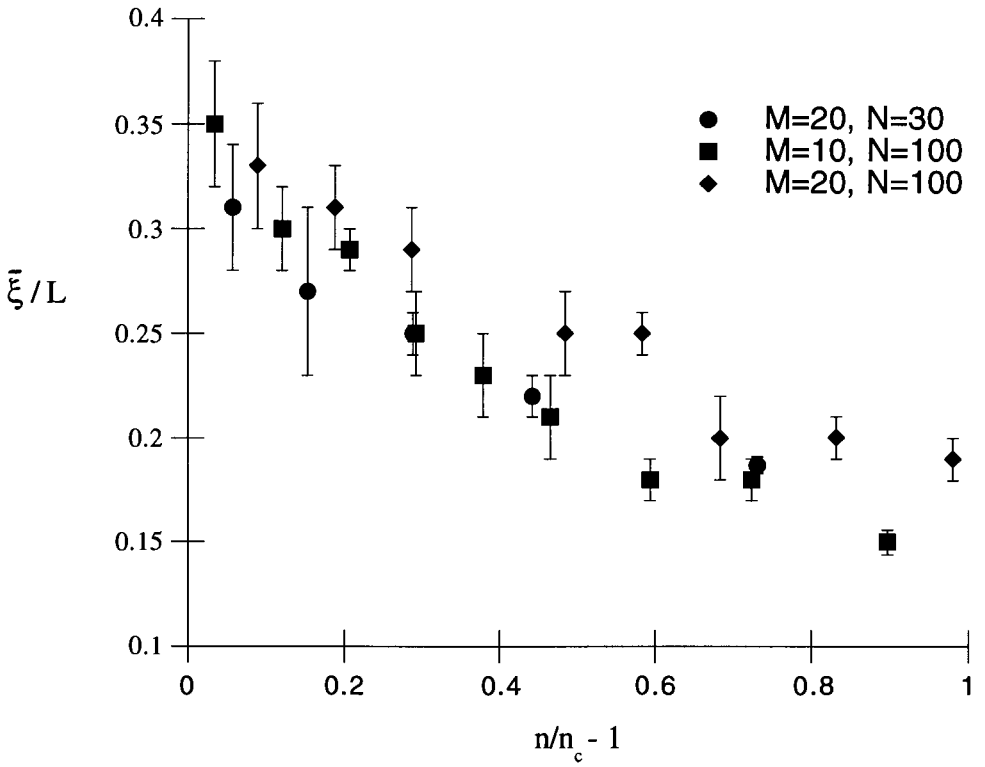

Figure 4.16: The average localization length as a function of crosslink density.

We have also measured the fraction of localized monomers Q. As mentioned above, in a simulation of finite length there is no unambiguous measure of localization. Monomers were considered localized if the localization length ξ was less than some fraction f of the

box length, typically $f = L/5$ or $f = L/3$. The variation in Q with crosslink density for two different systems is shown in Figs. 4.17 and 4.18. The exponents β_Q are obtained by fitting

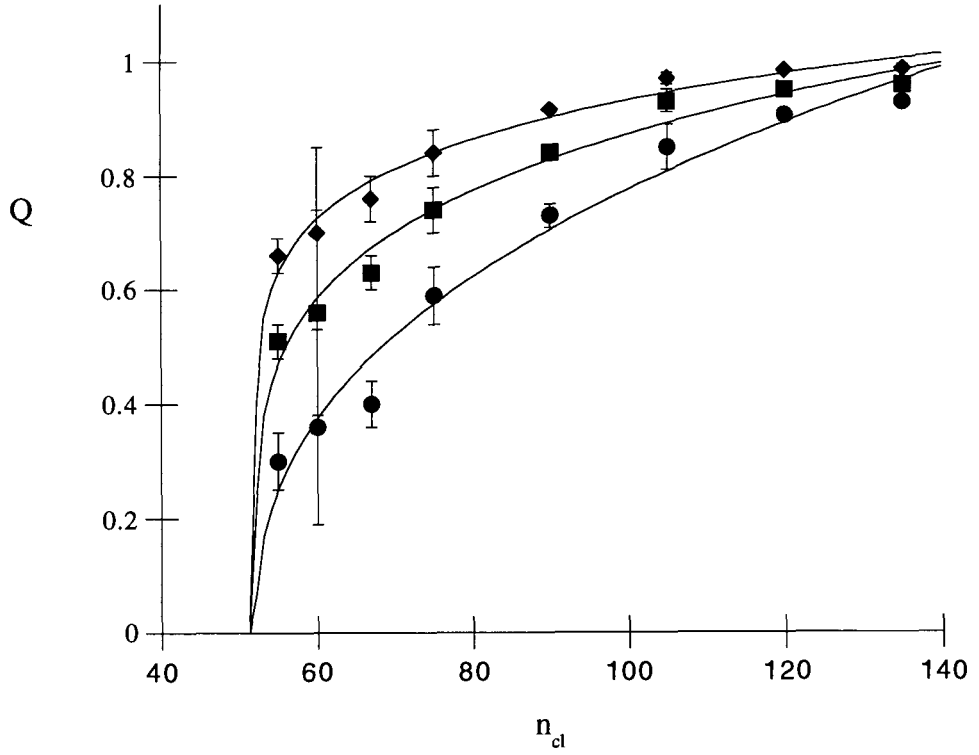

Figure 4.17: The variation of Q with the number of crosslinks is shown for the system of $M = 20$ and $N = 30$. The upper curve is Q when $f = L/3$, the middle curve is for $f = L/4$, and the bottom curve is for $f = L/5$. All curves are forced through the critical point $n_c = 52$.

Q to the equation $Q = A(n - n_c)^{\beta_Q}$. In all cases n_c was chosen to be the same as that found for q. If n_c were allowed to be a parameter to be fit then in all cases $n_c(Q)$ was found to be essentially the same as $n_c(q)$. The results for β_Q are shown in Table 4.5. The exponents quoted in this table are obtained by a fit to the values of Q closer to the transition, but the values remain the same if all the data shown in Figs. 4.17, 4.18 are included. The exponent predicted by [39] is $\beta_Q = 1$, from my data I cannot exclude this value. As discussed in the last chapter Goldbart *et al.* consider only the fraction of localized monomers to obtain the value of $\beta_Q = 1$, and clearly this is impossible to do in these simulations.

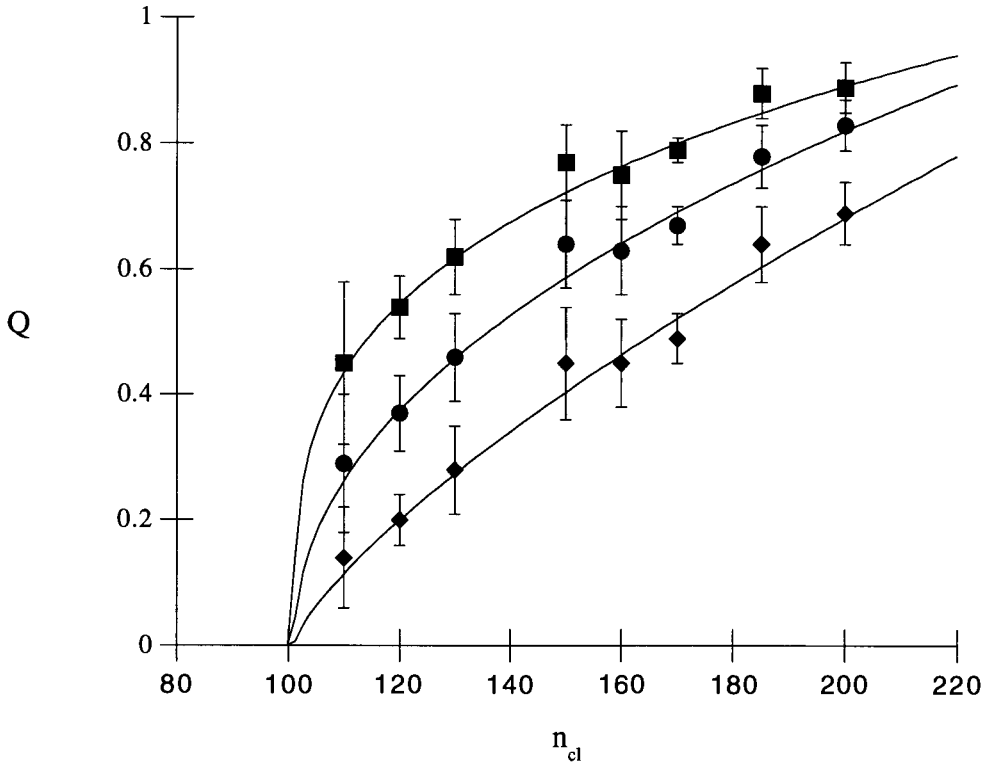

Figure 4.18: The variation of Q with the number of crosslinks is shown for the system of $M = 20$ and $N = 100$. The upper curve is Q when $f = L/3$, the middle curve is for $f = L/4$, and the bottom curve is for $f = L/5$. All curves are forced through the critical point $n_c = 101$.

M/N	$f = L/5$	$f = L/4$	$f = L/3$
20/30	0.46 ± 0.06	0.22 ± 0.02	0.14 ± 0.02
10/100	0.7 ± 0.1	0.45 ± 0.08	0.29 ± 0.06
20/100	0.7 ± 0.1	0.43 ± 0.09	0.28 ± 0.06

Table 4.5: A table showing the variation of β_Q with the fraction of the box f that was used as a criterion for localization.

4.5 Ergodicity Breaking

A central concept of statistical mechanics is that systems in equilibrium are ergodic. The ergodic hypothesis states that the time average of a quantity is equal to the phase-space average. This hypothesis is especially useful in numerical simulations. In this section I will discuss a technique developed by Thirumalai *et al.* [48] that distinguishes ergodic and non-ergodic behaviour in liquids and glasses with a particular focus on numerical simulations. Since simulations cannot reach $t \to \infty$, 'ergodicity' is only 'effective ergodicity' in the sense that the system is ergodic only over an observational time t_o. An ergodic system samples every point of a constant energy surface in phase space given infinite time. For $t = t_o$ the system is ergodic if effectively all regions of the energy surface are sampled. In the case of a non-ergodic system, the constant energy surface is decomposed into disjoint regions, and the barriers between the regions are large enough so that the system remains effectively trapped in one region over the observational time.

The following method was used by Thirumalai *et al.* to demonstrate broken ergodicity in a liquid to glass transition. An energy metric is defined as

$$d(t) = \frac{1}{\mathcal{N}} \sum_{j=1}^{\mathcal{N}} (\epsilon_{aj}(t) - \epsilon_{bj}(t))^2 , \tag{4.11}$$

where $\mathcal{N}$ is the total number of particles in the system, t is the time, j is a particle index and $\epsilon_{aj}(t)$ is the time-averaged energy of particle j at time t, $\epsilon_j(t) = \frac{1}{t}\sum_{t'=1}^{t} E_j(t')$ where $E_j(t')$ is the total energy of particle j at time t'. The labels a and b denote two different initial states of the system. The behaviour of $d(t)$ should characterize the degree of ergodicity of the system - if $d(t)$ decays rapidly to zero, then the two systems sample effectively the same region phase so that there are no barriers on the energy surface. However, if $d(t)$ approaches a non-zero plateau that decays very slowly, then the two systems are trapped in different regions of phase space, and over the observation time ergodicity is broken. This slow decay indicates the presence of energy barriers large enough to prevent the two states from sampling the same region of phase space. It should be noted that the two initial states of the system a, b should be widely separated in phase space, so as to start in different regions. Thirumalai *et al.* applied this method to liquids and supercooled glasses and found that the liquids were ergodic, while the glasses were not, over the length of the simulations.

The system considered by Thirumalai *et al.* is different from ours in that they have no quenched random variables, analogous to the crosslinks. I examined the function $d(t)$ for

different circumstances. For all crosslink densities, ranging from no crosslinks to well into the solid phase, $d(t)$ was monitored in the following way. Firstly, the crosslinks were imposed. Then, for a given realization of crosslinks two different systems were created by imposing different temperatures, and letting the system evolve in time. After a sufficient period of time had elapsed, approximately 10^8 integration steps, the two systems were brought to the same temperature and $d(t)$ was measured from this point on. Typical results for this are shown in curve a of Fig. 4.19. For all crosslink densities the curves $d(t)$ quickly decayed to a value close to zero. More disorder can be introduced by changing the distribution of crosslinks. In this case crosslinks were imposed on the melt, and from this crosslinked system a second system is created by changing one of the crosslinks. The two systems are allowed to relax at the same temperature before the comparison necessary for $d(t)$ is made. Results for this are shown in curve b of Fig. 4.19. The curve decays quickly to a value that is close to zero, but the difference in energy due to a single crosslink probably prevents $d(t)$ from actually attaining the value of zero. Finally, curve c of Fig. 4.19 compares two completely different distributions of crosslinks. Since $d(t)$ decays to a non-zero value, and only slowly decays from that value these systems are in different regions of phase space. Thus, once the crosslinks are imposed, the system is effectively ergodic by this measure, but, different distributions of crosslinks place the system in different regions of phase space, where the systems remain trapped for the length of a simulation and probably for much longer.

4.6 Conclusion

This chapter reported on the results of numerical simulations of randomly crosslinked polymer melts [43]. The aim of the simulations was to test some predictions of a recent theory of vulcanization, proposed in [39]. As a function of the number of crosslinks incorporated into the system Goldbart *et al.* predict an order parameter that is zero for the system in the liquid phase and non-zero when there is a sufficient density of crosslinks to form a solid, where this density is expected to be $n_c \sim 1$. They are able clearly to distinguish localized monomers from delocalized ones. The fraction of localized monomers is expected to increase with crosslink density as $Q \sim (n - n_c)^1$. The distribution of localization lengths of the localized monomers is predicted to be a single universal curve, when properly scaled.

We find that the order parameter q is zero until a critical density n_c of crosslinks. Due to strong system size fluctuations we are unable to confirm that $n_c = 1$ for all systems; but,

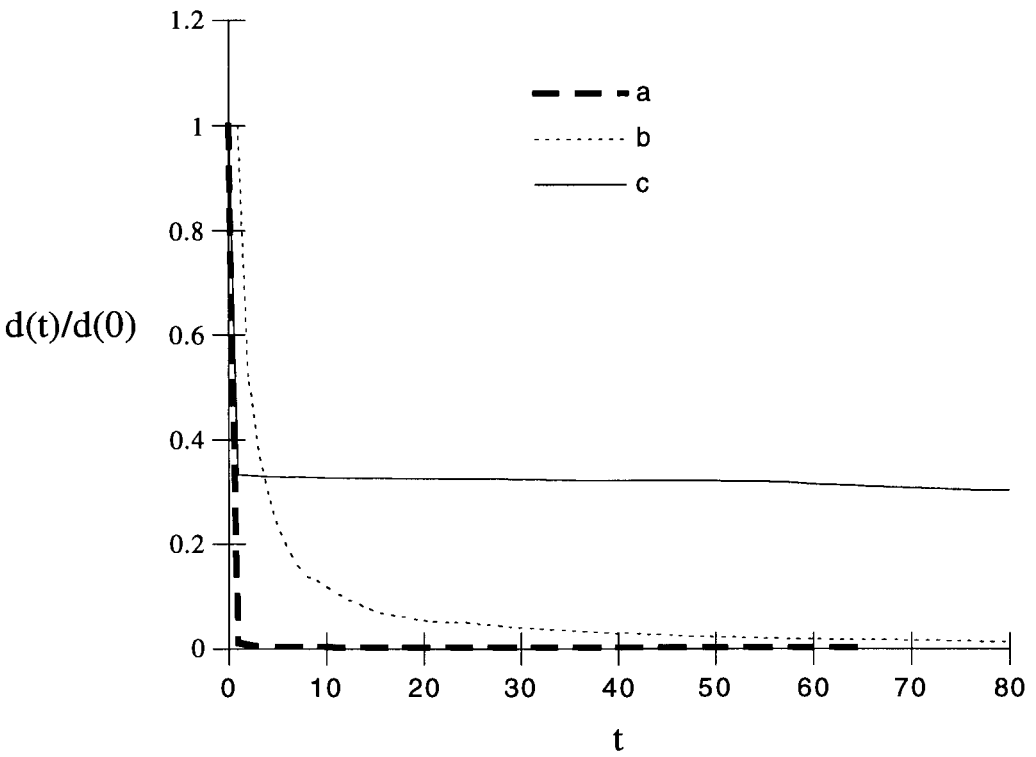

Figure 4.19: The function d(t) for $M = 20$, $N = 30$, and $n_{cl} = 60$ crosslinks. Time is measured in units of 10^7 integration steps. The different curves are explained in the text.

we do note that n_c decreases with increasing system size and that for the largest system $n_c \approx 1$. We are unable to find an unambiguous way of determining the fraction of localized particles. We have arbitrarily taken a fraction of the box size f, such that, if the average localization length of a monomer $\overline{\xi_j} < fL$, it was considered localized. For different values of f the exponent β_Q was calculated. Again, there was strong system-size dependence of the exponent, but the values of β_Q for the larger systems were consistent. The values of β_Q were extremely dependent on the particular value of f chosen. Finally, we considered the distribution of localization lengths. This distribution is expected to be a universal curve, and indeed this was found to be the case, when the localization lengths were scaled by the average localization length. Not only was the curve universal for a particular system, it was found that all systems collapsed to the same curve, although this curve is different from the one predicted by [39].

Finally, we implemented a test for ergodicity developed by Thirumalai *et al.* [48]. We find that, once the crosslinks are imposed, the system remains effectively ergodic, although the imposition of different realizations of crosslinks effectively places the system in different regions of phase space.

Chapter 5

Rigidity

5.1 Introduction

The elastic properties of vulcanized rubber are characteristically different from those of a crystalline solid. As noted in Chapter 1, rubber is capable of large elastic deformations on the order of hundreds of percent change. This is remarkable in that the deformations are reversible but the stress-strain relations are non-linear. For a crystalline solid the change in free energy due to external stresses arises primarily from the change in internal energy: The molecules change position relative to each other and their energy of interaction changes [49]. In vulcanized rubber the response to external stress is primarily entropic, that is the number of conformations available to the constituent chains changes.

In this section I describe the classical theory of high elasticity. In the next section I describe the implementation of this method to obtain the shear modulus as a function of crosslink density in the randomly crosslinked melts described in the previous chapter. The subsequent section describes the results of extensive simulations.

For the development of the analytic theory, a 'chain' denotes a segment of polymer between two crosslinking points. Defects such as dangling ends are not considered, although a significant fraction of monomers may be found in the dangling ends [46, 50]. Although there are many different chain lengths in a real network, the contour length or the number of monomers per chain is taken to be the same for each chain.

Starting from a polymer network in the shape of a cube, a deformation is applied to transform it to a rectangular parallelepiped, Fig. 5.1. The principal axes are stretched by amounts λ_1,λ_2,λ_3. The deformation is assumed to be affine, which means that, if a chain

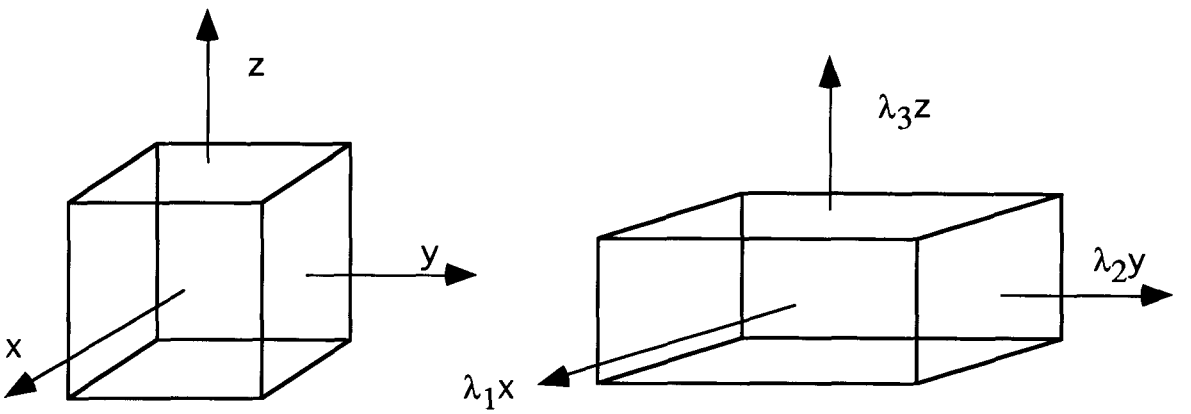

Figure 5.1: A deformation applied to a cube (left) results in a rectangular parallelepiped (right).

in the unstrained system has end-to-end vector length $\mathbf{R}_{ee} = (x, y, z)$, then in the deformed system this vector length is $\mathbf{R}'_{ee} = (\lambda_1 x, \lambda_2 y, \lambda_3 z)$. To calculate the total entropy change due to the deformation we begin by calculating the change in entropy of a single chain. This can be calculated by counting the number of configurations available to a random walk chain with end points fixed a distance $\mathbf{R}_{ee}$ apart. The entropy of this chain is

$$\mathcal{S} = A_c - k_B b^2 \mathbf{R}_{ee}^2, \tag{5.1}$$

where $b^2 = 3/(2Ma_0^2)$ is a constant related to the number M of monomers along the chain, a_0 is the bond length, and A_c is a constant. This is the proper form of the entropy for a chain whose ends are fixed.

The entropy after deformation is

$$\mathcal{S} = A_c - k_B b^2 \left(\lambda_1^2 x^2 + \lambda_2^2 y^2 + \lambda_3^2 z^2\right). \tag{5.2}$$

Thus, the contribution to the entropy of a single chain due to the deformation of the cube is

$$\Delta\mathcal{S} = -k_B b^2 \left((\lambda_1^2 - 1)x^2 + (\lambda_2^2 - 1)y^2 + (\lambda_3^2 - 1)z^2\right). \tag{5.3}$$

In a unit volume of the cube there are N_M chains each with M monomers and the entropy

change due to all these chains is

$$\Delta\mathcal{S} = -k_B b_M^2 \left((\lambda_1^2 - 1) \sum_{i=1}^{N_M} x_i^2 + (\lambda_2^2 - 1) \sum_{i=1}^{N_M} y_i^2 + (\lambda_3^2 - 1) \sum_{i=1}^{N_M} z_i^2 \right), \tag{5.4}$$

where $b_M = 3/\left(2Ma_0^2\right)$ is the appropriate constant for M monomers on a chain. Since these chains can be randomly oriented in the cube, on average

$$\sum_{i=1}^{N_M} x_i^2 = \sum_{i=1}^{N_M} y_i^2 = \sum_{i=1}^{N_M} z_i^2 = \frac{1}{3} \sum_{i=1}^{N_M} \mathbf{R}_{ee\,i}^2 = \frac{N_M}{3} \langle \mathbf{R}_{ee}^2(M) \rangle, \tag{5.5}$$

where $\langle \mathbf{R}_{ee}^2(M) \rangle^{1/2}$ is the average end-to-end length of a chain with M monomers. Now the assumption is made that we can replace $\langle \mathbf{R}_{ee}^2 \rangle$ by the expectation value of this quantity, for Gaussian chains

$$\langle \mathbf{R}_{ee}^2 \rangle = \int d\mathbf{R}_{ee}\, \mathbf{R}_{ee}^2 P(\mathbf{R}_{ee}) = \frac{3}{2b^2}, \tag{5.6}$$

(see Chapter 1). This gives for the change in entropy due to the N_M chains

$$\Delta\mathcal{S} = -k_B b_M^2 \frac{N_M}{3} \left(\lambda_1^2 + \lambda_2^2 + \lambda_3^2 - 3 \right) \frac{3}{2b_M^2}. \tag{5.7}$$

Now we sum the contributions from all the different lengths of chain M, $N = \sum_M N_M$. Thus the total change in entropy due to the deformation is

$$\Delta\mathcal{S} = -\frac{k_B N}{2} \left(\lambda_1^2 + \lambda_2^2 + \lambda_3^2 - 3 \right). \tag{5.8}$$

The change in entropy due to the deformation arises purely from the change in the number of configurations available to the chains when their endpoints are deformed and in this approximation, is insensitive to the particular details of the network. That means the entropy is not dependent upon the values of the lengths of chains in the network, the distribution of these lengths or other details of the chemistry, so long as the chains are long and flexible enough that the Gaussian model describes them accurately.

The change in free energy due to the deformation is

$$\Delta F = \Delta E_{\text{int}} - T\Delta\mathcal{S} \tag{5.9}$$

but, since the change is purely entropic, $\Delta F = -T\Delta\mathcal{S}$. Thus,

$$\Delta F = \frac{E}{2} \left(\lambda_1^2 + \lambda_2^2 + \lambda_3^2 - 3 \right), \tag{5.10}$$

where $E = Nk_BT$ is the appropriate elastic modulus. For a volume-conserving deformation E becomes the shear modulus.

From basic thermodynamics, for a reversible process the work done on a system is related to the internal energy by the relation $dE_{\text{int}} = dW + TdS$. This reduces to $\Delta W = -T\Delta S$, since the change in internal energy is negligible in this case. Considering only deformations which are explicitly volume conserving means that $\lambda_1\lambda_2\lambda_3 = 1$. For small changes in deformation this becomes

$$\frac{d\lambda_1}{\lambda_1} + \frac{d\lambda_2}{\lambda_2} + \frac{d\lambda_3}{\lambda_3} = 0 \tag{5.11}$$

Combining (5.11) with the change in work required to deform the system, we get

$$dW = E\left(\left(\lambda_1^2 - \lambda_3^2\right)\frac{d\lambda_1}{\lambda_1} + \left(\lambda_2^2 - \lambda_3^2\right)\frac{d\lambda_2}{\lambda_2}\right). \tag{5.12}$$

If the force per unit area on component α in the unstrained state is f_α and in the strained state is t_α, then $t_\alpha = f_\alpha\lambda_\alpha$. The work done by the applied forces to achieve the deformation is

$$\begin{aligned} dW &= f_1 d\lambda_1 + f_2 d\lambda_2 + f_3 d\lambda_3 \\ &= (f_1\lambda_1 - f_3\lambda_3)\frac{d\lambda_1}{\lambda_1} + (f_2\lambda_2 - f_3\lambda_3)\frac{d\lambda_2}{\lambda_2}. \end{aligned} \tag{5.13}$$

Equating (5.12) and (5.13) for any variation of stretch $d\lambda_\alpha$ gives the result

$$f_1\lambda_1 - f_2\lambda_2 = t_1 - t_2 = E\left(\lambda_1^2 - \lambda_2^2\right) \tag{5.14}$$

$$f_1\lambda_1 - f_3\lambda_3 = t_1 - t_3 = E\left(\lambda_1^2 - \lambda_3^2\right) \tag{5.15}$$

$$f_2\lambda_2 - f_3\lambda_3 = t_2 - t_3 = E\left(\lambda_2^2 - \lambda_3^2\right). \tag{5.16}$$

Since these equations are a function of the difference between the principal stresses and not their absolute values, the individual stresses can only be determined up to an overall hydrostatic pressure. This is a direct consequence of the imposition of a constant volume deformation, which is equivalent to stating that a polymer network is incompressible. This assumption is not unreasonable for vulcanized rubber. The work done on a polymer network due to a uniaxial stress f and a hydrostatic pressure is $dW = f\,dl - P\,dV$, where dV is the change in volume due to a hydrostatic pressure P. The change in $P\,dV$ is a factor of 10^{-4} smaller than $f\,dl$, [51], so at least to a first approximation the volume is constant.

The equations (5.14-5.16) relating the stress to the strain are the main result of the statistical theory of elasticity. In order to derive (5.14-5.16) there were several important

assumptions made. The first assumption was that Gaussian statistics adequately describe the end-to-end length of the chains. This assumption is justified only in a restricted set of conditions, because the network properties are sensitive to the method of formation of the network. In particular, Gaussian statistics are appropriate for a network formed by incorporating crosslinks via chemical agents or ionizing radiation into a dense melt of polymers [1]. If crosslinks were incorporated into a semi-dilute melt or into a dense melt into which is injected a good solvent the chains would not be ideal. Even if the melt itself is ideal, merely introducing crosslinks changes the equilibrium properties of the polymers. Monomers move to new equilibrium positions as a result of the crosslinks and the fluctuations of the chains are diminished by the presence of crosslinks [51]. An assumption related to that of Gaussian statistics is that the mean-square vector length of the chains in the network is the same as the mean square vector length of a polymer in the melt which was introduced in equation (5.6). A third assumption is that the deformation is affine, which implies that the ends of the chains remain fixed, or at least highly localized.

A more general theory of elasticity was created by James and Guth [52]. In their formulation the only fixed monomers are those that are at the surface. All other monomers including crosslink points are allowed complete freedom of movement. As well, they do not make the assumption that the mean square vector length of the chains is the same as a free chain in the melt, or that chains in the melt are Gaussian. They find a result similar to (5.14-5.16), but with E renormalized by factors not related to the strain. A limitation common to both theories is that only elastically active chains are considered. Defects such as dangling ends or self links are not included.

A series of experiments on natural rubber vulcanized with sulphur were done to test the validity of (5.14-5.16) [51]. Different types of stresses were imposed on the rubber, such as uniaxial elongation, two dimensional elongation, and various other compressions and shearing stresses. Deformations were reversible for up to 500% elongation. Equations (5.14-5.16) were verified for deformations up to 100%, i.e., $\lambda = 2$, in that the measured value of E was found to be independent of λ.

The method described above is not the only way to derive the elastic moduli. The isothermal elastic constants can be found by following a method first described by Squire *et al.*, [53]. This method is useful for systems that can be described by a potential U that depends only on the differences of positions of particles, taken pairwise. A set of orthonormal basis vectors $(\mathbf{a}_x, \mathbf{a}_y, \mathbf{a}_z)$ are defined for an undeformed system. A deformation is imposed

on the system, and the resultant strain tensor η_{ij} is calculated in terms of the basis vectors as

$$\eta_{ij} = \frac{1}{2}\left(a_{ij} - \delta_{ij}\right), \tag{5.17}$$

where δ_{ij} is the Kronecker delta, $a_{ij} = \mathbf{a}_i \cdot \mathbf{a}_j$ and the indices i, j range over the labels x, y, z. The strain tensor disappears in the undeformed system as expected, but is non-zero in a deformed system. The difference in position of any two particles k and l can be written as

$$r_{kl} = \sqrt{|\mathbf{r}_k - \mathbf{r}_l|}, \tag{5.18}$$

where $\mathbf{r}_k$ is the position of the k-th particle and can be expressed in basis vectors in the strained system $\mathbf{a}_i$ as $\mathbf{r}_k = x_{ki}\mathbf{a}_i$, where repeated indices are summed over. If we use this result, (5.18) becomes

$$\begin{aligned} r_{kl} &= \sqrt{\left(x_{ki} - x_{li}\right)\left(x_{kj} - x_{lj}\right)a_{ij}} \\ &= \sqrt{\left(x_{ki} - x_{li}\right)\left(x_{kj} - x_{lj}\right)\left(2\eta_{ij} + \delta_{ij}\right)}, \end{aligned} \tag{5.19}$$

where in the last step equation (5.17) was used. In such a system the partition function Z depends only on the potential U, so that

$$Z \sim \int \{d\mathbf{r}\} \exp\left(-\sum U(r)/k_B T\right). \tag{5.20}$$

The elastic moduli are defined as the derivatives of the free energy F with respect to the strain tensor,

$$C_{ijpq} = \frac{1}{V}\frac{\partial^2 F}{\partial \eta_{ij} \partial \eta_{pq}}. \tag{5.21}$$

Using (5.20) in the above equation leads to an expression for the elastic moduli C_{ijpq} in terms of expectation values of the derivatives of the potential with respect to r_{ij}. In a simulation these expectation values can easily be found as the time-averaged fluctuations of derivatives of U and, therefore, it is straightforward to apply this formalism to a system such as the one described in the previous chapter. Unfortunately, the implementation of this method for the calculation of elastic moduli leads to unstable results. That is, the uncertainties of the elastic constants were several times larger than the mean values.

Although much of the simulation work has focussed on polymer melts, there has been some work done on the shear modulus in crosslinked networks. Gao and Weiner [54] did simulations on a model of a crosslinked polymer network. Preserving some of the assumptions in the theory, their polymers had fixed end-to-end distance $\mathbf{R}$, and the polymers were

randomly oriented in a melt. Although the individual chains were not linked together, the orientations of the chains were fixed and the chains were allowed to diffuse through the system. They separately monitored the stresses arising from the connectivity of the monomers and the excluded volume interactions by varying the size of monomers σ while keeping the nearest-neighbour distance fixed. The range of variation of σ was sufficient to pass from the regime where the chains can easily pass through one another to the regime where they cannot. For small values of elongation, $\lambda \leq 1.5$, the stress-strain curves and, hence, the shear modulus were found to be virtually identical for all values of σ. For a substantial amount of elongation, $\lambda > 2$, the excluded volume contributions to the stress increased with increasing σ. This result is surprising only to the extent that the classical theory completely ignores the excluded volume effect, but, the result is consistent with the previously mentioned experiments in that the classical theory holds up to elongations of $\lambda = 2$.

Another set of simulations was done by Everaers, Kremer and Grest [55] who tested the effects of entanglements by slowly switching on the excluded volume interaction in a system of polymers set on interpenetrating diamond lattices. This system was fully mobile and the interpenetrating lattices explicitly created knots to entangle the polymers. The differing amounts of excluded volume allowed the knots to be trapped in some instances, while not in others. For extensions up to $\lambda = 2$ they found no difference in the force - elongation relationship for systems with and without knots.

5.2 Method

The details of the molecular dynamics simulations and of the equilibrated melts are described in Chapter 4. A number n_{cl} of random crosslinks were imposed in the manner detailed in the last chapter. The shear modulus was measured by imposing a volume conserving uniaxial elongation, so that $\lambda_1 = \lambda$ and $\lambda_2 = \lambda_3 = 1/\sqrt{\lambda}$ and stress was calculated by measuring the pressure tensor. In each of the principal directions the force per unit area was calculated by summing the force contributions from each of the monomers. The relation between the pressure tensor and the shear modulus is

$$\begin{aligned} P_1 - 1/3 < P > &= 2/3P_1 - 1/3P_2 - 1/3P_3 \\ &= -\frac{2}{3}\left(t_1 - \frac{1}{2}\left(t_2 + t_3\right)\right) \\ &= -\frac{2}{3}E\left(\lambda^2 - 1/\lambda\right). \end{aligned} \tag{5.22}$$

Thus, once the elongation is known, the pressure can be measured and the shear modulus is easily found.

The sizes of the systems were $N = 30$ polymers with $M = 20$ monomers per polymer; $N = 100$ polymers with each of $M = 10, 20$ monomers per polymer; and $N = 60$ polymers with $M = 50$ monomers. Three different values of elongation were applied of values $1.1L$, $1.2L$ and $1.3L$, where L is the length of the simulation box. These values of λ are small enough to ensure that the value of the shear modulus for each elongation will be the same, since the stress-strain relations are still in the linear regime. To calculate the shear modulus different values of crosslink density $n = n_{cl}/N$ were applied to each system. For each value of crosslink density at least seventy and often more than one hundred different realizations of crosslinks were used for the smaller systems. For the largest system of $M = 50$, $N = 60$ reasonably well converged results were obtained for fifteen to thirty samples. Before the incorporation of crosslinks, the monomers in the melt were assigned random velocities, such that $k_bT/\epsilon = 4$, and the equations of motion were integrated forward by 1000 time steps. The pressure tensor had a correlation time of approximately $50 - 100$ time steps, which was sufficient to randomize the force that each monomer experienced. This procedure was done so that the initial distribution of monomer positions would not unduly influence the calculation of the shear modulus. Once the crosslinks were imposed the pressure tensor was measured over a period of 10^5 time steps.

5.3 Results

A selection of the results is presented in Tables 5.1-5.2, and all the results are plotted in Figs. 5.2-5.4, the units of the shear elasticity are omitted but are ϵ/σ_0^3. The uncertainties are not shown in the figures but are quoted in the tables. The results for the tables and figures are the averages of the shear modulus for all the samples. The quoted uncertainties are obtained in the usual way as the standard deviation of the mean. The Figs.5.2 - 5.4 clearly show that the value of E is independent of the value of λ in this regime, as expected.

As can be seen from Tables 5.1-5.2 one consistent feature of these data is the decrease in standard deviation of E for a given number of crosslinks as λ is increased. The decrease in standard deviation is also evident for a given value of E as the system size is increased.

A direct comparison of the effects of polymer length is made in Fig.5.6. For $N = 100$

n_{cl}	$\lambda = 1.1$	$\lambda = 1.2$	$\lambda = 1.3$
0	-0.003 ± 0.03	$.003 \pm 0.01$	0.004 ± 0.009
50	0.007 ± 0.14	0.008 ± 0.06	
140	0.14 ± 0.21	0.11 ± 0.10	0.13 ± 0.08
150	0.11 ± 0.22	0.13 ± 0.12	0.13 ± 0.09
160	0.17 ± 0.23	0.16 ± 0.12	0.17 ± 0.09
170	0.23 ± 0.15	0.21 ± 0.09	
185	0.28 ± 0.28	0.26 ± 0.15	0.29 ± 0.13
200	0.31 ± 0.18	0.32 ± 0.13	

Table 5.1: A selection of the results for the shear modulus E for $M = 10$, $N = 100$. Entries are blank when there was not sufficient data to make an accurate estimate.

n_{cl}	$\lambda = 1.1$	$\lambda = 1.2$	$\lambda = 1.3$
0	-0.005 ± 0.02	0.003 ± 0.009	-0.002 ± 0.008
50	0.04 ± 0.05	0.02 ± 0.02	
150	0.11 ± 0.13	0.08 ± 0.06	0.08 ± 0.06
170	0.14 ± 0.15	0.10 ± 0.07	0.10 ± 0.04
185	0.16 ± 0.14	0.11 ± 0.08	0.11 ± 0.05
200	0.18 ± 0.15	0.15 ± 0.07	0.13 ± 0.07
220	0.21 ± 0.15	0.18 ± 0.08	0.23 ± 0.06
250	0.30 ± 0.14	0.25 ± 0.09	0.29 ± 0.06

Table 5.2: A selection of the results for the shear modulus E for $M = 20$, $N = 100$.

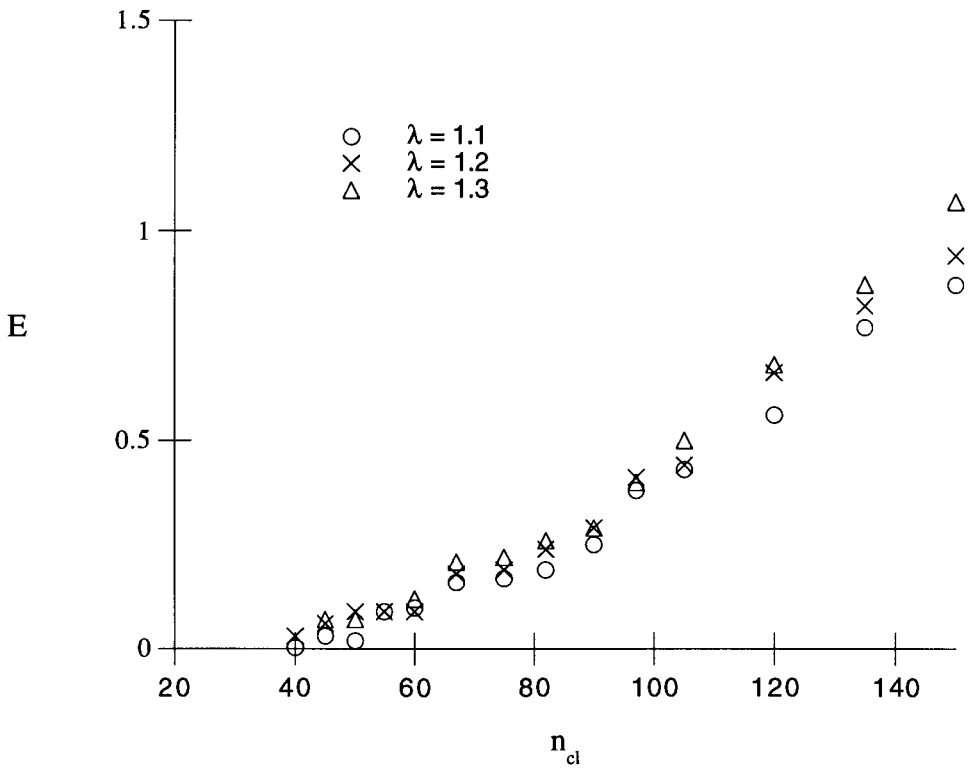

Figure 5.2: The shear modulus E as a function of the number of crosslinks for $N = 30$, $M = 20$.

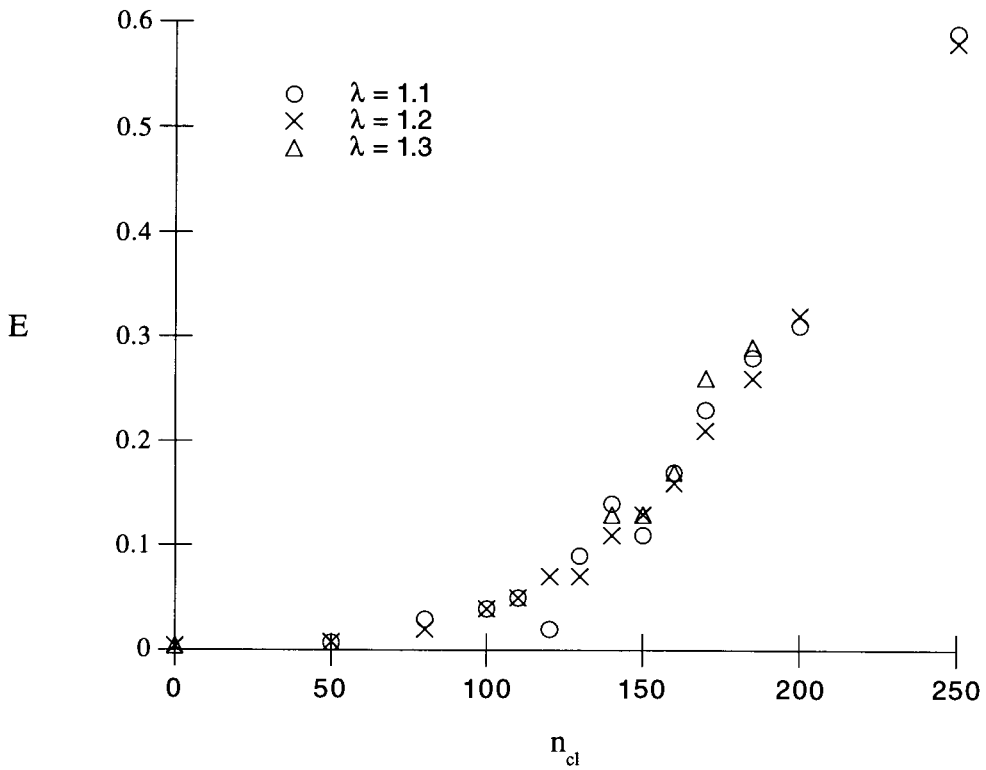

Figure 5.3: The shear modulus E as a function of the number of crosslinks for $N = 100$, $M = 10$.

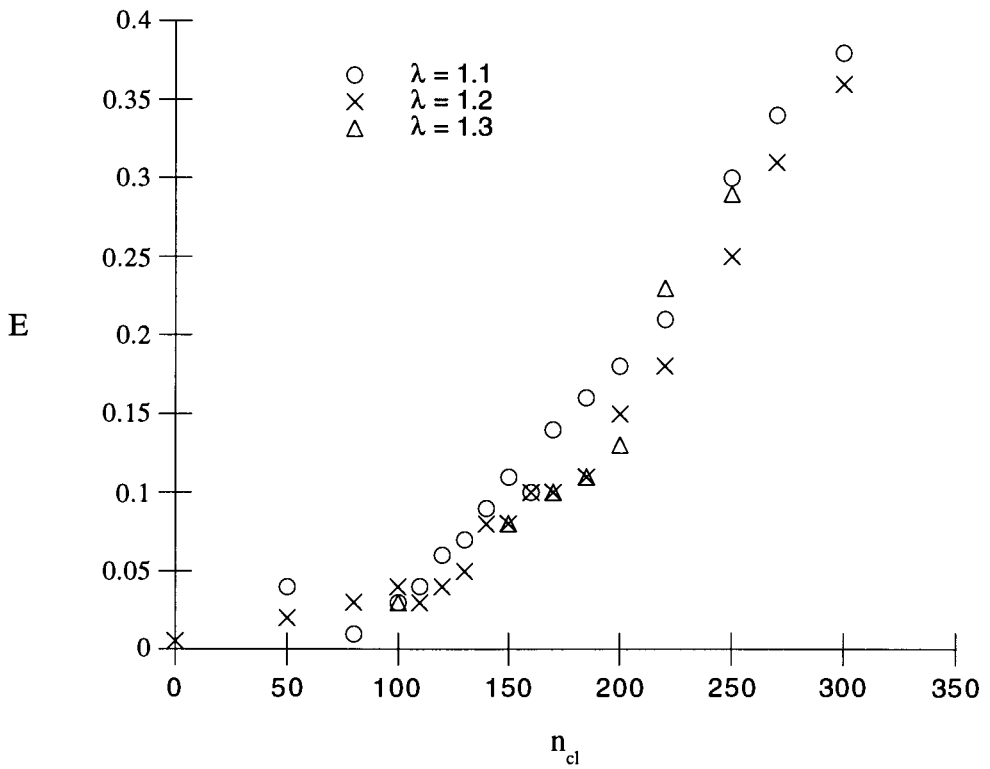

Figure 5.4: The shear modulus E as a function of the number of crosslinks for $N = 100$, $M = 20$.

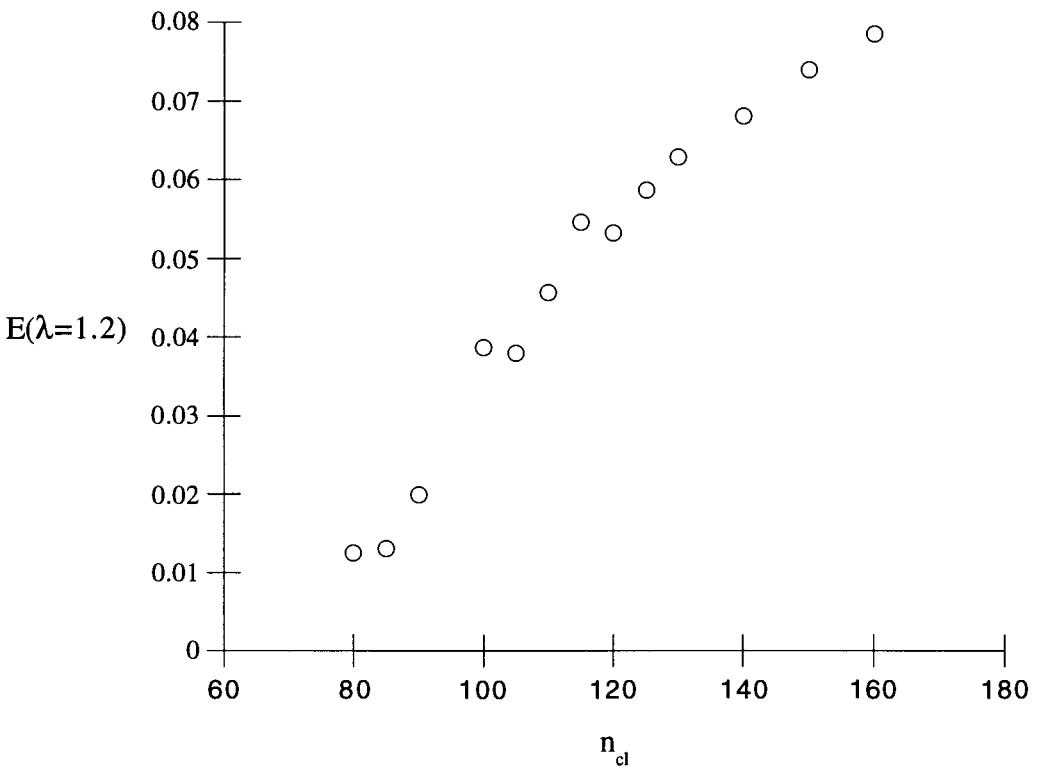

Figure 5.5: The shear modulus E as a function of the number of crosslinks for $N = 60$, $M = 50$.

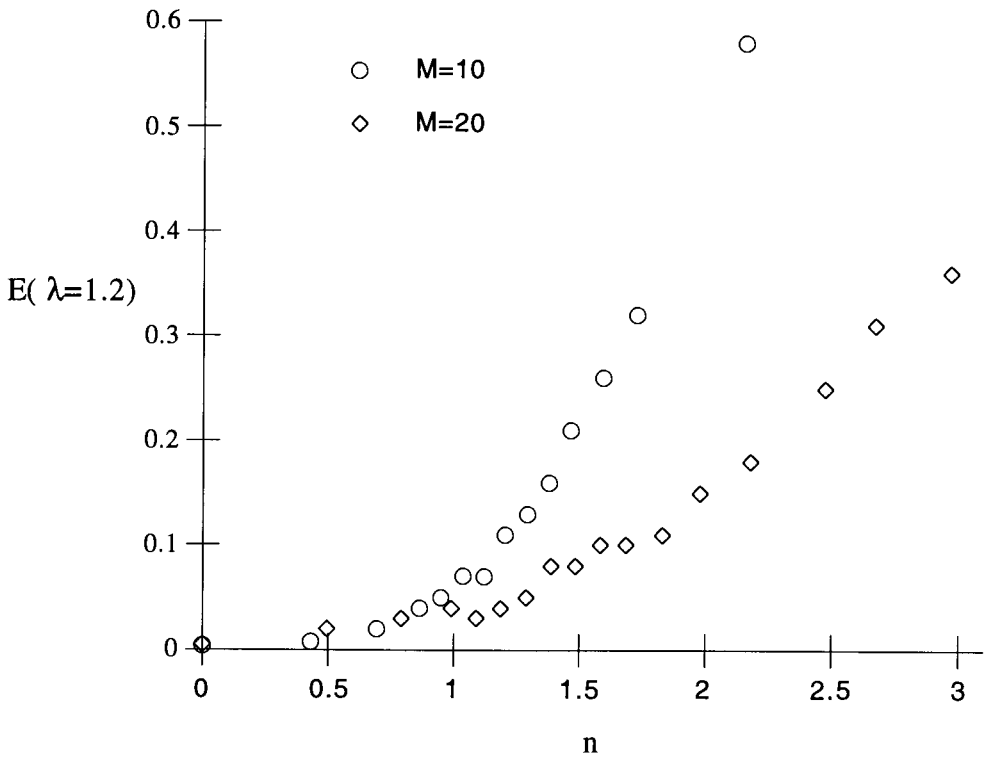

Figure 5.6: The shear modulus E for $N = 100$ polymers and $M = 10, 20$ monomers.

polymers the shear modulus as a function of crosslink density is plotted for $M = 10, 20$. The shear modulus increases at a much slower rate for longer polymers. This is contrary to the theoretical derivation of the shear modulus, where the change in entropy and hence the change in the value of the E is independent of the length of the chains, and the assumption that all the monomers were part of the infinite network was made. It is important to note that the incorporation of crosslinks partitions the chains into segments. A monomer or chain segment is considered to be elastically active if there are two independent paths which lead to the backbone of the network. This means that the elastically active part of a polymer, if there is one, is the section of chain between two crosslinks, or strand length. The average strand length of the chains has been measured, and was roughly constant as a function of the number of crosslinks but increased linearly with polymer length M. Although the chains in the melt obeyed Gaussian statistics, the elastically active part of the chains may be too short to be described in this way. This may be one reason for the discrepancy between our results and the theory as described in Section 5.1. As well, there is a clear decrease in the value of E with system size, for a given crosslink density, indicating that finite-size effects are non-negligible factors in the data.

An interesting comparison of the data is made by calculating the scaling exponents of E as a function of n. The exponent β_t is defined through $E \sim (n - n_c)^{\beta_t}$. Values for n_c can be estimated through a fit of the data. For $M = 10, 20$ the results of this fit give the same value of n_c, to within one standard deviation, as that found from the order parameter calculations. The values of n_c as found from the calculation of q will be used, and they are $n_c = 116, 101$ for $N = 100$, $M = 10, 20$, respectively, and $n_c = 1.7$ for $N = 30$, $M = 20$. For $M = 50$, $N = 60$ an independent estimate of n_c is not available. A free fit to the data in Fig. 5.5 gives an estimate of $n_c = 1.33 \pm 0.05$, and this is the value used to calculate the scaling exponent. The values of the scaling exponent are shown in Table 5.3.

As with the previous calculations there is a clear decrease in the scaling exponent with the system size. The value of the exponents for the four smaller systems are less than 1, which is somewhat surprising since the Figs. 5.2-5.4 might indicate that an exponent $\beta_t > 1$ may be more appropriate. The data used for the scaling exponents was close to the critical point, $n < 2$, and the forcing of the curves through the critical value n_c lowered the calculated value of β_t.

Clearly the scaling exponents predicted by the classical theory $\beta_t = 3$ or by percolation theory $\beta_t = 1.8$ [31] do not describe the data. Both these models assume that there are

M	N	β_t
20	30	0.93 ± 0.5
10	100	0.8 ± 0.5
20	100	0.73 ± 0.5
50	60	0.52 ± 0.07

Table 5.3: The values of the scaling exponents β_t for shear modulus. The values of E used for the fit were close to the transition regime, generally $1 \leq n_c \leq 2$. The large uncertainties arise because a weighted fit was done and the standard deviations of E were large, except in the case of $M = 50$, $N = 60$ where a weighted fit was not done.

few defects in the form of closed loops or dangling clusters. Previous computer simulations [56] have indicated that in systems similar to ours almost half of the monomers are found in dangling clusters. Since the theories seriously underestimate the number of monomers that are in the defects, this may account for some of the discrepancy in the values for the scaling exponent. As well, the shear modulus decreases to zero at a density of crosslinks greater than the percolation threshold. For a system with $N = 100$ chains, the percolation threshold occurs at a crosslink density of $n \sim 0.75$, whereas localization and rigidity occur at $n > 1$. This is consistent with previous studies that indicate that geometric percolation has a lower threshold than rigidity percolation [36].

5.4 Conclusion

In this chapter I have described a set of simulations performed to estimate the shear modulus of a system of polymer melts that were randomly crosslinked. The shear modulus E was calculated by performing a uniaxial extension on the polymer system and monitoring the resulting pressure along the principal axes. A large number of realizations of the calculations were necessary to obtain a stable estimate of E, and the standard deviation of E decreased with increasing system size, indicating that finite-size effects may be important.

There was a strong system-size dependence for the value of the shear modulus, contrary to the theoretical derivation. The origin of the inconsistency in not clear, but it is probably due to finite-size effects. Scaling exponents β_t were obtained by fitting the shear modulus to the equation $E \sim (n - n_c)^{\beta_t}$. The value of the exponent decreased from $\beta_t = 0.93$ for the smallest system to $\beta_t = 0.52$ for the largest. For the smaller systems the value of these

exponents may be affected by the fit through the critical crosslink density. Although there is a large uncertainty associated with these numbers because of the large standard deviations of the shear modulus, these exponents are clearly different from the classical prediction of $\beta_t = 3$, or the percolation prediction of $\beta_t = 1.8$. The values of n_c calculated from the shear modulus data were the same as those estimated from the order parameter calculation, when the comparison could be made, indicating that rigidity and localization occur in concert.

Bibliography

[1] A. Y. Grosberg and A.R. Khokhlov, *Statistical Physics of Macromolecules* (AIP Press, Woodbury NY,1994)

[2] M. Doi and S.F. Edwards, *The Theory of Polymer Dynamics* (Oxford University Press, Oxford, 1986)

[3] S. Stupp, S. Son, H. Lin and L. Li, Science **259**, 59 (1993)

[4] M. Spector, E. Naranjo, S. Chiruvolu and J. Zasadzinski, Phys. Rev. Lett. **73**, 2867 (1994)

[5] Damin Liu, thesis, Simon Fraser University 1992

[6] X. Wen, C. Garland, T. Hwa, M. Kardar, E. Kokufota, Y. Li, M. Orkisz and Y. Tanaka, Nature **355**, 426 (1992)

[7] Y. Kantor, M. Kardar and D. Nelson, Phys. Rev. Lett. **57**, 791 (1986); Y. Kantor, M. Kardar and D. Nelson, Phys. Rev. A **35** 3056 (1987)

[8] M. Plischke and D. Boal, Phys. Rev. A **38** 4943 (1988)

[9] A. Abraham, W. Rudge and M. Plischke, Phys. Rev. Lett. **62**, 1757 (1989)

[10] D. Boal, E. Levinson, D. Liu and M. Plischke, Phys. Rev. A **40**, 3292 (1989)

[11] J.-S. Ho and A. Baumgärtner, Phys. Rev. Lett. **63**, R1737 (1994), and references therein

[12] F. Abraham and D. Nelson, J. Phys. France **51**, 2653 (1990)

[13] Y. Kantor and D. Nelson, Phys. Rev. Lett. **58**, 2774 (1987)

[14] Y. Kantor and D. Nelson, Phys. Rev. A **36**, 4020 (1987)

[15] G. Grest and M. Murat, J. Phys. France **51**, 1415 (1990)

[16] M. Plischke and B. Fourcade, Phys. Rev. A **43**, 2056 (1991)

[17] Y. Kantor and K. Kremer, Phys. Rev. E **48**, 2490 (1993)

[18] M. Kardar and D. Nelson, Phys. Rev. Lett. **58**, 1298 (1987)

[19] B. Duplantier, Phys. Rev. Lett. **58**, 2733 (1987)

[20] J. Aronovitz and T. Lubensky, Europhys. Lett. **4**, 395 (1987)

[21] M. Paczuski, M. Kardar and D. Nelson Phys. Rev. Lett. **60**, 2638 (1988)

[22] M. Goulian, J. Phys. II France **1**, 1327 (1991)

[23] Le Doussal, J.Phys. A: Math. Gen. **25**, L469 (1992)

[24] G. Grest, Journal de Physique France I **1**, 169 (1991)

[25] D. Liu and M. Plischke, Phys. Rev. A **45**, 7139 (1992)

[26] I. Petsche and G. Grest, Phys. Rev. E **50**, 1324 (1989), and references therein

[27] M. Allen and D. Tildesley *Computer Simulations of Liquids* (Oxford University Press, Oxford, 1987)

[28] W. Hoover, *Computational Statistical Mechanics*, preprint

[29] J. Ray, M. Moody and A. Rahman, Phys. Rev. B **33**, 895 (1986)

[30] S. Barsky and M. Plischke, Phys. Rev. E **50**, 3911 (1994)

[31] P.G. de Gennes, *Scaling Concepts in Polymer Physics* (Cornell University Press, Ithaca NY, 1979)

[32] J. Essam in C. Domb and M. Green, *Phase Transitions and Critical Phenomena vol 2* (Academic Press, London, 1972)

[33] Martin Golubitsky and David Schaeffer, *Singularities and Groups in Bifurcation Theory vol 1* (Springer-Verlag, New York, 1985)

[34] P.G. de Gennes, La Recherche **7**, 919 (1976)

[35] P.G. de Gennes, J. Phys (Paris) **37**, L1 (1976)

[36] S. Feng and P. N. Sen, Phys. Rev. Lett. **52**, 216 (1984)

[37] A. R. Day, R. R. Tremblay and A-M. S. Tremblay, Phys. Rev. Lett. **56**, 2501 (1986)

[38] D. J. Jacobs and M. F. Thorpe, Phys. Rev. Lett. **75**, 4051 (1995)

[39] P. Goldbart, A. Zippelius and H. Castillo, preprint, and references therein

[40] R. Deam and S. F. Edwards, Philos. Trans. R. Soc. **280A**,317 (1976)

[41] K. Fischer and J. Hertz, *Spin Glasses* (Cambridge University Press 1991) page 76

[42] K. Kremer and G. Grest, J. Chem. Phys. **92**, 5057 (1990)

[43] S. Barsky and M. Plischke, Phys. Rev. E **53**, 871 (1996)

[44] J.D. Ferry *Viscoelastic Properties of Polymers* (Wiley and Sons, New York, 1970)

[45] J. Rudnick and G. Gaspari, Science **237**, 384 (1987)

[46] G. Grest and K. Kremer, Macromolecules **23,** 4994 (1990)

[47] G. Grest and K. Kremer, J. Phys. France **51**, 2829 (1990)

[48] D. Thirumalai, R. Mountain and T. Kirkpatrick, Phys. Rev. A **39**, 3563 (1989)

[49] L. Landau and E. Lifshitz *The Theory of Elasticity* (Pergamon Press, Oxford, 1986)

[50] L. Shy and B. Eichinger, Macromolecules **19**, 2787 (1986)

[51] L. Treloar, *The Physics of Rubber Elasticity* (Oxford Univeristy Press, Oxford, 1967)

[52] H. James and E. Guth, J. Chem. Phys. **11**, 455 (1943); H. James and E. Guth, J. Chem. Phys. **15**, 669 (1947)

[53] D. Squire, A. Holt and W. Hoover, Physica **42**, 388 (1969)

[54] J. Gao and J. Weiner, Macromolecules **24**, 1519 (1991)

[55] R. Everaers, K. Kremer and G. Grest, Macromolecular Symposia **93**, 53 (1995)

[56] K. Kremer and G. Grest in *Monte Carlo and Molecular Dynamics Simulations in Polymer Science* Ed. K. Binder (Oxford University Press, Oxford, 1995)